UNIVERSIDAD NACIONAL AUTÓNOMA DE MÉXICO

FACULTAD DE CIENCIAS

THE 2-FLAVOR SCHWINGER MODEL AT FINITE
TEMPERATURE AND IN THE DELTA-REGIME

T   E   S   I   S

QUE PARA OBTENER EL TÍTULO DE:

FÍSICO

P   R   E   S   E   N   T   A   :

JAIME FABIÁN NIETO CASTELLANOS

TUTOR

DR. WOLFGANG PETER BIETENHOLZ

CIUDAD UNIVERSITARIA, CDMX, 2021

Abstract

We present a study of the two-flavor Schwinger model by means of lattice simulations, using Wilson fermions and the Hybrid Monte Carlo algorithm. At finite temperature, we measure the masses of the bosons, which are related to m_π and m_η, as a function of the degenerate fermion mass m. We compare the results with the numerical solution of a set of equations obtained by Hosotani et al. based on bosonization, which predict these masses when $m \ll \sqrt{2g^2/\pi}$, where g is the gauge coupling. Furthermore, we measure the pion decay constant F_π in the so-called δ-regime, where finite size effects of the pion mass lead to $F_\pi = 0.6688(5)$. Finally, we measure the quenched topological susceptibility. Applying a two-dimensional version of the Witten-Veneziano formula, we compute the η meson decay constant $F_\eta = 0.374(3)$, which has a lower value than F_π. This is in contrast to large N_c Quantum Chromodynamics, where the two decay constants coincide.

Resumen

Se presenta un estudio del modelo de Schwinger con dos sabores por medio de simulaciones Monte Carlo, usando fermiones de Wilson y el algoritmo Monte Carlo Híbrido. A temperatura finita, se miden las masas de los bosones que aparecen en la teoría, las cuales se encuentran relacionadas con m_π y m_η, como función de la masa degenerada de los fermiones, m. Se comparan los resultados con la solución numérica a un conjunto de ecuaciones obtenidas por Hosotani et al. basándose en bosonización. Dichas ecuaciones predicen las masas de los bosones cuando $m \ll \sqrt{2g^2/\pi}$, donde g es la constante de acoplamiento de gauge. Asimismo, se mide la constante de decaimiento del pión F_π en el llamado régimen δ, donde efectos de volumen finito sobre la masa del pión conducen a $F_\pi = 0.6688(5)$. Finalmente, se mide la susceptibilidad topológica. Aplicando una versión bidimensional de la fórmula de Witten-Veneziano, se determina la constante de decaimiento del mesón η, $F_\eta = 0.374(3)$, la cual tiene un valor más bajo que el de F_π. Esto contrasta con Cromodinámica Cuántica con muchos colores, en donde ambas constantes de decaimiento coinciden.

Acknowledgments

First, I would like to thank my advisor, Dr. Wolfgang Bietenholz, for giving me the opportunity to collaborate in this project, for inviting me to present it in talks and for revising my work with a lot of commitment. I also want to thank Dr. Ivan Hip for providing me the codes to perform the simulations, for his advice to improve this thesis and for all his support during the past few months.

Quiero agradecer a mis padres, por apoyarme en mis decisiones y haberme dado una familia en lo que no carecí de nada. También agradezco a todos los amigos que hice en la carrera, en particular a Gabriela, Martín, Geovanny, César, Javier y Daniel, con quienes cursé la mayor parte de mis estudios y con quienes discutí varios problemas que me ayudaron a enriquecer mi entendimiento de los temas.

Agradezco también a cada persona en México que paga impuestos, por darme educación gratuita.

Finalmente, dedico este trabajo a mis abuelos María y Artemio y a la memoria de mi abuela Gloria.

Contents

Introduction

Quantum Chromodynamics (QCD) is the theory for the strong interaction. It is described in terms of quark and gluon fields. Phenomenologically, it is known that the quarks and gluons are confined and it is not possible to isolate them. Still, at high energies, the quarks are *asymptotically free* and we can study their interaction by means of perturbative methods. At low energy this is not possible.

A non-perturbative approach to the low energy regime of QCD are lattice simulations, which allow us to derive results from first principles. The first notions of this method were developed by Kenneth Wilson in the 1970s [1]. The general idea is based on the functional integral formalism. Performing a transition to Euclidean time (a Wick rotation), we can interpret the functional integral as a partition function of Statistical Mechanics. Then we discretize the Euclidean space-time and using the partition function we generate field configurations by means of Monte Carlo algorithms. With the configurations we can measure different observables. Numerous results have been obtained with this approach and they agree with experimental measurements, for instance, hadron masses, matrix elements and decay constants[1].

Perhaps, the most noticeable challenge of lattice QCD are the high computational resources that are needed. Therefore, it is more convenient to test numerical techniques in simpler models than QCD. The Schwinger model is a common choice as a toy model for QCD. It represents QED in two dimensions and has similar properties as QCD, such as confinement, topology and chiral symmetry breaking. Also, since the model is two dimensional, simulations do not require that much computer power. The model was introduced by J. Schwinger in 1969 [3,4]. Later, S. Coleman *et al.* proved the properties that we mentioned before [5,6].

For one massless fermion, the Schwinger model has an exact solution. However, for $N > 1$ massive flavors there is no precise analytic solution for the chiral condensate or the masses of the bosons that appear in the model. Even so, there have been several analytic approaches. In particular, in Chapter 3 we review the work done by Hosotani *et al.*, which uses *bosonization* to reduce the finite temperature Schwinger model to a quantum mechanical system. Assuming two degenerate flavors of mass m, they arrive at a set of equations, which can be solved numerically in order to compute the chiral condensate and the mass of the bosons that appear, for arbitrary values of m, as long as $m \ll \sqrt{2g^2/\pi}$, where g is the gauge coupling. We compare the solution of Hosotani's equations with lattice simulations of the Schwinger model at finite temperature.

Another non-perturbative approach to the low energy regime of QCD are effective field theories. A particularly successful one is *Chiral Perturbation Theory*. In this theory one considers the spontaneous symmetry breaking of the chiral flavor symmetry of QCD

$$\mathrm{SU}(N)_L \otimes \mathrm{SU}(N)_R \to \mathrm{SU}(N)_{L=R}$$

---

[1]A review of the most important lattice measurements at low energy can be found in ref. [2].

to write an effective Lagrangian, in terms of a field $U(x)$ in the coset space

$$U(x) \in (\mathrm{SU}(N)_L \otimes \mathrm{SU}(N)_R)/\mathrm{SU}(N)_{L=R} = \mathrm{SU}(N).$$

This field represents the lightest hadrons for N flavors, so at low energy they dominate the theory. Also, the meson field $U(x)$ replaces the quark and gluon fields.

In finite volume, several regimes of Chiral Perturbation Theory are established. We focus on the δ-regime, which consists of a small spatial volume but with a large Euclidean time extent. This regime has been little explored in the literature. Although it is unphysical, one can obtain physical results for the low energy constants of QCD. Also, it could be of interest because the small spatial volume enables faster simulations. Based on previous results obtained by Leutwyler, Hasenfratz and Niedermayer [7,8] for dimension $d \geq 3$, we make a conjecture about their two-dimensional version and we verify it by simulating the two-flavor Schwinger model. This allows us to compute the pion decay constant F_π in two dimensions.

Finally, we determine the *quenched topological susceptibility* and, by using the Witten-Veneziano formula [9,10], we obtain the decay constant of the η-meson in two dimensions. In large N_c QCD, it coincides with F_π. We verified whether the relation $F_\eta \simeq F_\pi$ is also valid in the Schwinger model.

Outline

This thesis is composed of the following chapters:

- Chapter 1: We discuss some important features of the Schwinger model and their relation with QCD.

- Chapter 2: We review the path integral and we explain the transition to Euclidean space. We discuss the main ideas about how a lattice simulation is carried out. We present the lattice formulation of Euclidean QED. Finally, we extend the ideas of the lattice formulation from QED to QCD.

- Chapter 3: We review the analytic approach to the Schwinger model by Hosotani *et al.* We compare the results of lattice simulations with a numerical solution to a set of equations, which allow us to compute the masses of the bosons that appear in the theory.

- Chapter 4: We review basic concepts of Chiral Perturbation Theory. We briefly describe three finite volume regimes, which can be used to perform lattice simulations of QCD, with a focus on the δ-regime. We present results of the measurement of the pion decay constant, F_π, in two dimensions.

- Chapter 5: We define the topological charge, the topological susceptibility and we compute them with lattice simulations. In this manner, we determine F_η in two dimensions by using the Witten-Veneziano formula for the Schwinger model.

- Chapter 6: We summarize our results and present the conclusions.

- Appendix: We describe the Hybrid Monte Carlo algorithm for a scalar field, a numerical integral, the jackknife error and the autocorrelation time.

Chapter 1

The Schwinger model

The Schwinger model represents Quantum Electrodynamics in 1+1 dimensions [4]. It is used as a toy model for Quantum Chromodynamics (QCD), because it has similar properties, such as: confinement, chiral symmetry breaking and topology. In contrast to QCD, however, this model does not have a running coupling constant. Its Lagrangian in Minkowski space-time (in natural units) for one flavor is given by

$$\mathcal{L} = -\frac{1}{4} F_{\mu\nu} F^{\mu\nu} + \overline{\psi}\gamma^\mu (i\partial_\mu - g A_\mu)\psi - m\overline{\psi}\psi, \tag{1.1}$$

where $F_{\mu\nu} = \partial_\mu A_\nu - \partial_\nu A_\mu$, $A_\mu(x)$ is the U(1) gauge field, g is the gauge coupling constant, ψ and $\overline{\psi}$ are independent Grassmann fields in the functional integral formulation (see Chapter 2) and γ^μ are the Dirac matrices. They can be chosen as

$$\gamma^0 = \sigma_3 = \begin{pmatrix} 1 & 0 \\ 0 & -1 \end{pmatrix}, \quad \gamma^1 = i\sigma_1 = \begin{pmatrix} 0 & i \\ i & 0 \end{pmatrix}, \tag{1.2}$$

which satisfy $(\gamma^\mu)^\dagger = \gamma^0 \gamma^\mu \gamma^0$, $\{\gamma^\mu, \gamma^\nu\} = 2g^{\mu\nu}$ with $g_{\mu\nu} = \text{diag}(1, -1)$. We assume $A_\mu(x)$ to be dimensionless and g to have dimension mass. With the γ matrices, we can define one more matrix

$$\gamma_5 \equiv \gamma^0 \gamma^1, \text{ which implies } \{\gamma^\mu, \gamma_5\} = 0, \quad \gamma_5^2 = \mathbb{I}, \quad \gamma_5^\dagger = \gamma_5. \tag{1.3}$$

The equations of motion can be obtained through the Euler-Lagrange equations

$$\partial_\mu \left(\frac{\partial \mathcal{L}}{\partial(\partial_\mu A_\nu)} \right) - \frac{\partial \mathcal{L}}{\partial A_\nu} = 0 \quad \Rightarrow \quad \partial_\nu F^{\nu\mu} = g J^\mu, \quad J^\mu \equiv \overline{\psi}\gamma^\mu\psi, \tag{1.4}$$

$$\partial_\mu \left(\frac{\partial \mathcal{L}}{\partial(\partial_\mu \psi)} \right) - \frac{\partial \mathcal{L}}{\partial \psi} = 0 \quad \Rightarrow \quad i\partial_\mu \overline{\psi}\gamma^\mu + m\overline{\psi} = -g\gamma^\mu A_\mu \overline{\psi}, \tag{1.5}$$

$$\partial_\mu \left(\frac{\partial \mathcal{L}}{\partial(\partial_\mu \overline{\psi})} \right) - \frac{\partial \mathcal{L}}{\partial \overline{\psi}} = 0 \quad \Rightarrow \quad i\gamma^\mu \partial_\mu \psi - m\psi = g\gamma^\mu A_\mu \psi. \tag{1.6}$$

Since $F^{\mu\nu}$ is antisymmetric, eq. (1.4) implies that J^μ is conserved

$$\partial_\mu J^\mu = 0. \tag{1.7}$$

If one applies a global axial transformation to the fields $\overline{\psi}$ and ψ

$$\psi \to \psi' = e^{i\alpha\gamma_5}\psi, \quad \overline{\psi} \to \overline{\psi}' = \overline{\psi}e^{i\alpha\gamma_5}, \quad \alpha \in \mathbb{R}, \tag{1.8}$$

the Lagrangian in eq. (1.1) transforms to

$$\mathcal{L} = -\frac{1}{4}F_{\mu\nu}F^{\mu\nu} + \overline{\psi}e^{i\alpha\gamma_5}\gamma^\mu(i\partial_\mu - gA_\mu)e^{i\alpha\gamma_5}\psi - m\overline{\psi}e^{2i\alpha\gamma_5}\psi. \tag{1.9}$$

Since $\{\gamma^\mu, \gamma_5\} = 0$, it follows that

$$e^{-i\alpha\gamma_5}\gamma^\mu = (\mathbb{I} - i\alpha\gamma_5 + \cdots)\gamma^\mu = \gamma^\mu(\mathbb{I} + i\alpha\gamma_5 + \cdots) = \gamma^\mu e^{i\alpha\gamma_5}, \tag{1.10}$$

and therefore

$$\mathcal{L} = -\frac{1}{4}F_{\mu\nu}F^{\mu\nu} + \overline{\psi}\gamma^\mu(i\partial_\mu - gA_\mu)\psi - m\overline{\psi}e^{2i\alpha\gamma_5}\psi. \tag{1.11}$$

We see that for $m = 0$, the Lagrangian has a symmetry under the transformation given in eq. (1.8). The Noether current of this symmetry, known as *axial current*, is

$$J_5^\mu = \overline{\psi}\gamma^\mu\gamma_5\psi. \tag{1.12}$$

Let us compute its divergence by taking into account the mass, using eq. (1.3) and relying on the equations of motion (1.5) and (1.6)

$$
\begin{aligned}
\partial_\mu J_5^\mu &= \partial_\mu\overline{\psi}\gamma^\mu\gamma_5\psi + \overline{\psi}\gamma^\mu\gamma_5\partial_\mu\psi \\
&= \partial_\mu\overline{\psi}\gamma^\mu\gamma_5\psi - \overline{\psi}\gamma_5\gamma^\mu\partial_\mu\psi \\
&= i(gA_\mu\overline{\psi}\gamma^\mu + m\overline{\psi})\gamma_5\psi + i\overline{\psi}\gamma_5(gA_\mu\gamma^\mu\psi + m\psi) \\
&= igA_\mu\overline{\psi}\gamma^\mu\gamma_5\psi + im\overline{\psi}\gamma_5\psi - igA_\mu\overline{\psi}\gamma^\mu\gamma_5\psi + im\overline{\psi}\gamma_5\psi \\
&= 2im\overline{\psi}\gamma_5\psi.
\end{aligned}
\tag{1.13}
$$

Hence, one would expect in the massless model J_5^μ to be conserved. However, it was proved that J_5^μ exhibits an anomaly at the quantum level [11, 12]. When $m = 0$ one actually has

$$\partial_\mu J_5^\mu = -\frac{g}{\pi}\frac{1}{2}\epsilon_{\mu\nu}F^{\mu\nu}. \tag{1.14}$$

This equation is known as the *axial anomaly*. In order to show that the theory is sensitive to this expression, we define

$$^*F \equiv \frac{1}{2}\epsilon_{\mu\nu}F^{\mu\nu} = F^{01} = -F_{01} = -E. \tag{1.15}$$

In 1+1 dimensions the Abelian strength field tensor is given by

$$F_{\mu\nu}(x) = \begin{pmatrix} 0 & E(x) \\ -E(x) & 0 \end{pmatrix}, \tag{1.16}$$

which confirms $^*F = -E$. Furthermore, $F_{\mu\nu} = \epsilon_{\mu\nu}F_{01} = \epsilon_{\mu\nu}E$, hence

$$F_{\mu\nu} = -\epsilon_{\mu\nu}{}^*F. \tag{1.17}$$

Let us note that

$$\epsilon^{01}\gamma_1 = -\epsilon_{01}\gamma_1 = -\gamma_1 = \gamma^1 = \gamma^0\gamma^0\gamma^1 = \gamma^0\gamma_5,$$
$$\epsilon^{10}\gamma_0 = -\epsilon_{10}\gamma_0 = \gamma_0 = \gamma^0 = -\gamma^0\gamma^1\gamma^1 = \gamma^1\gamma^0\gamma^1 = \gamma^1\gamma_5, \tag{1.18}$$

therefore $\epsilon^{\mu\nu}\gamma_\nu = \gamma^\mu\gamma_5$. With this expression we can rewrite eq. (1.12) as

$$J_5^\mu = \epsilon^{\mu\nu}J_\nu. \tag{1.19}$$

If we multiply by $\epsilon_{\sigma\mu}$ and use the property $\epsilon^{\nu\mu}\epsilon_{\mu\sigma} = \delta_\sigma^\nu$, eq. (1.19) takes the form

$$J_\sigma = \epsilon_{\sigma\mu}J_5^\mu, \qquad J^\sigma = \epsilon^{\sigma\mu}J_{5\,\mu}. \tag{1.20}$$

Substituting eq. (1.17) in eq. (1.4) leads to

$$-\partial_\mu\epsilon^{\mu\nu}\,{}^*F = gJ^\nu \tag{1.21}$$

and by using eq. (1.20) we have

$$-\partial_\mu\epsilon^{\mu\nu}\,{}^*F = g\epsilon^{\nu\mu}J_{5\,\mu}. \tag{1.22}$$

Multiplying by $\epsilon_{\nu\rho}$ yields

$$\partial_\rho\,{}^*F = gJ_{5\,\rho}. \tag{1.23}$$

We can take the derivative on both sides of the equation and rename the dummy index

$$\partial^\mu\partial_\mu\,{}^*F = g\partial^\mu J_{5\,\mu} = -\frac{g^2}{\pi}\,{}^*F. \tag{1.24}$$

Finally, substituting eq. (1.15) gives

$$\left(\partial^2 + \frac{g^2}{\pi}\right)E = 0, \tag{1.25}$$

which is the Klein-Gordon equation of a scalar field with the mass μ, $\mu^2 = g^2/\pi$. Therefore, in the massless one flavor Schwinger model, a boson of mass μ appears. This result has been generalized to an arbitrary number of N massless flavors [13], where a boson of mass $\mu^2 = Ng^2/\pi$ appears, along with $N-1$ massless bosons. For massive fermions no general solution exists, although there are several approaches. We will review one of those approaches in Chapter 3. Deeper discussions of QED in 1+1 dimensions can be found in refs. [14, 15].

1.1   Confinement

As we mentioned before, the Schwinger model exhibits confinement. We can illustrate this fact by analyzing the classical equations of motion

$$\partial_\mu F^{\mu\nu} = J^\nu. \tag{1.26}$$

Let us fix the gauge by setting $A_0 = 0$ and suppose that we place a charge g at the origin,

$$\partial_1 F^{10}(x) = g\delta(x) \quad \implies \quad \partial_x E(x) = g\delta(x) \quad \implies \quad E(x) = g\theta(x) + E_0, \tag{1.27}$$

where $\theta(x)$ is the Heaviside function and E_0 is a constant electric field. If we calculate the energy of this configuration, we see that it diverges

$$\frac{1}{2}\int_{-\infty}^{\infty} dx\, E^2 \to \infty. \tag{1.28}$$

This means that the finite energy states must be charge neutral. Now, let us consider two charges $\pm g$ at $x = \mp L/2$. The equation of motion reads

$$\partial_x E(x) = g\,\delta\left(x + \frac{L}{2}\right) - g\,\delta\left(x - \frac{L}{2}\right) \quad \implies \quad E(x) = g\,\theta\left(x + \frac{L}{2}\right) - g\,\theta\left(x - \frac{L}{2}\right) + E_0. \tag{1.29}$$
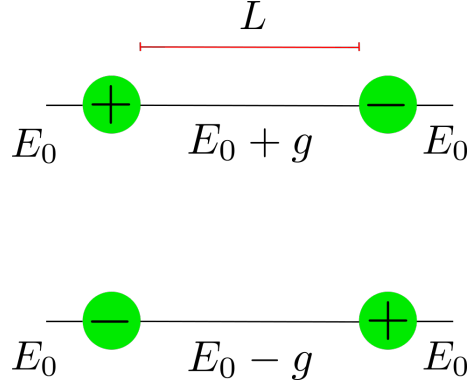
Figure 1.1: Electric field between an electron-positron pair in QED$_2$, considering the background field E_0.

If we set $E_0 = 0$, the electric field is

$$E(x) = \begin{cases} g & |x| < \frac{L}{2} \\ 0 & \text{otherwise.} \end{cases} \tag{1.30}$$

We can calculate the energy of this configuration,

$$\frac{1}{2} \int_{-\infty}^{\infty} dx\, E^2 = \frac{1}{2} \int_{-L/2}^{L/2} dx\, g^2 = \frac{g^2 L}{2}. \tag{1.31}$$

We see that the energy grows linearly with the separation of the charges, illustrating confinement. This property holds at the quantum level as well [5].

1.2 Vacuum angle

If we do not fix the background field E_0 to zero, it is possible to generate electron-positron pairs when the difference of the energy between both particles together and the background field is negative

$$\Delta H = \frac{1}{2} \int_{-L/2}^{L/2} dx\, \left[E(x)^2 - E_0^2 \right] < 0. \tag{1.32}$$

The electric field $E(x)$ between the particles is now given by (see figure 1.1)

$$E(x) = E_0 \pm g, \quad -\frac{L}{2} \leq x \leq \frac{L}{2}. \tag{1.33}$$

Pairs can be created when

$$\Delta H = \frac{L}{2} \left(g^2 \pm 2gE_0 \right) < 0$$

$$\Leftrightarrow \begin{cases} \frac{g}{2} < E_0 & \text{for } E(x) = E_0 - g \\ E_0 < -\frac{g}{2} & \text{for } E(x) = E_0 + g \end{cases}$$

$$\Leftrightarrow \frac{g}{2} < |E_0|. \tag{1.34}$$

In this context, the *vacuum angle* θ is introduced as

$$\theta = \frac{2\pi E_0}{g}. \tag{1.35}$$

4

Whenever $|\theta| > \pi$, pair production is favorable. $\theta = 0$ refers to confinement. This parameter was introduced to the Schwinger model by Coleman [6] and it adds the following term to the Lagrangian

$$\mathcal{L}_\theta = \frac{g\theta}{4\pi}\epsilon^{\mu\nu}F_{\mu\nu}. \tag{1.36}$$

We can rewrite $\epsilon^{\mu\nu}F_{\mu\nu}$ as

$$\epsilon^{\mu\nu}F_{\mu\nu} = \partial_\mu(2\epsilon^{\mu\nu}A_\nu), \tag{1.37}$$

which is a divergence. Therefore, $\mathcal{L}_\theta$ does not affect the equations of motion. In QCD a similar parameter appears.

1.3   Chiral symmetry breaking

As we will revise in a more detailed manner in Chapter 4, if one applies the chiral projection operators

$$P_L = \frac{\mathbb{I} - \gamma_5}{2}, \quad P_R = \frac{\mathbb{I} + \gamma_5}{2}, \tag{1.38}$$

to the fields ψ and $\overline{\psi}$, we can write the Lagrangian as

$$\mathcal{L} = -\frac{1}{4}F_{\mu\nu}F^{\mu\nu} + \overline{\psi}_L\gamma^\mu(i\partial_\mu - gA_\mu)\psi_L + \overline{\psi}_R\gamma^\mu(i\partial_\mu - gA_\mu)\psi_R - m(\overline{\psi}_R\psi_L + \overline{\psi}_L\psi_R),$$

$$\psi_R = P_R\psi, \quad \psi_L = P_L\psi, \quad \overline{\psi}_R = \overline{\psi}P_L, \quad \overline{\psi}_L = \overline{\psi}P_R, \tag{1.39}$$

which has a global symmetry under the transformations

$$\psi_L \to \psi'_L = e^{i\varphi_L}\psi_L, \quad \overline{\psi}_L \to \overline{\psi}'_L = \overline{\psi}_L e^{-i\varphi_L}, \quad e^{i\varphi_L} \in \mathrm{U}(1)_L, \tag{1.40}$$

$$\psi_R \to \psi'_R = e^{i\varphi_R}\psi_R, \quad \overline{\psi}_R \to \overline{\psi}'_R = \overline{\psi}_R e^{-i\varphi_R}, \quad e^{i\varphi_R} \in \mathrm{U}(1)_R \tag{1.41}$$

when $m = 0$. However, the *chiral condensate*, *i.e.* the vacuum expectation value $\langle\overline{\psi}\psi\rangle$ transforms as

$$\langle\overline{\psi}'\psi'\rangle = \left\langle \left(\overline{\psi}_R e^{i(\varphi_L - \varphi_R)}\psi_L + \overline{\psi}_L e^{i(\varphi_R - \varphi_L)}\psi_R\right) \right\rangle. \tag{1.42}$$

We see that it is invariant only when $\varphi_L = \varphi_R$, so $\mathrm{U}(1)_L \otimes \mathrm{U}(1)_R$ breaks to $\mathrm{U}(1)_{L=R}$.

In the N-flavor Schwinger model with degenerate fermion mass m, it has been shown [16] that the chiral condensate has the following dependence on m and θ when $m/\mu \ll 1$

$$\langle\overline{\psi}\psi\rangle = -\frac{\mu}{4\pi}\left(2e^\gamma \cos\frac{\theta}{2}\right)^{\frac{2N}{N+1}}\left(\frac{m}{\mu}\right)^{\frac{N-1}{N+1}}, \quad \mu = \frac{Ng^2}{\pi} \tag{1.43}$$

where γ is the Euler-Mascheroni constant. For the one flavor model we can see that

$$\langle\overline{\psi}\psi\rangle = -\frac{\mu}{2\pi}e^\gamma \cos\frac{\theta}{2}, \tag{1.44}$$

i.e. there is no dependence on the fermion mass. Hence the chiral condensate is non-vanishing even when $m = 0$. We also observe from eq. (1.43) that when $N > 1$, there is no chiral symmetry breaking in the massless Schwinger model, since $\langle\overline{\psi}\psi\rangle = 0$.

Chapter 2

Lattice formulation

Quantum Chromodynamics (QCD) is the established theory of the strong interaction. Its high energy regime can be managed through perturbation theory, since the quarks and gluons are asymptotically free. This means that the strong coupling α_s becomes small at high energies. It is known that

$$\alpha_s(q) \propto \frac{1}{\ln\left(\frac{q}{\Lambda_{\mathrm{QCD}}}\right)},$$

where q is the transfer momentum and Λ_{QCD} is the intrinsic energy scale of QCD. This enables one to perform expansions in powers of the coupling constant, when the energy is much larger than Λ_{QCD}. However, the low energy regime of QCD cannot be treated by perturbation theory, because the coupling becomes large. A non-perturbative approach to investigate this regime are lattice simulations. The main idea of this method is based on discretizing the space-time, on a four dimensional lattice. By means of the path integral and Monte Carlo simulations it is possible to generate field configurations that allow us to calculate relevant physical quantities. The first step to implement this procedure is a transition to *Euclidean time*, which is a rotation of the time coordinate to the imaginary axis. Some important properties of the Euclidean formulation will be discussed in the next section.

2.1   Path integral and Euclidean space-time

Let us begin by discussing the path integral for quantum mechanics in one dimension, the generalization to higher dimensions is straightforward. The starting point is the Green's function or time propagator $\hat{U}(t, t_0)$ of the Schrödinger equation, which satisfies

$$\left(\hat{H} - i\hbar\frac{\partial}{\partial t}\right)\hat{U}(t, t_0) = -i\hbar\hat{\mathbb{I}}\delta(t - t_0), \tag{2.1}$$

where $\hat{\mathbb{I}}$ is the identity operator and $\hat{H}$ the Hamilton operator. If $\hat{H}$ does not depend explicitly on time, the solution to eq. (2.1) reads

$$\hat{U}(t, t_0) = \theta(t - t_0)e^{-\frac{i}{\hbar}\hat{H}(t - t_0)}, \tag{2.2}$$

where θ is the Heaviside function. We assume $t > t_0$, hence $\theta = 1$. The propagator allows us to find the temporal evolution of a known state at t_0 by using

$$|\psi(t)\rangle = \hat{U}(t, t_0)|\psi(t_0)\rangle. \tag{2.3}$$

The idea now is finding an expression for the propagator. Let us consider a complete orthonormal set of position eigenstates $\{|x\rangle\}$, thus we define

$$U(x, t; x_0, t_0) = \langle x | \, \hat{U}(t, t_0) \, |x_0\rangle \, . \tag{2.4}$$

We will take $N - 1$ different intermediate times

$$t_0 < t_1 < \cdots < t_{N-1} < t. \tag{2.5}$$

Two consecutive times will be separated by an equidistant length $\epsilon = \frac{t-t_0}{N}$, i.e. $t_{j+1} - t_j = \epsilon$. We can write the propagator in the form

$$
\begin{aligned}
U(x, t; x_0, t_0) &= \langle x | \, e^{-\frac{i}{\hbar}\hat{H}(t-t_0)} \, |x_0\rangle \\
&= \langle x | \, e^{-\frac{i}{\hbar}\hat{H}(t-t_{N-1})} e^{-\frac{i}{\hbar}\hat{H}(t_{N-1}-t_{N-2})} \cdots e^{-\frac{i}{\hbar}\hat{H}(t_2-t_1)} e^{-\frac{i}{\hbar}\hat{H}(t_1-t_0)} \, |x_0\rangle \\
&= \langle x | \, e^{-\frac{i}{\hbar}\epsilon\hat{H}} \cdots e^{-\frac{i}{\hbar}\epsilon\hat{H}} \, |x_0\rangle \\
&= \langle x | \left(e^{-\frac{i}{\hbar}\epsilon\hat{H}} \right)^N |x_0\rangle \, .
\end{aligned}
\tag{2.6}
$$

Since $\{|x\rangle\}$ is complete, we apply the operator

$$\int dx \, |x\rangle \langle x| = \hat{\mathbb{1}} \tag{2.7}$$

$N - 1$ times, once at each intermediate time $t_1, \ldots, t_{N-1}$,

$$
\begin{aligned}
U(x, t; x_0, t_0) &= \int dx_1 \int dx_2 \cdots \int dx_{N-1} \, \langle x| \, e^{-\frac{i}{\hbar}\epsilon\hat{H}} \, |x_{N-1}\rangle \cdots \langle x_2| \, e^{-\frac{i}{\hbar}\epsilon\hat{H}} \, |x_1\rangle \\
&\times \langle x_1| \, e^{-\frac{i}{\hbar}\epsilon\hat{H}} \, |x_0\rangle \\
&= \int dx_1 \int dx_2 \cdots \int dx_{N-1} \prod_{j=0}^{N-1} \langle x_{j+1}| \, e^{-\frac{i}{\hbar}\epsilon\hat{H}} \, |x_j\rangle \, ,
\end{aligned}
\tag{2.8}
$$

where $x_N \equiv x$. We assume the Hamilton operator to have the standard form

$$\hat{H} = \frac{\hat{p}^2}{2m} + \hat{V}, \tag{2.9}$$

where $\hat{p}$ is the momentum operator with a complete orthonormal basis $\{|p\rangle\}$ and $\hat{V}$ is a potential term that only depends on the position operator $\hat{x}$. Now we use Trotter's formula[1], which states that for two bounded or semi-bounded (from below) operators $\hat{A}$ and $\hat{B}$ the following relation is satisfied

$$e^{\hat{A}+\hat{B}} = \lim_{n\to\infty} \left(e^{\hat{A}/n} e^{\hat{B}/n} \right)^n. \tag{2.10}$$

Since this is often the case of $\hat{p}^2$ and $\hat{V}$, we rewrite

$$\left(e^{-\frac{i}{\hbar}\epsilon\hat{H}} \right)^N = \lim_{N\to\infty} \left(e^{-\frac{i\epsilon\hat{p}^2}{2m\hbar}} e^{-\frac{i}{\hbar}\epsilon\hat{V}} \right)^N, \tag{2.11}$$

and conclude

$$U(x, t; x_0, t_0) = \lim_{N\to\infty} \int dx_1 \int dx_2 \cdots \int dx_N \prod_{j=0}^{N-1} \langle x_{j+1}| \, e^{-\frac{i\epsilon\hat{p}^2}{2m\hbar}} e^{-\frac{i}{\hbar}\epsilon\hat{V}} \, |x_j\rangle \, . \tag{2.12}$$

---

[1] See Section 2.3.1 of ref. [17] for a proof.

In order to simplify this expression we apply

$$\int dp \, |p\rangle \, \langle p| = \hat{\mathbb{1}} \tag{2.13}$$

to the matrix element

$$\langle x_{j+1}| \, e^{-\frac{i\epsilon \hat{p}^2}{2m\hbar}} e^{-\frac{i}{\hbar}\epsilon \hat{V}} \, |x_j\rangle = \int dp \, \langle x_{j+1}| \, e^{-\frac{i\epsilon \hat{p}^2}{2m\hbar}} \, |p\rangle \, \langle p| \, e^{-\frac{i}{\hbar}\epsilon \hat{V}} \, |x_j\rangle . \tag{2.14}$$

Since $\hat{V}$ only depends on $\hat{x}$, we obtain

$$e^{-\frac{i}{\hbar}\epsilon \hat{V}} \, |x_j\rangle = e^{-\frac{i}{\hbar}\epsilon V(x_j)} \, |x_j\rangle . \tag{2.15}$$

From

$$\langle p|x\rangle = \frac{1}{\sqrt{2\pi\hbar}} e^{-ipx/\hbar} = \langle x|p\rangle^* \tag{2.16}$$

we infer

$$\begin{aligned}
\langle x_{j+1}| \, e^{-\frac{i\epsilon \hat{p}^2}{2m\hbar}} e^{-\frac{i}{\hbar}\epsilon \hat{V}} \, |x_j\rangle &= \int dp \, e^{-\frac{i\epsilon p^2}{2m\hbar}} e^{-\frac{i}{\hbar}\epsilon V(x_j)} \, \langle x_{j+1}|p\rangle \, \langle p|x_j\rangle \\
&= \frac{1}{2\pi\hbar} \int dp \, e^{-\frac{i\epsilon p^2}{2m\hbar}} e^{-\frac{i}{\hbar}\epsilon V(x_j)} e^{\frac{i}{\hbar}p(x_{j+1}-x_j)} .
\end{aligned} \tag{2.17}$$

This is a Gaussian integral of the form

$$\int dx \, e^{-ax^2+bx} = \sqrt{\frac{\pi}{a}} e^{b^2/4a}, \quad \text{Re}(a) \geq 0, \quad a \neq 0. \tag{2.18}$$

The case $\text{Re}(a) = 0$ is non-trivial, but it can be shown by using Cauchy's integral theorem. Identifying $a = i\epsilon/(2m\hbar)$ and $b = i(x_{j+1} - x_j)/\hbar$, the result for the integral in eq. (2.17) reads

$$e^{-\frac{i}{\hbar}\epsilon V(x_j)} \sqrt{\frac{m}{2\pi i\hbar\epsilon}} e^{im\epsilon(x_{j+1}-x_j)^2/2\epsilon^2\hbar} . \tag{2.19}$$

Substituting this result in eq. (2.12) yields

$$\begin{aligned}
U(x,t;x_0,t_0) &= \lim_{N\to\infty} \int dx_1 \int dx_2 \cdots \int dx_{N-1} \left(\frac{m}{2\pi i\hbar\epsilon}\right)^{N/2} \\
&\times \quad \exp\left(\frac{i\epsilon}{\hbar} \sum_{j=0}^{N-1} \left[\frac{m}{2}\left(\frac{x_{j+1}-x_j}{\epsilon}\right)^2 - V(x_j)\right]\right) .
\end{aligned} \tag{2.20}$$

This expression is known as the path integral. It can be interpreted as a sum over all the possible trajectories that a non-relativistic particle can travel when moving from x_0 to x, because there is an integral over all positions at each intermediate time step t_j[2], see figure 2.1. In the continuum limit $N \to \infty \leftrightarrow \epsilon \to 0$, the argument of the exponential is the continuous time action

$$S[x] = \int dt \, \left(\frac{1}{2}m\dot{x}^2 - V\right) = \lim_{\epsilon\to0} \sum_{j=0}^{N-1} \epsilon \left[\frac{m}{2}\left(\frac{x_{j+1}-x_j}{\epsilon}\right)^2 - V(x_j)\right] . \tag{2.21}$$

---

[2]In field theory this interpretation is not right and one can question whether the name *path integral* is appropriate. For that reason, *functional integral* is used as well. Still, we will refer to it as path integral.
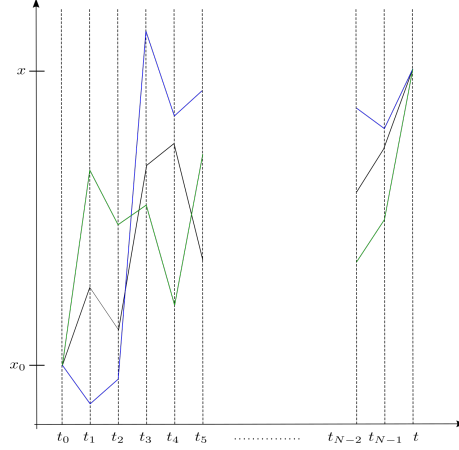
Figure 2.1: The path integral can be interpreted as a coherent sum over all possible paths from x_0 to x.

For this reason, the propagator can also be written as

$$U(x, t; x_0, t_0) = \int \mathcal{D}[x] e^{\frac{i}{\hbar} S[x]}, \quad \mathcal{D}[x] = \lim_{\epsilon \to 0} dx_1 dx_2 \cdots dx_{N-1} \left(\frac{m}{2\pi i \hbar \epsilon}\right)^{N/2}. \quad (2.22)$$

Further details about the path integral can be found in refs. [17, 18].

If we consider t as a purely imaginary parameter, we can perform the change of variable $it \to \tau$, where τ is known as *Euclidean time*. It follows that $d\tau^2 = (idt)^2 = -dt^2$. Thus, under this transformation all the terms of the interval ds^2 have the same sign, in contrast to Minkowski space-time. This change of coordinate transforms $\dot{x}(t) = ix'(\tau)$ and $dt = -id\tau$. As a result the action turns into

$$S[x] = \int dt \left(\frac{1}{2}m\dot{x}^2 - V\right) = i \int d\tau \left(\frac{1}{2}mx'^2 + V\right) = iS_E[x], \quad (2.23)$$

where we define the *Euclidean action* as

$$\begin{aligned} S_E[x] &= \int d\tau \left(\frac{1}{2}mx'^2 + V\right) \\ &= \lim_{a \to 0} \sum_{j=1}^{N-1} a \left[\frac{m}{2} \left(\frac{x_{j+1} - x_j}{a}\right)^2 + V(x_j)\right], \end{aligned} \quad (2.24)$$

where $a = i\epsilon$. By taking periodic boundary conditions $x_0 = x_N = x$, fixing $t_0 = 0$ (for convenience) and assuming that the system evolves during a Euclidean time $\tau_{\max} = Na$, we define the *Euclidean path integral* as

$$Z = \int dx \langle x| \hat{U}(\tau_{\max}, 0) |x\rangle = \int \mathcal{D}[x] e^{-S_E[x]/\hbar}, \quad \mathcal{D}[x] = \lim_{a \to 0} dx_1 dx_2 \cdots dx_N \left(\frac{m}{2\pi \hbar a}\right)^{N/2}$$

$$\hat{U}(\tau_{\max}, 0) = e^{-\tau_{\max} \hat{H}/\hbar}. \quad (2.25)$$

Note that there is an extra dx_N in $\mathcal{D}[x]$ that involves one more integration. This gives a link with statistical mechanics, where the partition function is given by

$$Z = \text{tr}\left[e^{-\beta \hat{H}}\right], \quad \beta = \frac{1}{k_B T}, \quad (2.26)$$

9

where T denotes temperature. In the case of the path integral, the factor β is

$$\beta = \frac{1}{\hbar}\tau_{\max}, \tag{2.27}$$

Thus, we see that the Euclidean path integral is mathematically equivalent to the partition function in statistical mechanics. This equivalence enables us to interpret

$$p[x] = \frac{1}{Z}e^{-S_E[x]/\hbar} \tag{2.28}$$

as the probability of the path $[x]$. A first calculation with this interpretation can be done if we consider the eigenstates $|n\rangle$ of $\hat{H}$

$$
\begin{aligned}
\int dx\,\langle x|\,\hat{U}(\tau_{\max},0)\,|x\rangle &= \mathrm{tr}\left[e^{-\beta\hat{H}}\right] \\
&= \mathrm{tr}\left[e^{-\frac{\tau_{\max}}{\hbar}\hat{H}}\right] \\
&= \sum_n \langle n|\,e^{-\frac{\tau_{\max}}{\hbar}\hat{H}}\,|n\rangle \\
&= \sum_n e^{-\frac{\tau_{\max}}{\hbar}E_n}.
\end{aligned} \tag{2.29}
$$

As $\tau_{\max}$ grows, only the exponential with the ground state energy E_0 (which we suppose non-degenerate) in its argument persists

$$\int dx\,\langle x|\,\hat{U}(\tau_{\max},0)\,|x\rangle \to e^{-\tau_{\max}E_0/\hbar}, \quad \text{for large } \tau_{\max}. \tag{2.30}$$

Therefore, it is possible to calculate the ground state energy through the decay of Z at large Euclidean time. Another consequence of the interpretation of the Euclidean path integral as a partition function is that one can calculate *thermal expectation values* using $\exp(-S_E[x]/\hbar)$ as a weight factor. For example, let us suppose an operator $\hat{A}$ that depends on the position operator $\hat{x}$; its expectation value is

$$\langle\hat{A}(\hat{x}(\tau))\rangle = \frac{1}{Z}\mathrm{tr}\left[\hat{A}(\hat{x}(\tau))e^{-\beta\hat{H}}\right] = \frac{1}{Z}\int \mathcal{D}[x]A(x(\tau))e^{-S_E[x]/\hbar}, \tag{2.31}$$

where Z is given by eq. (2.25). We obtain the correlation of two operators $\hat{A}(\hat{x})$ and $\hat{B}(\hat{x})$ as well

$$
\begin{aligned}
\langle\hat{A}(\hat{x}(\tau))\hat{B}(\hat{x}(0))\rangle &= \frac{1}{Z}\int \mathcal{D}[x]A(x(\tau))B(x(0))e^{-S_E[x]/\hbar} \\
&= \frac{1}{Z}\mathrm{tr}\left[\hat{A}(\hat{x}(\tau))\hat{B}(\hat{x}(0))e^{-\beta\hat{H}}\right] \\
&= \frac{1}{Z}\mathrm{tr}\left[e^{\tau\hat{H}/\hbar}\hat{A}(\hat{x}(0))e^{-\tau\hat{H}/\hbar}\hat{B}(\hat{x}(0))e^{-\beta\hat{H}}\right] \\
&= \frac{1}{Z}\sum_n \langle n|\,e^{\tau\hat{H}/\hbar}\hat{A}(\hat{x}(0))e^{-\tau\hat{H}/\hbar}\hat{B}(\hat{x}(0))e^{-\beta\hat{H}}\,|n\rangle \\
&= \frac{1}{Z}\sum_{n,m} \langle n|\,e^{\tau\hat{H}/\hbar}\hat{A}(\hat{x}(0))e^{-\tau\hat{H}/\hbar}\,|m\rangle\,\langle m|\,\hat{B}(\hat{x}(0))e^{-\beta\hat{H}}\,|n\rangle \\
&= \frac{1}{Z}\sum_{n,m} \langle n|\,\hat{A}(\hat{x}(0))\,|m\rangle\,e^{\tau(E_n-E_m)/\hbar}\,\langle m|\,\hat{B}(\hat{x}(0))\,|n\rangle\,e^{-\beta E_n} \\
&= \frac{1}{Z}\sum_{n,m} \langle n|\,\hat{A}(\hat{x}(0))\,|m\rangle\,\langle m|\,\hat{B}(\hat{x}(0))\,|n\rangle\,e^{-\tau E_m/\hbar}e^{-(\tau_{\max}-\tau)E_n/\hbar}. \tag{2.32}
\end{aligned}
$$

In the third line we made use of the fact that a time dependent operator can be written in Euclidean time according to the Heisenberg picture

$$\hat{O}(\tau) = e^{\tau\hat{H}/\hbar}\,\hat{O}(0)\,e^{-\tau\hat{H}/\hbar}. \tag{2.33}$$

In the other lines we have made use of the following properties

$$\sum_m |m\rangle\langle m| = \hat{\mathbb{I}}, \quad e^{\alpha\hat{H}}|m\rangle = e^{\alpha E_m}|m\rangle, \quad \langle m|e^{\alpha\hat{H}} = e^{\alpha E_m}\langle m|, \tag{2.34}$$

where α is a constant. In addition, we assume the eigenenergies to be non-degenerate. If we use eq. (2.29) for Z we can rewrite eq. (2.32) as

$$\langle\hat{A}(\hat{x}(\tau))\hat{B}(\hat{x}(0))\rangle = e^{\tau_{\max}E_0/\hbar}\frac{\sum_{n,m}\langle n|\hat{A}(\hat{x}(0))|m\rangle\langle m|\hat{B}(\hat{x}(0))|n\rangle\,e^{-\tau E_m/\hbar}e^{-(\tau_{\max}-\tau)E_n/\hbar}}{1 + e^{-\tau_{\max}(E_1-E_0)/\hbar} + e^{-\tau_{\max}(E_2-E_1)/\hbar} + \cdots}. \tag{2.35}$$

We have factorized $e^{-\tau_{\max}E_0/\hbar}$ from the partition function. Then

$$\langle\hat{A}(\hat{x}(\tau))\hat{B}(\hat{x}(0))\rangle = \frac{\sum_{n,m}\langle n|\hat{A}(\hat{x}(0))|m\rangle\langle m|\hat{B}(\hat{x}(0))|n\rangle\,e^{-\tau(E_m-E_0)/\hbar}e^{-(\tau_{\max}-\tau)(E_n-E_0)/\hbar}}{1 + e^{-\tau_{\max}(E_1-E_0)/\hbar} + e^{-\tau_{\max}(E_2-E_1)/\hbar} + \cdots}. \tag{2.36}$$

From this expression we see that if $\tau_{\max} \to \infty$ only those terms where $E_n = E_0$ will persist, giving as a result

$$\lim_{\tau_{\max}\to\infty}\langle\hat{A}(\hat{x}(\tau))\hat{B}(\hat{x}(0))\rangle = \sum_m \langle 0|\hat{A}(\hat{x}(0))|m\rangle\langle m|\hat{B}(\hat{x}(0))|0\rangle\,e^{-\tau(E_m-E_0)/\hbar}. \tag{2.37}$$

If now we take $\hat{A} = \hat{B}$ the correlator is

$$\begin{aligned}
\lim_{\tau_{\max}\to\infty}\langle\hat{A}(\hat{x}(\tau))\hat{A}(\hat{x}(0))\rangle &= |\langle 0|\hat{A}|0\rangle|^2 + |\langle 1|\hat{A}|0\rangle|^2 e^{-\tau(E_1-E_0)/\hbar} \\
&\quad + \sum_{m\geq 2}|\langle m|\hat{A}(\hat{x}(0))|0\rangle|^2 e^{-\tau(E_m-E_0)/\hbar}.
\end{aligned} \tag{2.38}$$

As τ becomes large, only the first two terms contribute, therefore

$$\lim_{\tau_{\max}\to\infty}\langle\hat{A}(\hat{x}(\tau))\hat{A}(\hat{x}(0))\rangle - |\langle 0|\hat{A}|0\rangle|^2 \simeq |\langle 1|\hat{A}|0\rangle|^2 e^{-\tau(E_1-E_0)/\hbar}, \quad \tau \text{ large}. \tag{2.39}$$

We see that this quantity decays exponentially in the Euclidean time. This decay depends directly on the energy gap $E_1 - E_0$, in that manner, this gap can be obtained by calculating the correlation $\langle\hat{A}(\hat{x}(\tau))\hat{A}(\hat{x}(0))\rangle$. This is relevant because $E_1 - E_0$ is related to the mass of a particle in field theory.

All these concepts can be described in bosonic fields by promoting the paths to field configurations

$$\begin{aligned}
x_i &\leftrightarrow \Phi(x), \\
\mathcal{D}[x] = \prod_i dx_i &\leftrightarrow \prod_x d\Phi_x = \mathcal{D}[\Phi], \\
S_E[x] &\leftrightarrow S_E[\Phi(x)],
\end{aligned} \tag{2.40}$$

where $S_E[\Phi(x)] = \int d^d x \left[\frac{1}{2}\partial_\mu\Phi(x)\partial_\mu\Phi(x) + \frac{m^2}{2}\Phi(x)^2\right]$. From now on let us set $\hbar = 1$. In this case, the partition function and the probability of a configuration $[\Phi]$ are

$$Z = \int\mathcal{D}[\Phi]e^{-S_E[\Phi]}, \quad p[\Phi] = \frac{1}{Z}e^{-S_E[\Phi]}. \tag{2.41}$$

The expectation values are calculated through

$$\langle \hat{A}(\tau) \rangle = \frac{1}{Z} \int \mathcal{D}[\Phi] e^{-S_E[\Phi]} \hat{A}[\Phi], \tag{2.42}$$

and the exponential decay of eq. (2.39) now occurs between the sites of the field configuration

$$\langle \Phi_x \Phi_y \rangle - \langle \Phi_x \rangle \langle \Phi_y \rangle \propto \exp\left(-\frac{|x-y|}{\xi}\right), \quad \text{for infinite volume.} \tag{2.43}$$

ξ is known as the *correlation length*, it is the inverse of the energy gap $E_1 - E_0$ and it sets the scale of the system. In actual simulations an infinite volume is impossible, so one often fixes a volume $(aL)^d$ with d the dimension of the system. By imposing periodic boundary conditions, the relation in eq. (2.43) is modified to

$$\langle \Phi_x \Phi_y \rangle - \langle \Phi_x \rangle \langle \Phi_y \rangle \propto \cosh\left(\frac{|x-y| - La/2}{\xi}\right). \tag{2.44}$$

In general, one can compute *n-point functions*

$$\langle \hat{\Phi}(x_1) \cdots \hat{\Phi}(x_n) \rangle = \frac{1}{Z} \int \mathcal{D}[\Phi] \Phi(x_1) \cdots \Phi(x_n) e^{-S_E[\Phi]}. \tag{2.45}$$

When one deals with fermion fields the path integral formulation is different, since they obey anticommutation rules. In order to define the path integral for fermions one has to treat the components of the spinor fields as *Grassmann numbers*, which are anticonmmuting variables. We will give a brief summary of the most important formulas to handle these numbers.

Let us define the Grassmann numbers η_i, $i = 1, 2, \ldots, N$ as a set of variables that satisfy the relation

$$\{\eta_i, \eta_j\} = 0. \tag{2.46}$$

This implies that $\eta_i^2 = 0$ and therefore any function that depends on these numbers can be written as

$$f(\eta) = f + \sum_i f_i \eta_i + \sum_{i,j} f_{ij} \eta_i \eta_j + \sum_{i,j,k} f_{ijk} \eta_i \eta_j \eta_k + \cdots, \tag{2.47}$$

where f, f_i, f_{ij} and f_{ijk} are complex numbers in general. The differentiation rules are

$$\frac{\partial \eta_i}{\partial \eta_j} = \delta_{ij}, \quad \frac{\partial(\eta_i \eta_j)}{\partial \eta_i} = \eta_j, \quad \frac{\partial(\eta_j \eta_i)}{\partial \eta_i} = -\eta_j, \quad i \neq j, \tag{2.48}$$

while the integration rules are

$$\int d\eta_i \, \eta_j = \delta_{ij}, \quad \int d\eta_i d\eta_j \, \eta_i \eta_j = -1, \quad i \neq j. \tag{2.49}$$

In this formalism, the spinor fields $\overline{\psi}$ and ψ are independent fields of N Grassmann components. The following relation can be proved for any arbitrary matrix M of dimension $N \times N$

$$\int \mathcal{D}[\overline{\psi}, \psi] \exp(-\overline{\psi} M \psi) = \det M,$$

$$\mathcal{D}[\overline{\psi}, \psi] = \prod_i d\overline{\psi}_i \, d\psi_i. \tag{2.50}$$

If M is also invertible, then

$$\int \mathcal{D}[\overline{\psi}, \psi] \; \psi_x \overline{\psi}_y \exp(-\overline{\psi} M \psi) = (M)^{-1}_{xy} \det M. \tag{2.51}$$

The partition function, without gauge interaction, is defined as the integral in eq. (2.50), but regarding M as a discretization of the Dirac operator. Further details about the Euclidan path integral and the Grassmann numbers can be found in refs. [19–21].

2.2   Concept of a lattice simulation

The idea of a lattice simulation is to generate field configurations $[\Phi]$, distributed according to the probability distribution in eq. (2.41). One can numerically compute n-point functions of the field configurations and obtain various observables, given by exponential decays, using expressions like eq. (2.44).

In order to obtain configurations with the desired probability distribution, one must rely on Monte Carlo algorithms. These algorithms create *Markov chains*, which are sequences of configurations where each new configuration is generated by considering only the previous one

$$[\Phi_1] \rightarrow [\Phi_2] \rightarrow [\Phi_3] \rightarrow \cdots \tag{2.52}$$

The Markov chains have to be *ergodic*, that is, if one has two arbitrary configurations $[\Phi]$ and $[\Phi']$, then the algorithm has to be able to move from $[\Phi]$ to $[\Phi']$ in a finite number of updates. They also have to satisfy the *detailed balance* condition, which will be explained below.

There are several algorithms to perform the configuration updates. Perhaps the simplest one to explain is the *Metropolis algorithm*, which we describe as a recipe for a scalar field.

1. First of all, one has to create an initial configuration $[\Phi]$. This can be done, for instance, by assigning the same value to all the elements $\Phi_x \in [\Phi]$ (*cold start*) or by the assignation of random values to each site (*hot start*).

2. Then one has to update the configuration. To do so one chooses a site x with the corresponding value Φ_x and calculates $\Phi_x + \epsilon$, with ϵ randomly selected in the interval $(-\epsilon_0, \epsilon_0)$, $\epsilon_0 > 0$. One has the freedom to set ϵ_0, normally it is the same for all the sites x.

3. Now, one considers the transition probability

$$\frac{W([\Phi] \rightarrow [\Phi'])}{W([\Phi'] \rightarrow [\Phi])} = \frac{p[\Phi']}{p[\Phi]} = e^{-\Delta S_E[\Phi, \Phi']}, \;\; \Delta S_E[\Phi, \Phi'] = S_E[\Phi'] - S_E[\Phi], \tag{2.53}$$

   where $W([A] \rightarrow [B])$ is the probability of moving from $[A]$ to $[B]$. The configurations $[\Phi]$ and $[\Phi']$ only differ at the site x, where $\Phi'_x = \Phi_x + \epsilon$. Equation (2.53) defines detailed balance. The Metropolis algorithm implements it as follows: if $\Delta S_E[\Phi, \Phi'] \leq 0$, the new configuration is $[\Phi']$, otherwise, the algorithm accepts the update $[\Phi] \rightarrow [\Phi']$ with a probability $\exp(-\Delta S_E[\Phi, \Phi'])$.

4. The first three steps are repeated for all x on the lattice. When the whole configuration has been updated we say that a *sweep* was performed. It can be proved (see e.g. ref. [22]) that this algorithm generates configurations with the required probability, after a large number of update steps.

Before measuring any type of quantity with the configurations generated through Monte Carlo algorithms, one has to perform a large number of sweeps until they have the correct distribution; this process is called *thermalization*. When the thermalization has been achieved, one can start to measure different observables numerically. For example, let us suppose that one wants to know the value of the field Φ at the site x of the lattice. The first step to do is thermalization, after that one can use "well-behaved"[3] configurations to measure $\langle \Phi_x \rangle$. Between each configuration that is used for measurements, one has to apply several sweeps, because each measurement has to be decorrelated (statistically independent) from the others.

2.3   QED in the continuum and on the lattice

In this section we review relevant features of the discretization of the action in Quantum Electrodynamics, S_{QED}. First, let us discuss some properties of its continuum action.

The first step to build S_{QED} refers to the action of the one flavor free fermion field

$$S_F[\psi, \overline{\psi}] = \int d^4x \, \overline{\psi}(x) \left(i\gamma^\mu \partial_\mu - m \right) \psi(x). \tag{2.54}$$

This equation is written in Minkowski space-time and in units of $\hbar = c = 1$, later we will rewrite everything in Euclidean space. This action is invariant under global U(1) transformations

$$\psi(x) \to \psi'(x) = \Omega\psi(x), \quad \overline{\psi}(x) \to \overline{\psi}\,'(x) = \overline{\psi}(x)\Omega^{-1}, \tag{2.55}$$

because the derivative does not act in Ω. However, if one promotes the global transformation to a local one, *i.e.* $\Omega \to \Omega(x)$, then S_F is not invariant anymore. In order to preserve the invariance one promotes the derivative ∂_μ to a covariant derivative D_μ that obeys

$$D'_\mu \psi'(x) = \Omega(x) D_\mu \psi(x), \tag{2.56}$$

where $\Omega(x) = e^{i\alpha(x)} \in \mathrm{U}(1)$. This holds if

$$D_\mu = \partial_\mu + igA_\mu(x), \tag{2.57}$$

where g is the coupling constant and $A_\mu(x)$ is a four vector potential or *gauge field*, that transforms as

$$A_\mu(x) \to A'_\mu(x) = A_\mu(x) - \frac{1}{g}\partial_\mu\alpha(x). \tag{2.58}$$

It can be checked that these expressions fulfill eq. (2.56),

$$\begin{aligned} D'_\mu \psi' &= \left(\partial_\mu + igA'_\mu \right) \Omega(x)\psi(x) \\ &= i\partial_\mu\alpha \, e^{i\alpha}\psi + e^{i\alpha}\partial_\mu\psi + igA_\mu e^{i\alpha}\psi - i\partial_\mu\alpha \, e^{i\alpha}\psi \\ &= \Omega D_\mu\psi. \end{aligned} \tag{2.59}$$

To finish constructing the QED action, we add the term

$$S_G[A] = -\frac{1}{4}\int d^4x \, F_{\mu\nu}F^{\mu\nu}, \tag{2.60}$$

---

[3]By "well-behaved" we mean that the configurations have the proper probability distribution.

where $F_{\mu\nu}$ is the field strength tensor given by $F_{\mu\nu} = \partial_\mu A_\nu - \partial_\nu A_\mu$. This tensor is invariant under the transformation in eq. (2.58). Therefore the complete QED action is

$$S_{\text{QED}}[\psi, \overline{\psi}, A] = -\frac{1}{4} \int d^4x \, F_{\mu\nu} F^{\mu\nu} + \int d^4x \, \overline{\psi}(i\gamma^\mu D_\mu - m)\psi. \tag{2.61}$$

To transform the action to Euclidean space we have to replace $x^0 \to -ix_4$, thus the integration measure now is $dx_1 dx_2 dx_3 (-idx_4) = -id^4x$. The index 4 is to mark the difference between Euclidean and real time. As a consequence of this change of coordinate, the time derivative and A^0 transform as well

$$\partial^0 \to i\partial_4, \quad A^0 \to iA_4. \tag{2.62}$$

The change of A^0 is because it has to behave as the derivative, due to eq. (2.58). We also introduce the Euclidean γ matrices, whose relation with the Minkowski γ matrices is

$$\gamma_4^E = \gamma^0, \quad \gamma_j^E = -i\gamma^j, \quad \gamma_5^E = \gamma_1^E \gamma_2^E \gamma_3^E \gamma_4^E. \tag{2.63}$$

These matrices satisfy $\{\gamma_\mu^E, \gamma_\nu^E\} = 2\delta_{\mu\nu}\mathbb{I}$, $\mu, \nu = 1, 2, 3, 4$. Then, S_F becomes

$$\begin{aligned}
S_F[\psi, \overline{\psi}, A] &= -i \int d^4x \, \overline{\psi} \left(i\gamma^0 D_0 + i\gamma^j D_j - m \right) \psi \\
&= -i \int d^4x \, \overline{\psi} \left(i\gamma_4^E i D_4 - \gamma_j^E D_j - m \right) \psi \\
&= iS_F^E[\psi, \overline{\psi}, A],
\end{aligned} \tag{2.64}$$

where $S_F^E[\psi, \overline{\psi}, A]$ is defined by

$$S_F^E[\psi, \overline{\psi}, A] = \int d^4x \, \overline{\psi} \left(\gamma_\mu^E D_\mu + m \right) \psi. \tag{2.65}$$

The pure gauge term transforms as

$$S_G[A] = iS_G^E[A], \quad S_G^E[A] = \frac{1}{4} \int d^4x \, F_{\mu\nu} F_{\mu\nu}. \tag{2.66}$$

Therefore, the action is (see ref. [21] for further details)

$$S_{\text{QED}} = iS_{\text{QED}}^E, \quad S_{\text{QED}}^E = \frac{1}{4} \int d^4x \, F_{\mu\nu} F_{\mu\nu} + \int d^4x \, \overline{\psi} \left(\gamma_\mu^E D_\mu + m \right) \psi. \tag{2.67}$$

We proceed to discretize S_{QED}^E by taking into account two important properties:

1. In the continuum limit, the discretization has to yield eq. (2.67).

2. The action on the discretized space has to preserve the gauge invariance, in analogy to the continuum.

Let us consider a four dimensional hypercubic lattice

$$V = \{\vec{n} = (n_1, n_2, n_3, n_4) \mid n_\mu = 0, 1, \ldots, N_\mu - 1; \mu = 1, 2, 3, 4\}, \tag{2.68}$$

where $\vec{n}$ labels a point in the Euclidean space. We will assume that the points are separated by a length a, named lattice constant. The fermion fields are only defined at the sites labeled by $\vec{n}$: $\overline{\psi}(\vec{n})$, $\psi(\vec{n})$. Now, we begin in the same way as in the continuum, that is, by

considering the Euclidean action of a free fermion field, eq. (2.65). A first discretization can be obtained by replacing the continuum derivative by a discrete one,

$$\partial_\mu \psi(x) \rightarrow \frac{\psi(\vec{n} + \hat{\mu}) - \psi(\vec{n} - \hat{\mu})}{2a}, \qquad \text{(central finite differences)}, \qquad (2.69)$$

where $\vec{n} \pm \hat{\mu}$ are the nearest neighbors of the site $\vec{n}$ in the μ-direction. This leads to the following discrete version of S_F^E

$$S_F^E[\overline{\psi}, \psi] = a^4 \sum_{\vec{n}} \overline{\psi}(\vec{n}) \left(\sum_{\mu=1}^4 \gamma_\mu^E \frac{\psi(\vec{n} + \hat{\mu}) - \psi(\vec{n} - \hat{\mu})}{2a} + m\psi(\vec{n}) \right). \qquad (2.70)$$

We would like this action to remain invariant under local transformations $\Omega(\vec{n}) \in \mathrm{U}(1)$,

$$\psi'(\vec{n}) = \Omega(\vec{n})\psi(\vec{n}), \quad \overline{\psi}(\vec{n}) = \overline{\psi}'(\vec{n})\Omega^{-1}(\vec{n}). \qquad (2.71)$$

The mass term in eq. (2.70) does indeed remain invariant, since the transformations $\Omega(\vec{n})$ and $\Omega^{-1}(\vec{n})$ cancel. The discretized derivative, however, does not remain invariant

$$\overline{\psi}'(\vec{n})\psi'(\vec{n} + \hat{\mu}) = \overline{\psi}(\vec{n})\Omega^{-1}(\vec{n})\Omega(\vec{n} + \hat{\mu})\psi(\vec{n} + \hat{\mu}) \neq \overline{\psi}(\vec{n})\psi(\vec{n} + \hat{\mu}). \qquad (2.72)$$

This expression shows that eq. (2.70) is not a proper discretization if we want to preserve local invariance. This forces us to introduce a gauge field in order to preserve the local symmetry, as in the continuum. We introduce a field $U_\mu(\vec{n})$ that transforms as

$$U_\mu \rightarrow U'_\mu(\vec{n}) = \Omega(\vec{n})U_\mu(\vec{n})\Omega^{-1}(\vec{n} + \hat{\mu}). \qquad (2.73)$$

That way, the product $\psi(\vec{n})U_\mu(\vec{n})\psi(\vec{n} + \hat{\mu})$ is locally U(1) invariant

$$\begin{aligned} \psi'(\vec{n})U'_\mu(\vec{n})\psi'(\vec{n} + \hat{\mu}) &= \overline{\psi}(\vec{n})\Omega^{-1}(\vec{n})\Omega(\vec{n})U_\mu(\vec{n})\Omega^{-1}(\vec{n} + \hat{\mu})\Omega(\vec{n} + \hat{\mu})\psi(\vec{n} + \hat{\mu}) \\ &= \psi(\vec{n})U_\mu(\vec{n})\psi(\vec{n} + \hat{\mu}). \end{aligned} \qquad (2.74)$$

In order to preserve the symmetry of the term $\overline{\psi}(\vec{n})\psi(\vec{n} - \hat{\mu})$, we multiply by $U_\mu^\dagger(\vec{n} - \hat{\mu})$, because its transformation rule is

$$\begin{aligned} U'^\dagger_\mu(\vec{n} - \hat{\mu}) &= \left[\Omega(\vec{n} - \hat{\mu})U_\mu(\vec{n} - \hat{\mu})\Omega^{-1}(\vec{n}) \right]^\dagger \\ &= \Omega(\vec{n})U_\mu^\dagger(\vec{n} - \hat{\mu})\Omega^{-1}(\vec{n} - \hat{\mu}). \end{aligned}$$

This implies that

$$\begin{aligned} \overline{\psi}'(\vec{n})U'^\dagger_\mu(\vec{n} - \hat{\mu})\psi'(\vec{n} - \hat{\mu}) &= \overline{\psi}(\vec{n})\Omega^{-1}(\vec{n})\Omega(\vec{n})U_\mu^\dagger(\vec{n} - \hat{\mu})\Omega^{-1}(\vec{n} - \hat{\mu})\Omega(\vec{n} - \hat{\mu})\psi(\vec{n} - \hat{\mu}) \\ &= \overline{\psi}(\vec{n})U_\mu^\dagger(\vec{n} - \hat{\mu})\psi(\vec{n} - \hat{\mu}). \end{aligned} \qquad (2.75)$$

The field $U_\mu(\vec{n})$ provides a link between the sites $\vec{n}$ and $\vec{n} + \hat{\mu}$, for that reason it is known as *link variable*. A schematic representation of these links is shown in figure 2.2.

With the link variables one can discretize the action S_F^E in a gauge invariant way

$$S_F^E[\overline{\psi}, \psi, U] = a^4 \sum_{\vec{n}} \overline{\psi}(\vec{n}) \left(\sum_{\mu=1}^4 \gamma_\mu^E \frac{U_\mu(\vec{n})\psi(\vec{n} + \hat{\mu}) - U_\mu^\dagger(\vec{n} - \hat{\mu})\psi(\vec{n} - \hat{\mu})}{2a} + m\psi(\vec{n}) \right). \qquad (2.76)$$
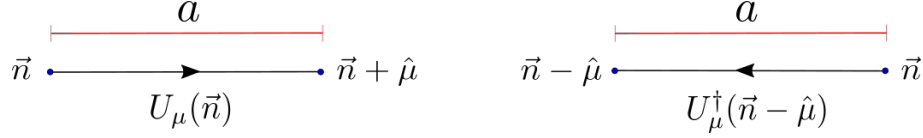
Figure 2.2: The link variables connect nearest neighbors lattice sites: $U_\mu(\vec{n})$ connects $\vec{n}$ with $\vec{n} + \hat{\mu}$, while $U_\mu^\dagger(\vec{n} - \hat{\mu})$ connects $\vec{n}$ with $\vec{n} - \hat{\mu}$.

Up to this point we have not yet related the link variables to continuum QED. In order to do that we are going to revise the analogue of these variables in the continuum. Let us suppose that we want to preserve gauge invariance of the product $\overline{\psi}(x)\psi(y)$, which for arbitrary $\Omega(x)$ and $\Omega(y)$ transforms as

$$\overline{\psi}'(x)\psi'(y) = \overline{\psi}(x)\Omega^{-1}(x)\Omega(y)\psi(y) \neq \overline{\psi}(x)\psi(y), \quad \text{for } x \neq y. \tag{2.77}$$

To maintain the symmetry one uses the so-called *paralell transporter* or *Schwinger line integral*

$$U(x,y) = e^{ig\int_{\mathcal{C}} A_\mu dx_\mu}, \tag{2.78}$$

where $A_\mu(x)$ is the gauge field, g the gauge coupling constant and $\mathcal{C}$ is a curve connecting x and y. The important property of this term is that it transforms under U(1) as

$$U(x,y) \to U'(x,y) = \Omega(x)U(x,y)\Omega^{-1}(y), \tag{2.79}$$

then

$$\begin{aligned}
\overline{\psi}'(x)U'(x,y)\psi'(y) &= \overline{\psi}(x)\Omega^{-1}(x)\Omega(x)U(x,y)\Omega^{-1}(y)\Omega(y)\psi(y) \\
&= \overline{\psi}(x)U(x,y)\psi(y).
\end{aligned} \tag{2.80}$$

Let us consider $|\epsilon_\mu| \ll 1$, thus

$$U(x, x + \epsilon_\mu) \approx e^{ig\epsilon_\mu A_\mu(x)}, \tag{2.81}$$

where we have approximated the line integral by the product of $A_\mu(x)$ with $(x + \epsilon_\mu) - x$. This suggests the following expression for the link variables

$$U_\mu(\vec{n}) = e^{igaA_\mu(\vec{n})}. \tag{2.82}$$

In order to verify that this expression is appropriate, we need to check that in the limit $a \to 0$, the continuum action is recovered. As we will see, eq. (2.82) does this correctly. By expanding the link variables we obtain

$$\begin{aligned}
U_\mu(\vec{n}) &= 1 + igaA_\mu(\vec{n}) + \mathcal{O}(a^2), \\
U_\mu^\dagger(\vec{n} - \hat{\mu}) &= 1 - igaA_\mu(\vec{n} - \hat{\mu}) + \mathcal{O}(a^2).
\end{aligned} \tag{2.83}$$

Substituting in eq. (2.76) yields

$$\begin{aligned}
S_F^E &= a^4 \sum_{\vec{n}} \overline{\psi}(\vec{n}) \left(\sum_{\mu=1}^{4} \gamma_\mu^E \frac{(1 + igaA_\mu(\vec{n}))\psi(\vec{n} + \hat{\mu}) - (1 - igaA_\mu(\vec{n} - \hat{\mu}))\psi(\vec{n} - \hat{\mu})}{2a} \right. \\
&\quad + \left. m\psi(\vec{n}) + \mathcal{O}(a) \right) \\
&= a^4 \sum_{\vec{n}} \overline{\psi}(\vec{n}) \left(\sum_{\mu=1}^{4} \gamma_\mu^E \frac{\psi(\vec{n} + \hat{\mu}) - \psi(\vec{n} - \hat{\mu})}{2a} \right. \\
&\quad + \left. \frac{ig}{2}(A_\mu(\vec{n})\psi(\vec{n} + \hat{\mu}) + A_\mu(\vec{n} - \hat{\mu})\psi(\vec{n} - \hat{\mu})) + m\psi(\vec{n}) + \mathcal{O}(a) \right).
\end{aligned} \tag{2.84}$$

17

The first term in the parentheses is a discrete version of $\gamma_\mu^E \partial_\mu \psi(x)$, while in the second term we will take $\psi(\vec{n} \pm \hat{\mu}) A_\mu(\vec{n} - \hat{\mu}) = \psi(\vec{n}) A_\mu(\vec{n}) + \mathcal{O}(a)$ because the sites are separated by a distance a. Then, eq. (2.84) reduces to

$$S_F^E = a^4 \sum_{\vec{n}} \overline{\psi}(\vec{n}) \left(\sum_{\mu=1}^{4} \gamma_\mu^E \frac{\psi(\vec{n} + \hat{\mu}) - \psi(\vec{n} - \hat{\mu})}{2a} + ig A_\mu(\vec{n}) \psi(\vec{n}) + m\psi(\vec{n}) + \mathcal{O}(a) \right). \quad (2.85)$$

In the limit $a \to 0$ we obtain

$$\begin{aligned} S_F^E &= \int d^4 x \, \overline{\psi}(x) \left[\gamma_\mu^E (\partial_\mu + ig A_\mu(x)) + m \right] \psi(x) \\ &= \int d^4 x \, \overline{\psi}(x) (\gamma_\mu^E D_\mu + m) \psi(x). \end{aligned} \quad (2.86)$$

Therefore, the discretization in eq. (2.76) of S_F^E satisfies the two conditions that we mentioned at the beginning. However, this expression is not completely right for a non-trivial reason that we will revise in the next section[4].

For now let us continue with the discretization of the pure gauge term

$$S_G^E = \frac{1}{4} \int d^4 x \, F_{\mu\nu} F_{\mu\nu}. \quad (2.87)$$

Again we have to make sure that the expression we use is gauge invariant and that in the limit $a \to 0$ eq. (2.87) is recovered. For this purpose, we define a *plaquette variable*

$$U_{\mu\nu}(\vec{n}) \equiv U_\mu(\vec{n}) U_\nu(\vec{n} + \hat{\mu}) U_\mu^\dagger(\vec{n} + \hat{\nu}) U_\nu^\dagger(\vec{n}), \quad (2.88)$$

where $\hat{\mu}$ and $\hat{\nu}$ denote different directions. From eq. (2.82) we see that the link variables are group elements of U(1) and as a result $U_{\mu\nu} \in$ U(1) as well. Geometrically, the plaquette $U_{\mu\nu}(\vec{n})$ connects the sites $\vec{n}, \vec{n} + \hat{\mu}, \vec{n} + \hat{\mu} + \hat{\nu}$ and $\vec{n} + \hat{\nu}$ (see figure 2.3). Besides, by using the following transformation rules

$$\begin{aligned} U_\mu'(\vec{n}) &= \Omega(\vec{n}) U_\mu(\vec{n}) \Omega^{-1}(\vec{n} + \hat{\mu}), \\ U_\nu'(\vec{n} + \hat{\mu}) &= \Omega(\vec{n} + \hat{\mu}) U_\nu(\vec{n} + \hat{\mu}) \Omega^{-1}(\vec{n} + \hat{\mu} + \hat{\nu}), \\ U_\mu'^\dagger(\vec{n} + \hat{\nu}) &= \Omega(\vec{n} + \hat{\mu} + \hat{\nu}) U_\mu^\dagger(\vec{n} + \hat{\nu}) \Omega^{-1}(\vec{n} + \hat{\nu}) \\ U_\nu'^\dagger(\vec{n}) &= \Omega(\vec{n} + \hat{\nu}) U_\nu^\dagger(\vec{n}) \Omega^{-1}(\vec{n}), \end{aligned} \quad (2.89)$$

we can see that the plaquette transforms as

$$U_{\mu\nu}'(\vec{n}) = \Omega(\vec{n}) U_{\mu\nu}(\vec{n}) \Omega^{-1}(\vec{n}). \quad (2.90)$$

Since $\Omega(\vec{n})$ and $U_{\mu\nu}(\vec{n})$ belong to U(1), which is an Abelian group (*i.e.* its elements commute), we conclude that

$$U_{\mu\nu}'(\vec{n}) = U_{\mu\nu}(\vec{n}). \quad (2.91)$$

Hence, the plaquettes are gauge invariant when the transformation group is U(1). Based on this property, we define the *Wilson gauge action* as

$$S_G^E[U] = \frac{1}{g^2} \sum_{\vec{n}} \sum_{\mu<\nu} \left[1 - \frac{1}{2} \left(U_{\mu\nu}(\vec{n}) + U_{\mu\nu}^\dagger(\vec{n}) \right) \right]. \quad (2.92)$$

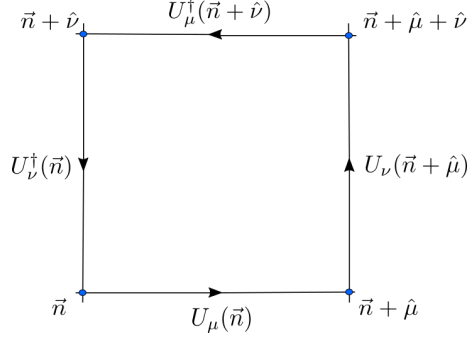[4]Equation (2.76) is known as the *naive fermion action*.

Figure 2.3: Schematic representation of the plaquette variable $U_{\mu\nu}$. It links the points $\vec{n}$, $\vec{n} + \hat{\mu}$, $\vec{n} + \hat{\mu} + \hat{\nu}$ and $\vec{n} + \hat{\nu}$ on the lattice by using the link variables.

Let us verify that this action coincides with eq. (2.87) in the limit $a \to 0$. We can substitute eq. (2.82) in the definition of the plaquette

$$U_{\mu\nu}(\vec{n}) = e^{igaA_\mu(\vec{n})}e^{igaA_\nu(\vec{n}+\hat{\mu})}e^{-igaA_\mu(\vec{n}+\hat{\nu})}e^{-igaA_\nu(\vec{n})}. \tag{2.93}$$

The exponents can be rearranged

$$
\begin{aligned}
U_{\mu\nu}(\vec{n}) &= e^{iga^2\left(\frac{A_\nu(\vec{n}+\hat{\mu})-A_\nu(\vec{n})}{a} - \frac{A_\mu(\vec{n}+\hat{\nu})-A_\mu(\vec{n})}{a}\right)} \\
&= e^{iga^2(\partial_\mu A_\nu(\vec{n})-\partial_\nu A_\mu(\vec{n})+\mathcal{O}(a))} \\
&= e^{iga^2(F_{\mu\nu}(\vec{n})+\mathcal{O}(a))}. \tag{2.94}
\end{aligned}
$$

Then

$$
\begin{aligned}
U_{\mu\nu}(\vec{n}) + U_{\mu\nu}^\dagger(\vec{n}) &= 2 - g^2a^4(F_{\mu\nu}(\vec{n})+\mathcal{O}(a))^2 + g^4a^8(F_{\mu\nu}+\mathcal{O}(a))^4 + \cdots \\
&= 2 - g^2a^4 F_{\mu\nu}(\vec{n})F_{\mu\nu}(\vec{n}) + \mathcal{O}(a^5) \tag{2.95}
\end{aligned}
$$

Substituting in eq. (2.92) yields

$$
\begin{aligned}
S_G^E[U] &= \frac{1}{g^2}\sum_{\vec{n}}\sum_{\mu<\nu}\frac{g^2a^4}{2}F_{\mu\nu}(\vec{n})F_{\mu\nu}(\vec{n}) + \mathcal{O}(a^5) \\
&= \frac{1}{4}a^4\sum_{\vec{n}}\sum_{\mu,\nu}F_{\mu\nu}(\vec{n})F_{\mu\nu}(\vec{n}) + \mathcal{O}(a^5). \tag{2.96}
\end{aligned}
$$

The factor of 2 comes from the fact that on the right-hand side $F_{\mu\nu}$ is antisymmetric and that the sum extends over all possible values of μ and ν, not only those where $\mu < \nu$. When $a \to 0$ the Wilson action converges to the continuum action (2.87). Finally, the complete naive discretization of the Euclidean QED action takes the form

$$
\begin{aligned}
S_{\text{QED}}^E[\psi, \overline{\psi}, U] &= a^4\sum_{\vec{n}}\overline{\psi}(\vec{n})\left(\sum_{\mu=1}^4\gamma_\mu^E\frac{U_\mu(\vec{n})\psi(\vec{n}+\hat{\mu}) - U_\mu^\dagger(\vec{n}-\hat{\mu})\psi(\vec{n}-\hat{\mu})}{2a} + m\psi(\vec{n})\right) \\
&\quad + \frac{1}{g^2}\sum_{\vec{n}}\sum_{\mu<\nu}\left[1 - \frac{1}{2}\left(U_{\mu\nu}(\vec{n}) + U_{\mu\nu}^\dagger(\vec{n})\right)\right]. \tag{2.97}
\end{aligned}
$$

2.4   Wilson fermions

As we mentioned in the previous section, the discretization of the fermion action given in eq. (2.76) is not fully correct. To see why, let us rewrite it as follows

$$S_F^E[\psi, \overline{\psi}, U] = a^4 \sum_{\vec{n}, \vec{m}} \overline{\psi}(\vec{n}) D(\vec{n}, \vec{m}) \psi(\vec{m}),$$

$$D(\vec{n}, \vec{m}) = \sum_{\mu=1}^{4} \gamma_\mu^E \frac{U_\mu(\vec{n}) \delta_{\vec{n}+\hat{\mu}, \vec{m}} - U_\mu^\dagger(\vec{n}-\hat{\mu}) \delta_{\vec{n}-\hat{\mu}, \vec{m}}}{2a} + m \delta_{\vec{n}, \vec{m}}, \tag{2.98}$$

where $D(\vec{n}, \vec{m})$ is the Dirac operator. Let us suppose for the moment that we are working in the chiral limit, *i.e.* $m = 0$ and that there are no gauge fields. We will compute the inverse of the Dirac operator $D^{-1}(\vec{n}, \vec{m})$. To do so we use the Fourier transform, defined for an arbitrary function $f(\vec{n})$ as

$$\tilde{f}(\vec{p}) = \frac{1}{\sqrt{|V|}} \sum_{\vec{n}} f(\vec{n}) e^{-i\vec{p} \cdot \vec{n} a}, \qquad |V| \equiv N_1 N_2 N_3 N_4. \tag{2.99}$$

The inverse transformation is

$$\tilde{f}(\vec{n}) = \frac{1}{\sqrt{|V|}} \sum_{\vec{p}} \tilde{f}(\vec{p}) e^{i\vec{p} \cdot \vec{n} a},$$

$$\tilde{V} = \left\{ \vec{p} = (p_1, p_2, p_3, p_4) \mid p_\mu = \frac{2\pi}{aN_\mu} k_\mu, \ k_\mu = -\frac{N_\mu}{2} + 1, -\frac{N_\mu}{2} + 2, \dots, \frac{N_\mu}{2} \right\}. \tag{2.100}$$

Then, if one transforms the fermion fields the Dirac operator takes the form

$$\begin{aligned}
\tilde{D}(\vec{p}, \vec{q}) &= \frac{1}{|V|} \sum_{\vec{n}, \vec{m}} e^{-i\vec{p} \cdot \vec{n} a} D(\vec{n}, \vec{m}) e^{i\vec{q} \cdot \vec{m} a} \\
&= \frac{1}{|V|} \sum_{\vec{n}} e^{-i(\vec{p}-\vec{q}) \cdot \vec{n} a} \sum_{\mu=1}^{4} \gamma_\mu^E \left(\frac{e^{i\vec{q} \cdot \hat{\mu} a} - e^{-i\vec{q} \cdot \hat{\mu} a}}{2a} \right) \\
&= \frac{1}{|V|} \sum_{\vec{n}} e^{i(\vec{p}-\vec{q}) \cdot \vec{n} a} \sum_{\mu=1}^{4} \left(\gamma_\mu^E \frac{i}{a} \sin(q_\mu a) \right).
\end{aligned} \tag{2.101}$$

The first sum can be expressed as

$$\frac{1}{|V|} \sum_{\vec{n}} e^{i(\vec{p}-\vec{q}) \cdot \vec{n} a} = \prod_{\nu=1}^{4} \frac{1}{N_\nu} \sum_{n_\nu=0}^{N_\nu-1} e^{i(p_\nu - q_\nu) n_\nu a}, \tag{2.102}$$

where $p_\nu = 2\pi k_\nu/(aN_\nu)$ and $q_\nu = 2\pi k_\nu'/(aN_\nu)$. When $k_\nu = k_\nu'$ the product is equal to one. Now let us analyze its value when $k_\nu \neq k_\nu'$,

$$\begin{aligned}
\frac{1}{N_\nu} \sum_{n_\nu=0}^{N_\nu-1} e^{i(p_\nu - q_\nu) n_\nu a} &= \frac{1}{N_\nu} \sum_{n_\nu=0}^{N_\nu-1} \left(e^{i(p_\nu - q_\nu) a} \right)^{n_\nu} \\
&= \frac{1}{N_\nu} \frac{1 - e^{i(p_\nu - q_\nu) N_\nu a}}{1 - e^{i(p_\nu - q_\nu) a}} \\
&= \frac{1}{N_\nu} \frac{1 - e^{i 2\pi (k_\nu - k_\nu')}}{1 - e^{i 2\pi (k_\nu - k_\nu')/N_\nu}}.
\end{aligned} \tag{2.103}$$

Since $k_\nu - k'_\nu \in \mathbb{Z}$, the numerator vanishes. Hence

$$\frac{1}{|V|} \sum_{\vec{n}} e^{i(\vec{p}-\vec{q})\cdot\vec{n}a} = \delta_{p_1,q_1}\delta_{p_2,q_2}\delta_{p_3,q_3}\delta_{p_4,q_4} = \delta_{\vec{p},\vec{q}}. \tag{2.104}$$

Substituting in eq. (2.101) yields

$$\tilde{D}(\vec{p},\vec{q}) = \delta_{\vec{p},\vec{q}}\tilde{D}(\vec{p}), \quad \tilde{D}(\vec{p}) = \frac{i}{a}\sum_{\mu=1}^{4}\left(\gamma_\mu^E \sin(p_\mu a)\right). \tag{2.105}$$

In order to calculate $D^{-1}(\vec{n},\vec{m})$ we use the inverse transformation

$$D^{-1}(\vec{n},\vec{m}) = \frac{1}{|V|}\sum_{\vec{p}}\tilde{D}^{-1}(\vec{p})e^{i\vec{p}\cdot(\vec{n}-\vec{m})a}. \tag{2.106}$$

To find $\tilde{D}^{-1}(\vec{p})$ we multiply

$$-\tilde{D}(\vec{p})\tilde{D}(\vec{p}) = \frac{1}{a^2}\left[\sum_{\mu=1}^{4}\left(\gamma_\mu^E\right)^2 \sin^2(p_\mu a) + \sum_{\mu\neq\nu}\gamma_\mu^E\gamma_\nu^E \sin(p_\mu a)\sin(p_\nu a)\right]. \tag{2.107}$$

Since $\{\gamma_\mu^E,\gamma_\nu^E\} = 2\delta_{\mu\nu}\mathbb{I}$, the product reduces to

$$-\tilde{D}(\vec{p})\tilde{D}(\vec{p}) = \frac{1}{a^2}\sum_{\mu=1}^{4}\sin^2(p_\mu a), \tag{2.108}$$

thus

$$\tilde{D}^{-1}(\vec{p}) = \frac{\frac{-i}{a}\sum_\mu \gamma_\mu^E \sin(p_\mu a)}{\frac{1}{a^2}\sum_\mu \sin^2(p_\mu a)}. \tag{2.109}$$

As a consequence of the Fourier transform, the momentum components are in $(-\pi/a, \pi/a]$ (first Brillouin zone). When $a \to 0$ one obtains the propagator in the continuum

$$\tilde{D}^{-1}(\vec{p}) = \frac{-i\sum_\mu \gamma_\mu^E p_\mu}{p^2}. \tag{2.110}$$

We see that in the continuum there is only one pole at $\vec{p} = \vec{0}$; this is correct since the poles of the propagator represent particles and we are dealing with just one fermion. On the other hand, the discrete version has poles at $\vec{p} = \vec{0}$ and when each component of $\vec{p}$ is either 0 or π/a. Thus the discrete version has 16 poles, with 15 of them being unphysical[5]. This is known as the *fermion doubling* problem and shows that the naive discretization that we gave in the last section is wrong, even though it is gauge invariant and converges to the right expression in the continuum limit. A way of solving this issue was proposed by Kenneth Wilson [1]: the idea is modifying the Dirac operator by adding a term that eliminates the unwanted particles, but that vanishes when $a \to 0$. The term he adds is called the Wilson term and it is a discretization of the Laplace operator multiplied by $-a/2$

$$W = -\frac{a}{2}\sum_{\mu=1}^{4}\frac{\delta_{\vec{n}+\hat{\mu},\vec{m}} - 2\delta_{\vec{n},\vec{m}} + \delta_{\vec{n}-\hat{\mu},\vec{m}}}{a^2}. \tag{2.111}$$

---

[5]In d dimensions $2^d - 1$ unwanted fermions appear.

The sum is just a discrete version of $\partial_\mu \partial_\mu$, so the full term convergences to zero when $a \to 0$. In the case with gauge fields, to preserve the gauge invariance we have to insert the link variables

$$W = -\frac{a}{2} \sum_{\mu=1}^{4} \frac{U_\mu(\vec{n})\delta_{\vec{n}+\hat{\mu},\vec{m}} - 2\delta_{\vec{n},\vec{m}} + U_\mu^\dagger(\vec{n} - \hat{\mu})\delta_{\vec{n}-\hat{\mu},\vec{m}}}{a^2}. \tag{2.112}$$

Adding this term to the Dirac operator yields

$$D_{\mathrm{W}} = \left(m - \frac{4}{a}\right)\delta_{\vec{n},\vec{m}} - \frac{1}{2a}\sum_{\mu=1}^{4}\left[(1 - \gamma_\mu^E)U_\mu(\vec{n})\delta_{\vec{n}+\hat{\mu},\vec{m}} + (1 - \gamma_\mu^E)U_\mu^\dagger(\vec{n} - \hat{\mu})\delta_{\vec{n}-\hat{\mu},\vec{m}}\right]. \tag{2.113}$$

This version of the Dirac operator eliminates the fermion doublers, by sending them to a cutoff energy of $O(1/a)$. The fermions simulated with this formulation are known as *Wilson fermions* and they were implemented in a Hybrid Monte Carlo (HMC) algorithm to obtain results with the Schwinger model (see Appendix A for a discussion of this algorithm with a scalar field). Unfortunately, there is one problem with this formulation: it breaks chiral symmetry explicitly, even when $m = 0$. This can be seen if one substitutes the chiral transformations

$$\overline{\psi}(\vec{n}) \to \overline{\psi}'(\vec{n}) = \overline{\psi}(\vec{n})e^{i\alpha\gamma_5}, \ \ \psi(\vec{n}) \to \psi'(\vec{n}) = e^{i\alpha\gamma_5}\psi(\vec{n}), \ \ \alpha \in \mathbb{R} \tag{2.114}$$

and considers W when multiplied by the fermion fields

$$\overline{\psi}'(\vec{n})W\psi'(\vec{m}) = \overline{\psi}(\vec{n})We^{i\alpha\gamma_5^E}e^{i\alpha\gamma_5^E}\psi(\vec{m}) \neq \overline{\psi}(\vec{n})W\psi(\vec{m}). \tag{2.115}$$

If it is intact, the chiral symmetry prevents additive mass renormalization. This is not the case for Wilson fermions, so additive mass renormalization sets in, and approaching the chiral limit requires a fine tuning of the bare fermion mass. The expectation values can be calculated through

$$\langle \hat{A} \rangle = \frac{1}{Z}\int \mathcal{D}[\overline{\psi},\psi]\mathcal{D}[U]e^{-S_{\mathrm{QED}}^E[\psi,\overline{\psi},U]}A[\psi,\overline{\psi},U],$$

$$Z = \int \mathcal{D}[\overline{\psi},\psi]\mathcal{D}[U]e^{-S_{\mathrm{QED}}^E[\psi,\overline{\psi},U]},$$

$$\mathcal{D}[U] = \prod_{\vec{n}\in L}\prod_{\mu=1}^{4} dU_\mu(\vec{n}) \quad \text{(Haar measure)}. \tag{2.116}$$

There are more ways of discretizing $D(\vec{n},\vec{m})$ that deal with the doubling problem and they introduce other kind of fermions, such as *staggered fermions, Ginsparg-Wilson fermions*, etc. Reviews of those formulations can be found in refs. [20, 23], however they will not be used in this work.

To finish this section, we make a comment about the scale fixing in the lattice framework. Usually, the discretized Euclidean action of the Schwinger model is rewritten in terms of the dimensionless parameter

$$\beta \equiv \frac{1}{(ag)^2}, \tag{2.117}$$

where a is the lattice constant and g the gauge coupling. One can approximate the continuum limit by making β larger. For that reason, it is very common to set $a = 1$ and to vary the separation between the lattice sites by using the gauge coupling as a free parameter. This kind of units are known as *lattice units* and we will use them to present our results.

2.5   QCD on the lattice

In this section we extend the ideas of the discretization of the QED action to QCD, which is a non-Abelian gauge theory. We begin by considering the Euclidean action

$$\int d^4x\, \overline{\psi}(\gamma_\mu^E D_\mu + m)\psi + \frac{1}{4}\int d^4x\, \text{tr}\left[G_{\mu\nu}(x)G_{\mu\nu}(x)\right], \tag{2.118}$$

where $G_{\mu\nu} = \partial_\mu A_\nu - \partial_\nu A_\mu + ig[A_\mu, A_\nu]$ is the gluon field strength tensor and $A_\mu(x) \in \text{SU}(3)$. In order to assure invariance under local SU(3) transformations, the covariant derivative must satisfy

$$D'_\mu \psi'(x) = \Omega(x)D_\mu \psi(x), \quad \Omega(x) \in \text{SU}(3), \tag{2.119}$$

which is accomplished if A_μ transforms as

$$A_\mu(x) \rightarrow A'_\mu(x) = \Omega(x)A_\mu(x)\Omega^{-1}(x) - \frac{i}{g}\Omega(x)\partial_\mu\Omega^{-1}(x). \tag{2.120}$$

We verify this by substitution

$$
\begin{aligned}
D'_\mu \psi' &= \left(\partial_\mu + igA'_\mu\right)\Omega(x)\psi(x) \\
&= \partial_\mu\Omega\psi + \Omega\partial_\mu\psi + ig\Omega A_\mu\psi + \Omega\partial_\mu\Omega^{-1}\Omega\psi \\
&= \partial_\mu\Omega\psi + \Omega\partial_\mu\psi + ig\Omega A_\mu\psi + \Omega\partial_\mu(\Omega^{-1}\Omega)\psi - \Omega\Omega^{-1}\partial_\mu\Omega\psi \\
&= \Omega(\partial_\mu\psi + igA_\mu\psi) \\
&= \Omega D_\mu\psi.
\end{aligned} \tag{2.121}
$$

The discretization of the Dirac operator is the same as in QED, *i.e.* the discretization without the fermion doublers corresponds to eq. (2.113). The link variables definition is analogous to eq. (2.82). Also, the plaquette variables are defined as in eq. (2.88), but in this case one has to preserve the order of the operations because the link variables are matrices. Even though these definitions are analogous, the construction of the gauge action is different, since the plaquettes are not gauge invariant due to the non-commutativity of the link variables. Still, we can construct a gauge invariant Wilson action using the trace operator as follows

$$S_G^E[U] = \frac{3}{g^2}\sum_{\vec{n}\in L}\sum_{\mu<\nu}\left(1 - \frac{1}{3}\text{Re tr}\left[U_{\mu\nu}(\vec{n})\right]\right), \quad U_{\mu\nu} \in \text{SU}(3). \tag{2.122}$$

Let us verify that this action converges to the correct expression in the continuum. First we simplify the plaquettes expression

$$U_{\mu\nu}(\vec{n}) = e^{igaA_\mu(\vec{n})}e^{igaA_\nu(\vec{n}+\hat{\mu})}e^{-igaA_\mu(\vec{n}+\hat{\nu})}e^{-igaA_\nu(\vec{n})}, \tag{2.123}$$

by using the Baker-Campbell-Hausdorff formula, which states that for two matrices A and B

$$e^{aA}e^{aB} = e^{aA+aB+\frac{a^2}{2}[A,B]+\mathcal{O}(a^3)}. \tag{2.124}$$

If we apply the formula to (2.123) we obtain

$$U_{\mu\nu}(\vec{n}) = \exp\Bigg\{iga\bigg(A_\mu(\vec{n}) + A_\nu(\vec{n}+\hat{\mu}) - A_\mu(\vec{n}+\hat{\nu}) - A_\nu(\vec{n})\bigg) - \frac{g^2a^2}{2}[A_\mu(\vec{n}), A_\nu(\vec{n}+\hat{\mu})]$$

$$+\frac{g^2a^2}{2}[A_\mu(\vec{n}), A_\mu(\vec{n}+\hat{\nu})] + \frac{g^2a^2}{2}[A_\nu(\vec{n}+\hat{\mu}), A_\mu(\vec{n}+\hat{\nu})] + \frac{g^2a^2}{2}[A_\mu(\vec{n}), A_\nu(\vec{n})]$$

$$+\frac{g^2a^2}{2}[A_\nu(\vec{n}+\hat{\mu}), A_\nu(\vec{n})] - \frac{g^2a^2}{2}[A_\mu(\vec{n}+\hat{\nu}), A_\nu(\vec{n})] + \mathcal{O}(a^3)\Bigg\}. \tag{2.125}$$

Now, if we use a Taylor expansion for the field

$$A_\nu(\vec{n} + \hat{\mu}) = A_\nu(\vec{n}) + a\,\partial_\mu A_\nu(\vec{n}) + \mathcal{O}(a^2), \tag{2.126}$$

we reduce eq. (2.125) to

$$
\begin{aligned}
U_{\mu\nu}(\vec{n}) &= e^{iga^2(\partial_\mu A_\nu(\vec{n}) - \partial_\nu A_\mu(\vec{n}) + ig[A_\mu(\vec{n}), A_\nu(\vec{n})]) + \mathcal{O}(a^3)} \\
&= e^{iga^2(G_{\mu\nu}(\vec{n}) + \mathcal{O}(a))}.
\end{aligned} \tag{2.127}
$$

Then

$$\mathrm{Re}\ \mathrm{tr}[U_{\mu\nu}(\vec{n})] = \mathrm{tr}\left[\mathbb{I} - \frac{a^4 g^2}{2} G_{\mu\nu}(\vec{n}) G_{\mu\nu}(\vec{n})\right] + \mathcal{O}(a^5). \tag{2.128}$$

Substituting in eq. (2.122) yields

$$
\begin{aligned}
S_G^E[U] &= \frac{3}{g^2} \sum_{\vec{n} \in L} \sum_{\mu < \nu} \frac{a^4 g^2}{6}\, \mathrm{tr}\left[G_{\mu\nu}(\vec{n}) G_{\mu\nu}(\vec{n})\right] + \mathcal{O}(a^5) \\
&= \frac{a^4}{4} \sum_{\vec{n} \in L} \sum_{\mu,\nu} \mathrm{tr}\left[G_{\mu\nu}(\vec{n}) G_{\mu\nu}(\vec{n})\right] + \mathcal{O}(a^5).
\end{aligned} \tag{2.129}
$$

In the limit $a \to 0$, we obtain the gauge action

$$S_G^E = \frac{1}{4} \int d^4x\ \mathrm{tr}\left[G_{\mu\nu}(x) G_{\mu\nu}(x)\right]. \tag{2.130}$$

Deeper discussions of lattice QCD can be revised in refs. [20, 21, 24].

Chapter 3

Hosotani's approach to the Schwinger model

In the 1990s, Yukio Hosotani *et al.* published several studies of the massive Schwinger model for an arbitrary number of $N > 1$ flavors at finite temperature T, where they reduced the massive model to a quantum mechanical system of $N-1$ degrees of freedom [16,25–27]. This allowed them to derive analytic predictions for the boson masses that appear, and for the chiral condensate. In the massless N flavor model, it is known that a boson mass $\mu = \sqrt{Ng^2/\pi}$ appears [13]. In the Schwinger model with degenerate non-zero fermion mass the approach by Hosotani gives as a result N bosons, $N-1$ of them with the same mass μ_2 and one with mass $\mu_1 > \mu_2$. In the limit $m \to 0$ one obtains $\mu_2 \to 0$ and $\mu_1 \to \mu$ [26,27].

We will review the most important equations of this approach without complete derivations, together with a numerical solution for the predictions of the boson masses and the chiral condensate in the two flavor model at finite temperature. The reliability of these solutions is limited to $m \ll \mu$, as explained in Sections 6 and 8 of ref. [27].

3.1 Reduction to a quantum mechanical system

The QED Lagrangian for the N flavor Schwinger model in Euclidean space is given by

$$\mathcal{L} = \frac{1}{4} F_{\mu\nu} F_{\mu\nu} + \sum_{f=1}^{N} \overline{\psi}_f \left[\gamma_\mu^E \left(\partial_\mu + ig A_\mu \right) + m_f \right] \psi_f. \tag{3.1}$$

The index f denotes the flavor. We consider degenerate fermion masses, that is $m_f \equiv m$. The idea is to map the model onto a circumference of length L_t and to impose the following boundary condition on the fermion fields and the gauge field

$$\psi_f \left(\tau + \frac{1}{T}, x \right) = -e^{2\pi i \alpha_f} \psi_f(\tau, x),$$

$$A_\mu \left(\tau + \frac{1}{T}, x \right) = A_\mu \left(\tau, x \right), \tag{3.2}$$

where α_f is a phase factor and $T = 1/L_t$ denotes the temperature. By setting $\alpha_f = 0$ it is possible to relate the model on the circle with the finite temperature Schwinger model.

Next one uses the *bosonization method* to reduce the model to a quantum mechanical system of $N-1$ degrees of freedom. The main idea is to write the fields in terms of bosonic operators that obey certain commutation relations, see e.g. refs. [16,27]. However,

those steps are rather tedious and here we only review the resulting formulation. After bosonization, the eigenvalue equation

$$\hat{H}\,|\Phi_0\rangle = E_0\,|\Phi_0\rangle, \tag{3.3}$$

where $\hat{H}$ is the Hamilton operator, $|\Phi_0\rangle$ is the vacuum state and E_0 its energy, is reduced to

$$[-\triangle_\varphi + \kappa_0 F_N(\varphi_1, ..., \varphi_N)]\,g(\varphi_1, ..., \varphi_N) = \epsilon g(\varphi_1, ..., \varphi_N),$$

$$\kappa_0 = \frac{N}{\pi(N-1)} m L_t \overline{B} e^{-\pi/(\mu N L_t)}, \quad F_N(\varphi_1, ..., \varphi_N) = -\sum_{f=1}^{N} \cos\varphi_f,$$

$$\overline{B} = [B(\mu_1 L_t)]^{1/N} [B(\mu_2 L_t)]^{1-1/N}, \quad \epsilon = \frac{N L_t E_0}{2\pi} + \frac{\pi N^2}{12},$$

$$B(z) = \frac{z}{4\pi} \exp\left[\gamma + \frac{\pi}{z} - 2\int_1^\infty \frac{du}{(e^{uz} - 1)\sqrt{u^2 - 1}}\right]. \tag{3.4}$$

$\gamma = 0.57721566490...$ is the Euler-Mascheroni constant. The angular variables φ_f are constrained by

$$\varphi_N = \theta - \sum_{f=1}^{N-1} \varphi_f, \tag{3.5}$$

where θ is the vacuum angle, which can be restricted to $(-\pi, \pi]$. It coincides with the vacuum angle that we introduced in Section 1.2 in a different form. $\triangle_\varphi$ is the Laplacian of the system, given by

$$\triangle_\varphi = \sum_{f=1}^{N-1}\left(\frac{\partial}{\partial\varphi_f} - i\beta_f\right)^2 - \frac{2}{N-1}\sum_{f<f'}^{N-1}\left(\frac{\partial}{\partial\varphi_f} - i\beta_f\right)\left(\frac{\partial}{\partial\varphi_{f'}} - i\beta_{f'}\right)$$

$$\beta_f = \alpha_f - \alpha_N. \tag{3.6}$$

The function $B(z)$ has no direct physical meaning, but it appears in the equations. We show its behavior in figure 3.1. ϵ has to be determined together with $g(\varphi_1, ..., \varphi_N)$, μ_1 and μ_2 by solving the first line of eqs. (3.4) and other equations below. We are interested in a solution for μ_1 and μ_2.

The first line in eq. (3.4) is an eigenvalue problem for a system of $N - 1$ degrees of freedom, due to the restriction (3.5). We simplify eqs. (3.4) for $N = 2$. The Laplacian is now given by

$$\triangle_\varphi = \left(\frac{d}{d\varphi_1} + i\delta\alpha\right)^2 = -\left(i\frac{d}{d\varphi_1} - \delta\alpha\right)^2, \tag{3.7}$$

with $\delta\alpha = \alpha_2 - \alpha_1$. In virtue of the constraint (3.5), the function $F_2(\varphi_1, \varphi_2)$ is expressed as

$$F_2(\varphi_1) = -\cos(\varphi_1) - \cos(\varphi_1 - \theta) = -2\cos\frac{\theta}{2}\cos\left(\varphi_1 - \frac{\theta}{2}\right). \tag{3.8}$$

Substituting $\triangle_\varphi$ and $F_2(\varphi_1)$ in the first line of eqs. (3.4) yields

$$\left[\left(i\frac{d}{d\varphi_1} - \delta\alpha\right)^2 - 2\kappa_0 \cos\frac{\theta}{2}\cos\left(\varphi_1 - \frac{\theta}{2}\right)\right]g(\varphi_1) = \epsilon g(\varphi_1). \tag{3.9}$$

Let us define

$$\kappa \equiv 2\kappa_0 \cos\frac{\theta}{2} = \frac{4}{\pi} m L_t \cos\frac{\theta}{2}\,[B(\mu_1 L_t)B(\mu_2 L_t)]^{1/2}\,e^{-\pi/(2\mu L_t)}, \tag{3.10}$$
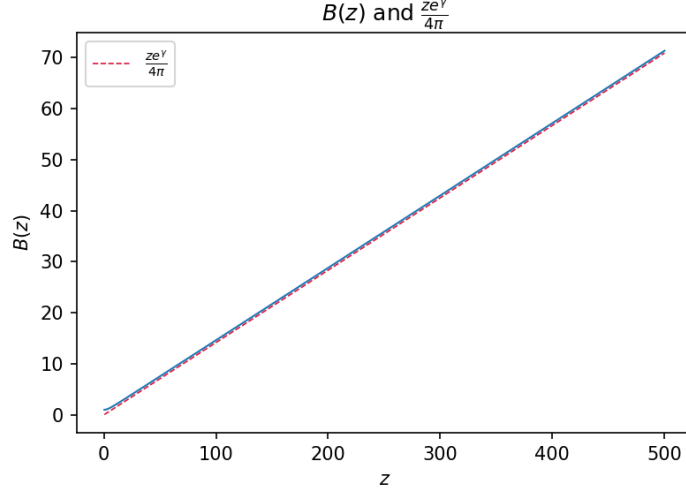
Figure 3.1: $B(z)$ defined in eq. (3.4). For large z, $B(z) \approx \frac{ze^{\gamma}}{4\pi}$.

thus, eq. (3.9) can be written as

$$\left[\left(i\frac{d}{d\varphi_1} - \delta\alpha \right)^2 - \kappa \cos\left(\varphi_1 - \frac{\theta}{2} \right) \right] g(\varphi_1) = \epsilon g(\varphi_1). \tag{3.11}$$

Finally, we substitute $\varphi = \varphi_1 - \frac{\theta}{2}$ and define $f(\varphi) = g(\varphi + \frac{\theta}{2})$. Then, eq. (3.11) takes the form

$$\left[\left(i\frac{d}{d\varphi} - \delta\alpha \right)^2 - \kappa \cos\varphi \right] f(\varphi) = \epsilon f(\varphi). \tag{3.12}$$

In refs. [16, 25–27], it is shown that the masses μ_1, μ_2 and the chiral condensate $-\langle \overline{\psi}\psi \rangle_\theta$ can be obtained through the following equations, when $m \ll \mu$,

$$\mu_2^2 = \frac{2\pi^2}{L_t^2}\kappa \int_{-\pi}^{\pi} d\varphi \cos\varphi\, |f_0(\varphi)|^2,$$

$$\mu_1^2 = \mu^2 + \mu_2^2,$$

$$\langle \overline{\psi}\psi \rangle_\theta = -\frac{\mu_2^2}{4\pi m}, \tag{3.13}$$

where $f_0(\varphi)$ denotes the ground state function of eq. (3.12), which obeys $f_0(\varphi+2\pi) = f_0(\varphi)$ and has to be normalized.

Now we need to find a solution to eq. (3.12) in order to calculate μ_2; however, κ also depends on μ_2. This means that eqs. (3.10), (3.12) and (3.13) must be solved in a self-consistent way. Analytically this is hardly possible for general values, but it can be done numerically. Still, there is one limiting case that is worth analyzing, because it will provide a cross-check with the numerical solutions of the next section. Let us set $\delta\alpha = 0$. We see in figure 3.1 that $B(z)$ is monotonically increasing, so if we restrict ourselves to the case $\cos(\theta/2) \geq 0$, for $\mu L_t \gg 1$ we have $\kappa \gg 1$. According to ref. [26], this allows us to approximate[1] $\cos\varphi \approx 1 - \frac{\varphi^2}{2}$ and eq. (3.12) reduces to

$$-\frac{d^2f}{d\varphi^2} - \kappa\left(1 - \frac{\varphi^2}{2} \right) f = \epsilon f. \tag{3.14}$$

---

[1]In Hosotani's work this approximation is not clearly argued, but it is necessary in order to obtain a limiting case that is already known in the literature, as we mention at the end of this section.

With the ansatz $f(\varphi) = e^{-b\varphi^2}$ we obtain

$$-\frac{d^2 f}{d\varphi^2} - \kappa \left(1 - \frac{\varphi^2}{2}\right) f = \left(2b - 4b^2\varphi^2 - \kappa + \kappa\frac{\varphi^2}{2}\right) e^{-b\varphi^2}, \qquad (3.15)$$

then

$$\epsilon = 2b - 4b^2\varphi^2 - \kappa + \kappa\frac{\varphi^2}{2}. \qquad (3.16)$$

Let us remember that ϵ is a constant (see for instance the third line of eq. (3.4)), so it cannot depend on φ, which forces us to fix $b = \sqrt{\kappa/8}$. As a result, the normalized solution to eq. (3.12), under the previous assumptions, is

$$f(\varphi) = \frac{e^{-\sqrt{\frac{\kappa}{8}}\varphi^2}}{\int_{-\pi}^{\pi} d\varphi |e^{-\sqrt{\frac{\kappa}{8}}\varphi^2}|^2}. \qquad (3.17)$$

To calculate μ_2 we denote

$$I \equiv \frac{\int_{-\pi}^{\pi} d\varphi \left(1 - \frac{\varphi^2}{2}\right) e^{-\sqrt{\frac{\kappa}{2}}\varphi^2}}{\int_{-\pi}^{\pi} d\varphi \, e^{-\sqrt{\frac{\kappa}{2}}\varphi^2}}, \qquad (3.18)$$

in that manner we can rewrite the first line of eqs. (3.13) as

$$\mu_2^2 = \frac{2\pi^2}{L_t^2}\kappa I = \frac{8}{L_t^2\pi}mL_t \cos\frac{\theta}{2}\left[B(\mu_2 L_t)B(\mu_1 L_t)\right]^{1/2} e^{-\pi/(2\mu L_t)}I. \qquad (3.19)$$

Since we consider $\mu L_t \gg 1$ then $e^{-\pi/(2\mu L_t)} \approx 1$. We are also able to obtain a simpler form of the function $B(z)$ in eq. (3.4). We see directly from its expression that if $z \gg 1$ the exponential term in the denominator of the integrand vanishes. Thus the integral is suppressed, together with the factor π/z. Then

$$B(z) \approx \frac{ze^{\gamma}}{4\pi}, \qquad z \gg 1, \qquad (3.20)$$

see figure 3.1. With this result the value for μ_2 is approximately

$$\begin{aligned}
\mu_2^2 &\approx \frac{8\pi^2}{L_t^2\pi}mL_t \cos\frac{\theta}{2}\left(\frac{\mu_1 L_t e^{\gamma}}{4\pi}\right)^{1/2}\left(\frac{\mu_2 L_t e^{\gamma}}{4\pi}\right)^{1/2} I \\
&= 2m\cos\frac{\theta}{2}e^{\gamma}\sqrt{\mu_1\mu_2}I. \qquad (3.21)
\end{aligned}$$

Equation (3.13) is valid when $m \ll \mu$. That way, we can approximate μ_1 by $\mu = \sqrt{2}g/\sqrt{\pi}$, since it is its value when the fermions are massless. Now, let us analyze the integral I in eq. (3.18)

$$I = 1 - \frac{\int_{-\pi}^{\pi} d\varphi \, \frac{\varphi^2}{2} e^{-\sqrt{\frac{\kappa}{2}}\varphi^2}}{\int_{-\pi}^{\pi} d\varphi \, e^{-\sqrt{\frac{\kappa}{2}}\varphi^2}}. \qquad (3.22)$$

We can use the error function to express the denominator

$$\int_{-\pi}^{\pi} d\varphi \, e^{-a\varphi^2} = \sqrt{\frac{\pi}{a}}\text{erf}(\sqrt{a}\pi), \quad \text{where } a = \sqrt{\frac{\kappa}{2}}, \quad \text{erf}(x) = \frac{2}{\sqrt{\pi}}\int_0^x dt \, e^{-t^2}. \qquad (3.23)$$

By using the following property (see ref. [28] for the error function properties)

$$\int dx \, \text{erf}(\sqrt{a}x) = x\,\text{erf}(\sqrt{a}x) + \frac{1}{\sqrt{\pi a}}e^{-ax^2} + \text{constant} \qquad (3.24)$$
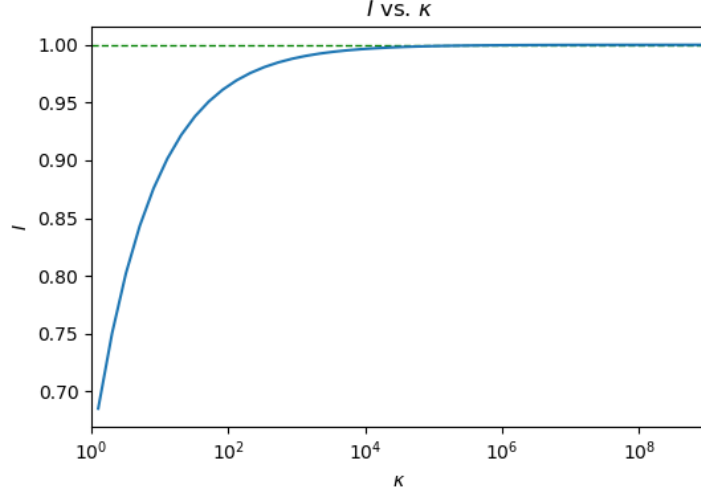
Figure 3.2: $I(\kappa)$ defined in eq. (3.22).

and integrating by parts, it is possible to show that

$$\int_0^\pi d\varphi \, \varphi^2 e^{-a\varphi^2} = \frac{\sqrt{\pi}}{4a^{3/2}} \operatorname{erf}(\sqrt{a}\pi) - \frac{\pi}{2a} e^{-a\pi^2}. \tag{3.25}$$

Therefore

$$\frac{\int_{-\pi}^\pi d\varphi \, \frac{\varphi^2}{2} e^{-\sqrt{\frac{\kappa}{2}}\varphi^2}}{\int_{-\pi}^\pi d\varphi \, e^{-\sqrt{\frac{\kappa}{2}}\varphi^2}} = \frac{1}{2a} - \frac{\sqrt{\frac{\pi}{a}} e^{-a\pi^2}}{\operatorname{erf}(\sqrt{a}\pi)}. \tag{3.26}$$

In the limit $L_t \to \infty$ we have $\kappa \to \infty$ and as a consequence $a \to \infty$. Thus, considering that

$$\lim_{a \to \infty} \operatorname{erf}(\sqrt{a}\pi) = 1, \tag{3.27}$$

we conclude

$$\lim_{L_t \to \infty} I = 1, \quad \text{when } \cos\frac{\theta}{2} \geq 0. \tag{3.28}$$

This can also be seen numerically, as shown in figure 3.2. Then, eq. (3.21) is simplified to

$$\mu_2^2 = 2e^\gamma m \sqrt{\mu\mu_2} \cos\frac{\theta}{2} \tag{3.29}$$

We are finally left with

$$\mu_2 = \left(4e^{2\gamma} \mu m^2 \cos^2\frac{\theta}{2} \right)^{1/3} = \left(4e^{2\gamma} \sqrt{\frac{2}{\pi}} g m^2 \cos^2\frac{\theta}{2} \right)^{1/3}. \tag{3.30}$$

We evaluate the constant terms

$$\left(4e^{2\gamma} \sqrt{\frac{2}{\pi}} \right)^{1/3} = 2.1633\ldots \tag{3.31}$$

Therefore

$$\mu_2 = 2.1633\ldots \left(m^2 g \cos^2\frac{\theta}{2} \right)^{1/3}, \quad L_t \to \infty, \quad \cos\frac{\theta}{2} \geq 0, \quad m \ll \mu. \tag{3.32}$$

The two flavor massive Schwinger model has a certain analogy to QCD, that way we can relate μ_1 with the mass of the η' meson and μ_2 with the pion mass (see Chapter 5). Anyhow, we will refer to the boson of mass μ_1 as η. So from now on we will denote $\mu_1 = m_\eta$ and $\mu_2 = m_\pi$. There are two predictions for m_π at infinite volume and small fermion mass m. The first one is a semi-classical prediction [29], that is equal to eq. (3.32) by taking $\theta = 0$. The other prediction was deduced by A. Smilga [30] and it is slightly different from the semi-classical one: $m_\pi = 2.008(m^2 g)^{1/3}$.

It is possible to derive further expressions for limiting cases, however, the rest of the analysis will be done numerically.

3.2   Numerical solution

The first step to solve eqs. (3.10), (3.12) and (3.13) is to find a solution of the differential equation that involves $f(\varphi)$ with the condition $f(\varphi + 2\pi) = f(\varphi)$, $\varphi \in (-\pi, \pi]$. If one sets $\delta\alpha = 0$, performs the change of variable $\varphi = 2x$ and defines $a \equiv 4\epsilon$, $q \equiv -2\kappa$, then eq. (3.12) takes the form

$$\frac{d^2 f}{dx^2} + (a - 2q \cos 2x)f = 0, \quad f(x + \pi) = f(\pi), \quad x \in \left(-\frac{\pi}{2}, \frac{\pi}{2}\right], \qquad (3.33)$$

which is the quantum pendulum equation [26] or the *Mathieu equation*. Furthermore, if $\delta\alpha \neq 0$ one can perform the change of variable $f(\varphi) = e^{-i\varphi \, \delta\alpha} g(\varphi)$. Thus, the derivatives and the boundary condition become

$$\begin{aligned}
\frac{df}{d\varphi} &= e^{-i\delta\alpha}\left(\frac{dg}{d\varphi} - ig\,\delta\alpha\right), \\
\frac{d^2 f}{d\varphi^2} &= e^{-i\varphi\,\delta\alpha}\left(-2i\delta\alpha\frac{dg}{d\varphi} - \delta\alpha^2 + \frac{d^2 g}{d\varphi^2}\right), \\
g(\varphi + 2\pi) &= e^{i2\pi\delta\alpha} g(\varphi).
\end{aligned} \qquad (3.34)$$

Substituting in eq. (3.12) yields

$$-\frac{d^2 g}{d\varphi^2} - \kappa \cos\varphi\, g = \epsilon g. \qquad (3.35)$$

This is the same equation for $f(\varphi)$ when $\delta\alpha = 0$ but with a different boundary condition given by the last line of eqs. (3.34)[2].

The solutions to eq. (3.33) are the *Mathieu functions* of first kind, denoted by

$$\frac{1}{\sqrt{\pi}}\mathrm{ce}_n\left(\frac{\varphi}{2}, -2\kappa\right), \quad \frac{1}{\sqrt{\pi}}\mathrm{se}_n\left(\frac{\varphi}{2}, -2\kappa\right), \quad n \text{ an even number}, \qquad (3.36)$$

while the solutions to eq. (3.35) are non-periodic solutions to the Mathieu equation, known as *Floquet solutions*. There are some analytic expressions for the Mathieu functions ce_n, se_n, and the Floquet solutions. The former can be expressed as a linear combination of the sine and cosine functions, while the Floquet solutions are sought by using the so-called *Floquet theorem*, which allows us to find solutions of the form

$$F_\nu(\varphi) = e^{i\nu\varphi} P(\varphi). \qquad (3.37)$$

Here ν is a constant, determined by the boundary condition, and $P(\varphi)$ is a periodic function. However, the result is quite complicated, see for example refs. [28,32]. The best

---

[2]For this reason, eq. (3.12) is also known as the *Damped Mathieu Equation*, see e.g. ref. [31].

way to proceed is by discretizing eq. (3.12) in order to obtain a matrix eigenvalue problem that will allows us to find the ground state function $f_0(\varphi)$.

Let us expand eq. (3.12)

$$-\frac{d^2 f}{d\varphi^2} - 2i\delta\alpha \frac{df}{d\varphi} + \delta\alpha^2 f - \kappa \cos\varphi = \epsilon f \tag{3.38}$$

and divide the interval $(-\pi, \pi]$ in $N+1$ sites separated by $\Delta\varphi = 2\pi/N$. Then we replace the continuum derivatives by discrete derivatives

$$f_j = f(\varphi_j), \quad \frac{df}{d\varphi} \to \frac{f_{j+1} - f_{j-1}}{2\Delta\varphi}, \quad \frac{d^2 f}{d\varphi^2} \to \frac{f_{j+1} - 2f_j + f_{j-1}}{\Delta\varphi^2},$$

$$\varphi \in (-\pi, \pi], \quad f_0 = f_N. \tag{3.39}$$

Substituting them in eq. (3.38) yields

$$-\frac{f_{j+1} - 2f_j + f_{j-1}}{\Delta\varphi^2} - 2i\delta\alpha \frac{f_{j+1} - f_{j-1}}{2\Delta\varphi} + \delta\alpha^2 f_j - \kappa \cos\varphi_j f_j = \epsilon f_j. \tag{3.40}$$

The index j runs from 0 to $N-1$ (we are assuming $f_{-1} = f_{N-1}$ since f is periodic). Thus we have N algebraic equations that can be written in matrix form if we substitute

$$\frac{f_{j+1} - 2f_j + f_{j-1}}{\Delta\varphi^2} \quad \longrightarrow \quad \frac{1}{\Delta\varphi^2} \underbrace{\begin{pmatrix} -2 & 1 & 0 & 0 & \cdots & \cdots & \cdots & 1 \\ 1 & -2 & 1 & 0 & \cdots & \cdots & \cdots & 0 \\ 0 & 1 & -2 & 1 & \cdots & \cdots & \cdots & 0 \\ \vdots & \vdots & \vdots & \vdots & \cdots & 1 & -2 & 1 \\ 1 & 0 & 0 & 0 & \cdots & 0 & 1 & -2 \end{pmatrix}}_{\mathbb{M}_1} \underbrace{\begin{pmatrix} f_0 \\ f_1 \\ f_2 \\ \vdots \\ f_{N-1} \end{pmatrix}}_{\vec{f}},$$

$$\frac{f_{j+1} - f_{j-1}}{2\Delta\varphi} \quad \longrightarrow \quad \frac{1}{2\Delta\varphi} \underbrace{\begin{pmatrix} 0 & 1 & 0 & 0 & 0 & \cdots & 0 & -1 \\ -1 & 0 & 1 & 0 & 0 & \cdots & 0 & 0 \\ 0 & -1 & 0 & 1 & 0 & \cdots & 0 & 0 \\ 0 & 0 & -1 & 0 & 1 & \cdots & 0 & 0 \\ \vdots & \vdots & \vdots & \vdots & \vdots & \vdots & \vdots & \vdots \\ 0 & 0 & 0 & 0 & 0 & \cdots & 0 & 1 \\ 1 & 0 & 0 & 0 & 0 & \cdots & -1 & 0 \end{pmatrix}}_{\mathbb{M}_2} \begin{pmatrix} f_0 \\ f_1 \\ f_2 \\ \vdots \\ f_{N-1} \end{pmatrix},$$

$$\delta\alpha^2 f_j - \kappa \cos\varphi_j f_j \quad \longrightarrow \quad \underbrace{\text{diag}(\delta\alpha^2 - \kappa \cos\varphi_0, \dots, \delta\alpha^2 - \kappa \cos\varphi_{N-1})}_{\mathbb{M}_3} \vec{f}. \tag{3.41}$$

In that manner, the N algebraic equations can be expressed as

$$\left(-\frac{\mathbb{M}_1}{\Delta\varphi^2} - \frac{i\delta\alpha}{\Delta\varphi} \mathbb{M}_2 + \mathbb{M}_3 \right) \vec{f} = \epsilon \vec{f}, \tag{3.42}$$

where $\mathbb{M}_1$, $\mathbb{M}_2$, $\mathbb{M}_3$ and $\vec{f}$ are defined in eq. (3.41). This is a linear algebra eigenvalue problem that can be solved using standard subroutines, e.g. LAPACK. Then, the eigenvectors $\vec{f}$ are obtained. However they are not yet normalized as $\int_{-\pi}^{\pi} d\varphi |f(\varphi)|^2 = 1$, so

one must use a numerical integral (see Appendix B) to normalize the resultant vector $\vec{f}$. Reference [26] mentions some limiting case solutions of the ground state of eq. (3.38)

$$f_0(\varphi) \approx \begin{cases} \frac{1}{\sqrt{2\pi}} \left[1 + \frac{\kappa}{1-4\delta\alpha^2}(\cos\varphi - 2i\delta\alpha\sin\varphi) \right] & \text{for } \frac{\kappa}{1\pm2\delta\alpha} \ll 1 \\ \\ \frac{1}{\sqrt{2\pi}} \left[\frac{1}{\sqrt{2}} \left(1 + e^{\mp i\varphi} \right) + \frac{\kappa}{4\sqrt{2}} \left(e^{\pm i\varphi} + e^{\mp 2i\varphi} \right) \right] & \text{for } \delta\alpha = \pm\frac{1}{2}, \quad \kappa \ll 1 \\ \\ \frac{1}{\int_{-\pi}^{\pi} |e^{-i\delta\alpha\varphi - \sqrt{\frac{\kappa}{8}}\varphi^2}|^2 d\varphi} e^{-i\delta\alpha\varphi - \sqrt{\frac{\kappa}{8}}\varphi^2} & \text{for } \kappa \gg 1. \end{cases} \qquad (3.43)$$

One can compare the numerical result with these particular expressions in order to verify the outcome of diagonalizing eq. (3.42). In figure 3.3 the comparison is shown.

The next step is to find solutions for m_π and the chiral condensate $\langle \overline{\psi}\psi \rangle = -m_\pi^2/(4\pi m)$. Equations (3.13) correspond to the following system of equations

$$\left[\left(i\frac{d}{d\varphi} - \delta\alpha \right)^2 - \kappa\cos\varphi \right] f(\varphi) = \epsilon f(\varphi),$$

$$(m_\pi L_t)^2 = 2\pi^2\kappa \int_{-\pi}^{\pi} d\varphi \, \cos\varphi \, |f_0(\varphi)|^2,$$

$$\kappa = \frac{4}{\pi} m L_t \cos\frac{\theta}{2} \left[B(m_\eta L_t) \right]^{1/2} \left[B(m_\pi L_t) \right]^{1/2} e^{-\pi/2\mu L_t}. \qquad (3.44)$$

Below we are going to use the notation $\beta = 1/g^2$ and we recall that $\mu^2 = 2g^2/\pi$.

Equations (3.44) can be solved as a non-linear system of equations or in a self-consistent way. We explain both procedures as recipes. To solve eqs. (3.44) as a non-linear system one performs the following steps:

- First, one has to assign values to the input parameters κ, $\delta\alpha$, θ, β and m; that way one has to determine m_π and L_t.

- Then, the ground state function is calculated numerically by using eq. (3.42) for the κ and $\delta\alpha$ values that we chose, and the result is normalized.

- With f_0 already calculated, one computes $m_\pi L_t$ with the second equation of (3.44), using once again a numerical integrator.

- Note that $m_\pi L_t$ is already known from the previous step, but in order to find L_t and m_π separately one has to determine the "L_t-roots" of the last equation in (3.44). This can be done using a root finder, for instance bisection.

Following these four steps the system can be solved. It is important to note, however, that with this procedure one does not have control over L_t, but over κ, so if a solution for a specific L_t is desired, then a scan for several values of κ has to be applied. Still, it is possible to have control over L_t, but then one cannot give an initial value for m and it has to be determined in the same way we computed L_t in the last four steps. That is, one would have to do the following steps instead:

- Assign values to κ, $\delta\alpha$, θ, β, L_t and leave m_π and m undetermined.

- Calculate the normalized groundstate $f_0(\varphi)$.

- With f_0 already calculated, one computes m_π with the second equation of (3.44).

- Now one has to determine m in the last equation of (3.44). In this case one can solve for m analytically, there is no need for a root finder.
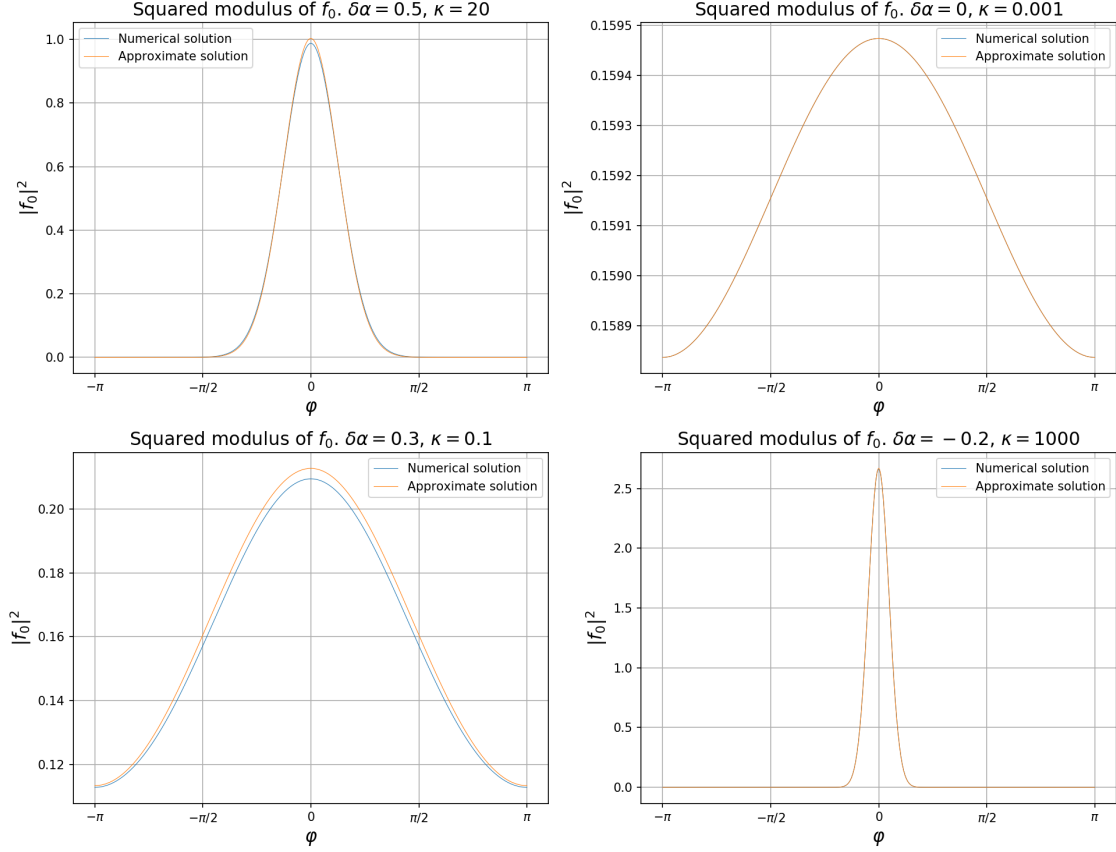
Figure 3.3: Ground state function of eq. (3.38). The approximate solutions correspond to the expressions in eq. (3.43). In the two plots on the right-hand side it is hard to distinguish the two curves. We use $N + 1 = 10^3$ points in the discretization.

On the other hand, if one wants to have total control over both variables, L_t and m, then the system has to be solved self-consistently. The idea is to carry out the following steps:

- Assign a value to $\delta\alpha$, θ, β, L_t, m and start from an initial guess for the pion mass m_π^{ini}. The pion mass will be determined self-consistently.

- Calculate κ.

- Calculate a new value of the pion mass, m_π^{new}, using the second equation of (3.44).

- If $|m_\pi^{\text{new}} - m_\pi^{\text{ini}}|$ is smaller than an error that one desires, then m_π^{new} is the result for m_π. Otherwise, one has to use m_π^{new} as m_π^{ini} and repeat these four steps until the final value has converged within the error. We cannot guarantee that the iteration converges, but in the examples that we tested the result always converges to the same values that one obtains with the two previous methods.

We implemented these three methods with Python and all of them give the same results. In general, the last one is most expensive computationally since one does not know how long the algorithm takes to converge and it depends on the initial guess. Anyhow, this method is most useful since we can fix arbitrary values of L_t and m. We choose these two parameters to be dimensionless, that way we set the energy scale of the system and compare the solution with the results of lattice simulations.

The first result to be revised is eq. (3.32), because it helps to verify the numerical solution and it also allows us to check the outcome with the three different methods

explained above. To do so, we substitute m_η for its value in the chiral limit ($m_\eta = \mu$) and then we solve eqs. (3.44). In figure 3.4 the pion mass is shown as a function of $(m^2g)^{1/3}$ for different values of L_t and $\delta\alpha = \theta = 0$, $\beta = 4$. We see that when L_t becomes larger, the values move closer to the semi-classical prediction.
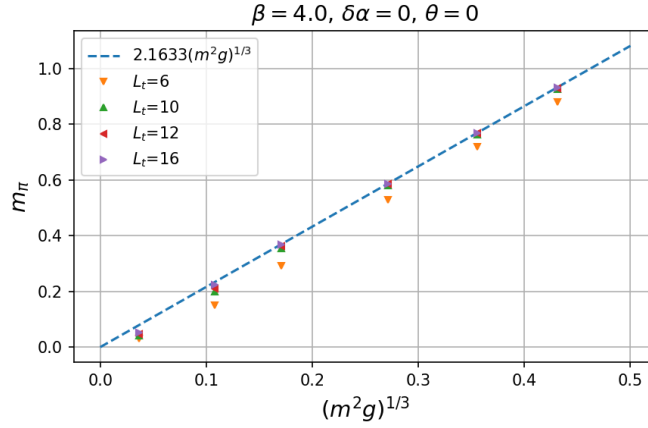
(a) Fixing m and determining L_t
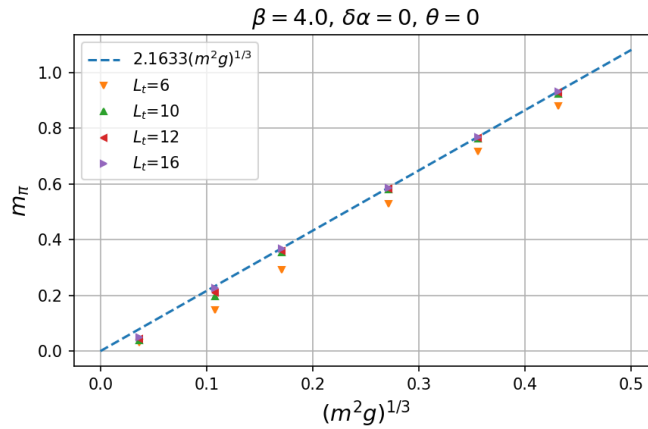
(b) Fixing L_t and determining m
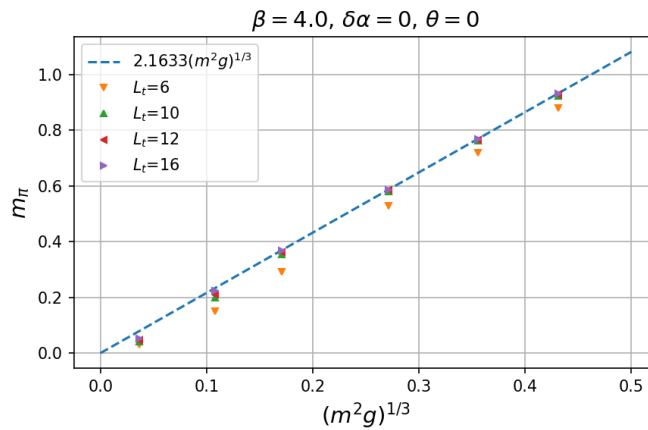
(c) Self-consistent solution

Figure 3.4: Solution for the pion mass as function of $(m^2g)^{1/3}$ when one substitutes $m_\eta \approx \mu$. Each plot was made with one of the three different methods described above. We observe that the results coincide.

If one does not substitute $m_\eta \approx \mu$ and instead uses $m_\eta = \sqrt{m_\pi^2 + \mu^2}$, the result of figure 3.4 is different, since m_π will not converge to eq. (3.32). In figure 3.5, the pion mass as a function of $(m^2 g)^{1/3}$ and m_η as a function of m are shown, but taking into account the change in m_η. The chiral condensate can be calculated as well by using the third line of eqs. (3.13). Different values of this quantity as function of L_t and the temperature are shown in figure 3.6.

(a)

(b)
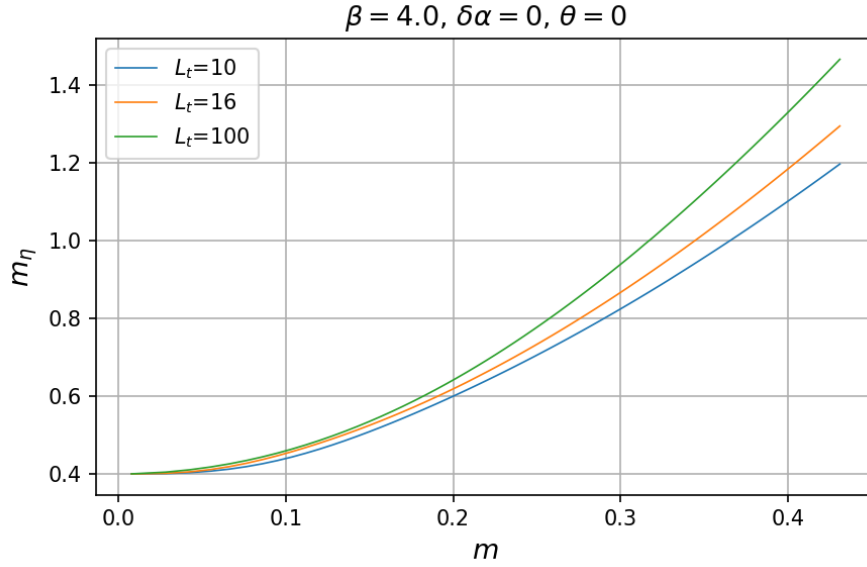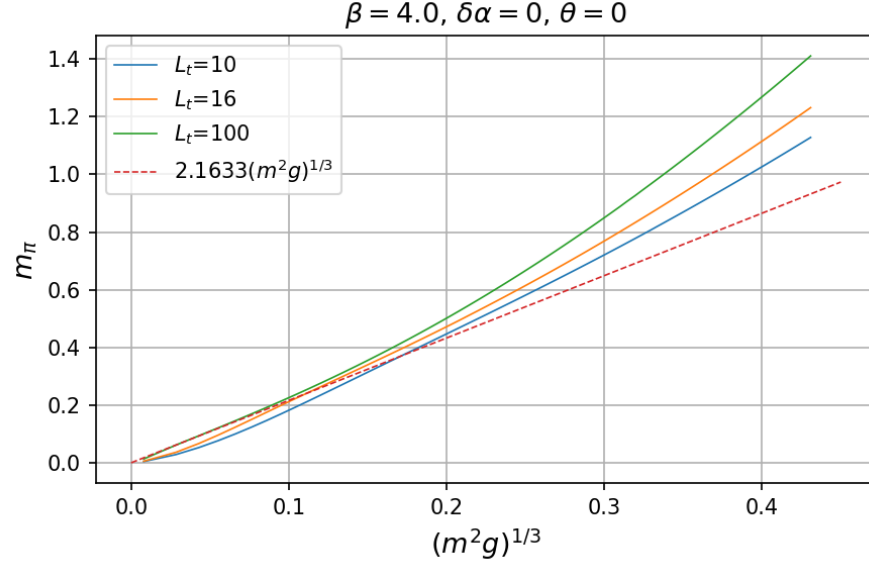
Figure 3.5: Predictions of m_η and m_π for different fermion masses and values of L_t. We see that as L_t becomes larger, for small m the value of m_π approaches to the semi-classical prediction and in the chiral limit it vanishes. We also observe that m_η converges to $\mu = \sqrt{2 \times 0.5^2/\pi} \simeq 0.39$ when $m \to 0$.
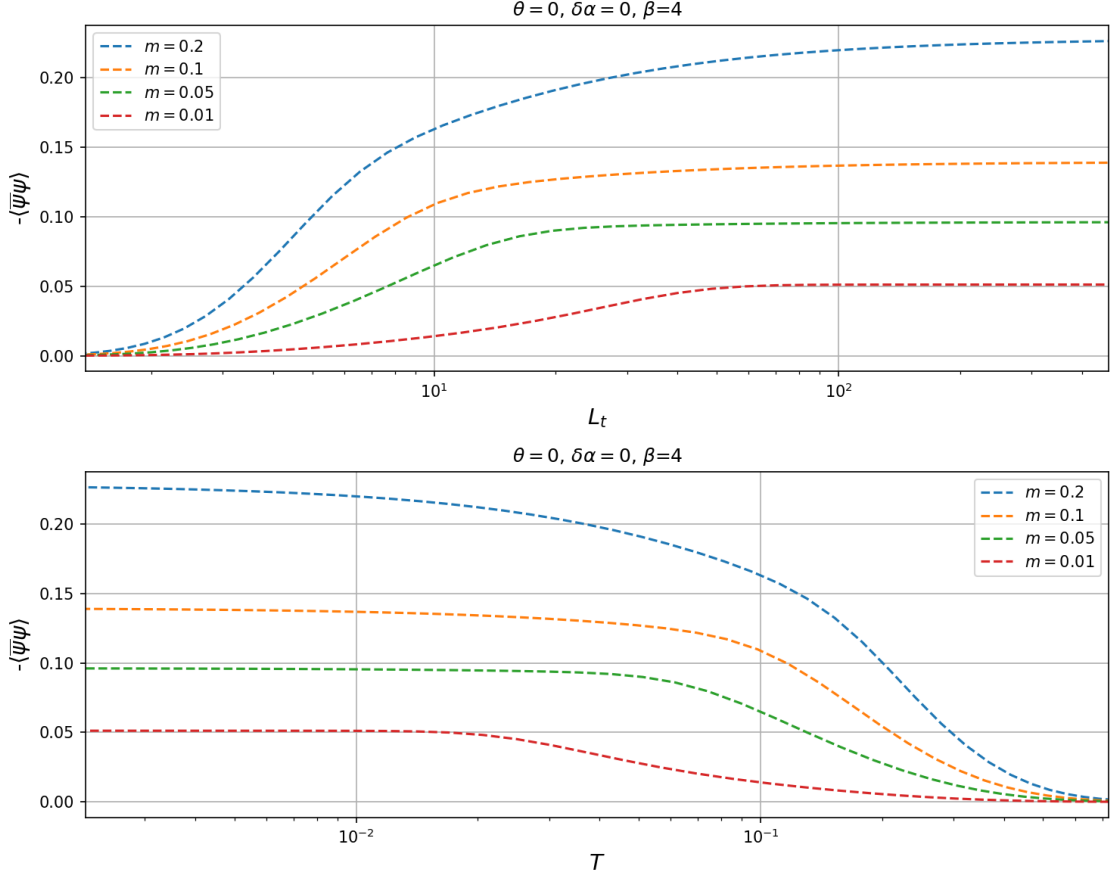
Figure 3.6: Predictions of the chiral condensate $-\langle \overline{\psi}\psi \rangle$ as a function of L_t and the temperature T. In the limit $m \to 0$, $\langle \overline{\psi}\psi \rangle$ vanishes. At high temperature the chiral condensate vanishes faster. We anticipated this result in Chapter 1, where we mentioned that only when we consider one flavor, $\langle \overline{\psi}\psi \rangle$ does not go to zero in the chiral limit.

3.3 Lattice simulations results

In this section we show results of m_π and m_η obtained with lattice simulations at finite temperature for $\beta = 1/g^2 = 4$. Each value of m_π and m_η was obtained through 10^3 measurements separated by 10 sweeps. 500 sweeps were performed to thermalize the configurations. The fermion mass was also measured, since it undergoes renormalization and one cannot use the bare Wilson fermion mass. We determined m by using the PCAC relation, see Section 4.4. We compare the results of the simulations with the prediction given by Hosotani, by setting $\delta\alpha = \theta = 0$. In figures 3.7, 3.8 and 3.9 results of m_π vs. $(m^2 g)^{1/3}$ and m_η vs. m for a spatial volume $L = 64$ and a time extent $L_t = 10, 12, 16$ are shown, respectively. These plots are in lattice units, *i.e.* we have set the lattice constant $a = 1$, so the masses do not have dimensions.

For $\beta = 4$, the mass of η in the chiral limit is $\sqrt{2 \times 0.5^2/\pi} \simeq 0.39$; then, one would expect Hosotani's prediction to match the simulation results for a fermion mass $m \ll 0.39$. This implies that the prediction should be valid when $(m^2 g)^{1/3} \ll 0.42$. In figure 3.7 we see that when $(m^2 g)^{1/3} \lesssim 0.1$, the analytic approach matches well the results of the simulations. For larger m, the values of m_π and m_η obtained by means of the simulations disagree with the prediction. Still, in both cases m_π is above the semi-classical prediction.

Now, if $(m^2 g)^{1/3} \lesssim 0.1$, then $m \lesssim 0.044$. According to figure 3.7 (b), in this region the prediction coincides with the simulation results. Both sets of results converge to a value

very close to 0.4, which is compatible with $m_\eta = \sqrt{2g^2/\pi}$. However, for masses larger than 0.05 we see again a discrepancy between the simulations and the analytic approach. In figures 3.8 and 3.9 we increase L_t and the agreement between the simulations and the prediction by Hosotani occurs when $m \lesssim 0.05$.

With the simulations we can also measure the chiral condensate. Even so, we cannot compare directly this result with the prediction by Hosotani, because, as we mentioned in Chapter 2, Wilson fermions break the chiral symmetry. Therefore, we do not see that $\langle \overline{\psi}\psi \rangle$ vanishes as m goes to zero. For instance, in figure 3.10 we show $\langle \overline{\psi}\psi \rangle$ for $L_t = 10$ and $L = 64$ as a function of the fermion mass.

Based on these results, we can affirm that the predictions of eqs. (3.44) do not allow us to perform a study for masses $m \gtrsim \sqrt{2g^2/\pi}$. Nevertheless, it is still useful to compare values near the chiral limit. The approach analyzed in this chapter for the Schwinger model at finite temperature would be more useful to compare results for the boson masses and the chiral condensate for arbitrary values of θ, close to $m = 0$. In principle, this is what Hosotani intended when he developed his solution. At finite θ, lattice simulations are not feasible due to the *sign problem*, where the action becomes complex and we cannot use $\exp(-S)$ as a probability weight factor. In this chapter we revised how far one can go with the outcome of eqs. (3.44) to study the finite temperature Schwinger model for arbitrary fermion mass.

(a) m_π vs. $(m^2 g)^{1/3}$
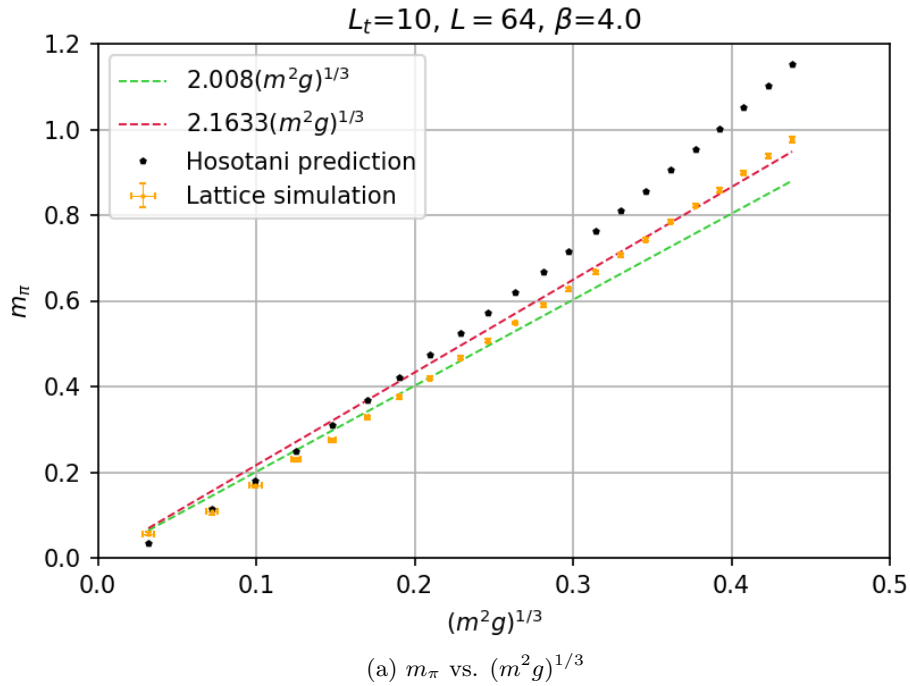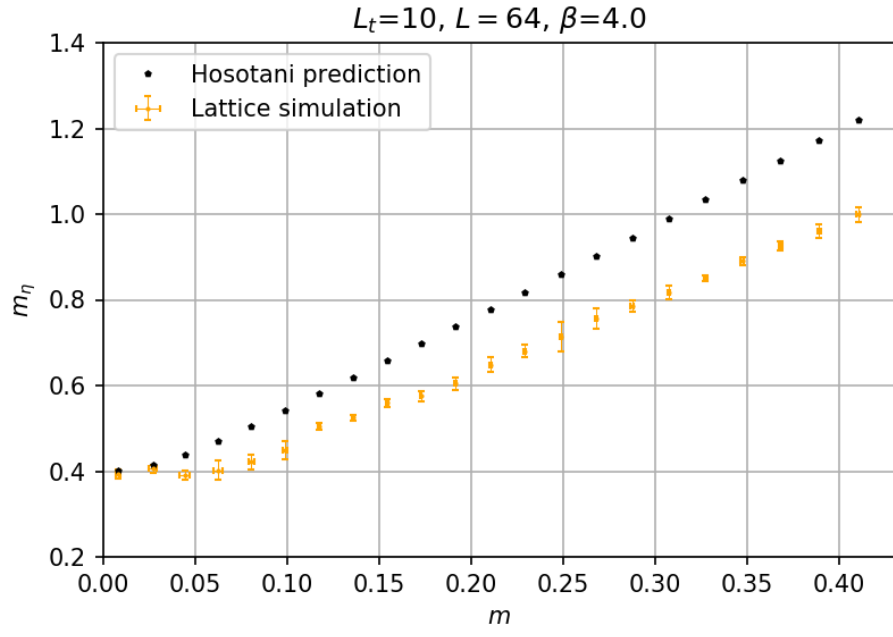
(b) m_η vs. m

Figure 3.7: Masses of the η and π mesons as a function of the degenerate fermion mass m for $L_t = 10$.

(a) m_π vs. $(m^2 g)^{1/3}$
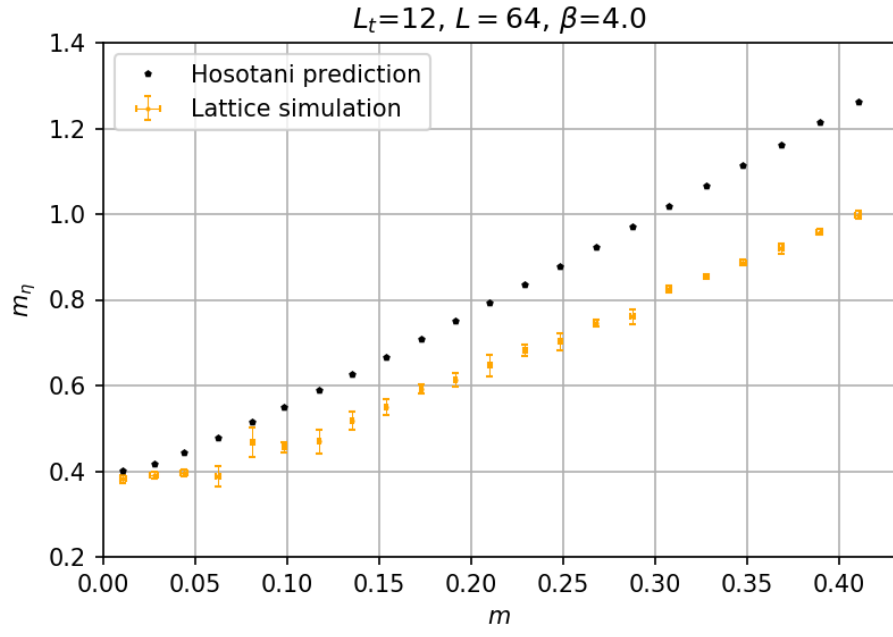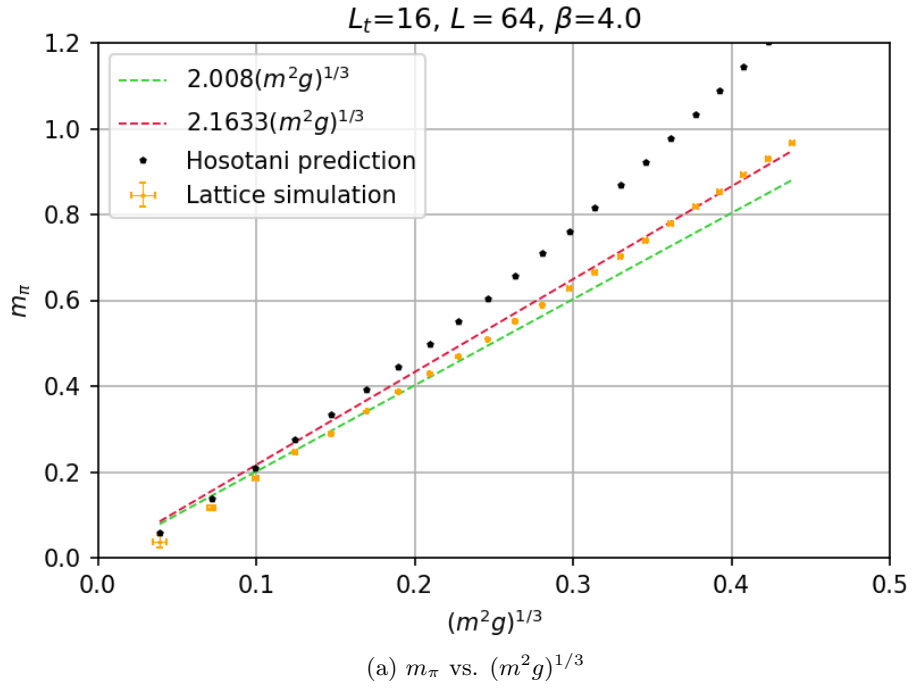
(b) m_η vs. m
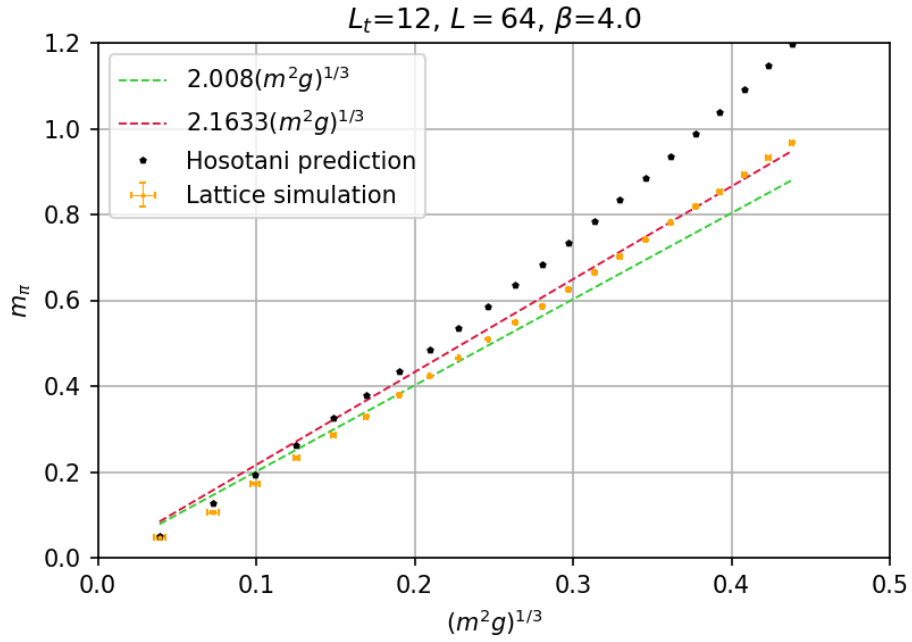
Figure 3.8: Masses of the η and π mesons as a function of the degenerate fermion mass m for $L_t = 12$.

(a) m_π vs. $(m^2 g)^{1/3}$

(b) m_η vs. m
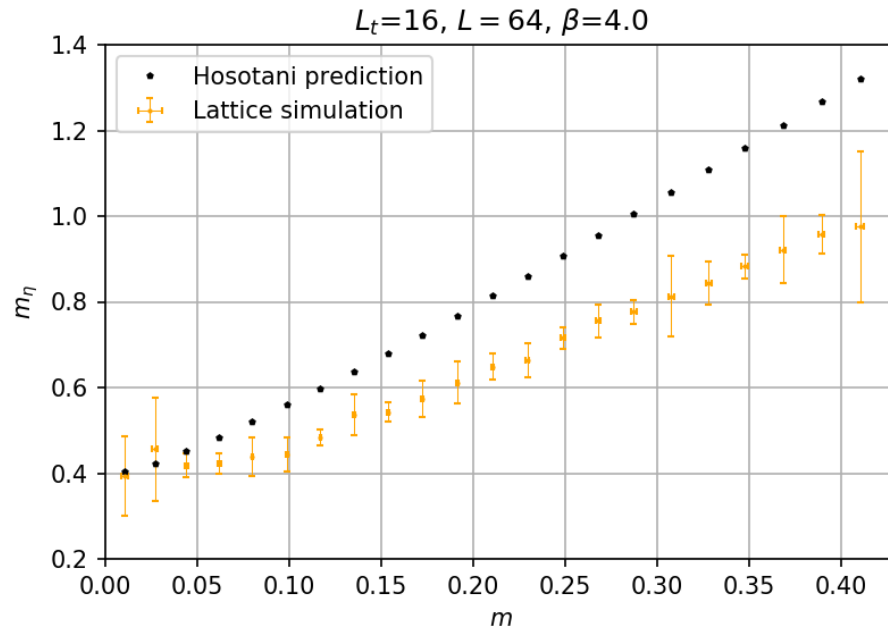
Figure 3.9: Masses of the η and π mesons as a function of the degenerate fermion mass m for $L_t = 16$.
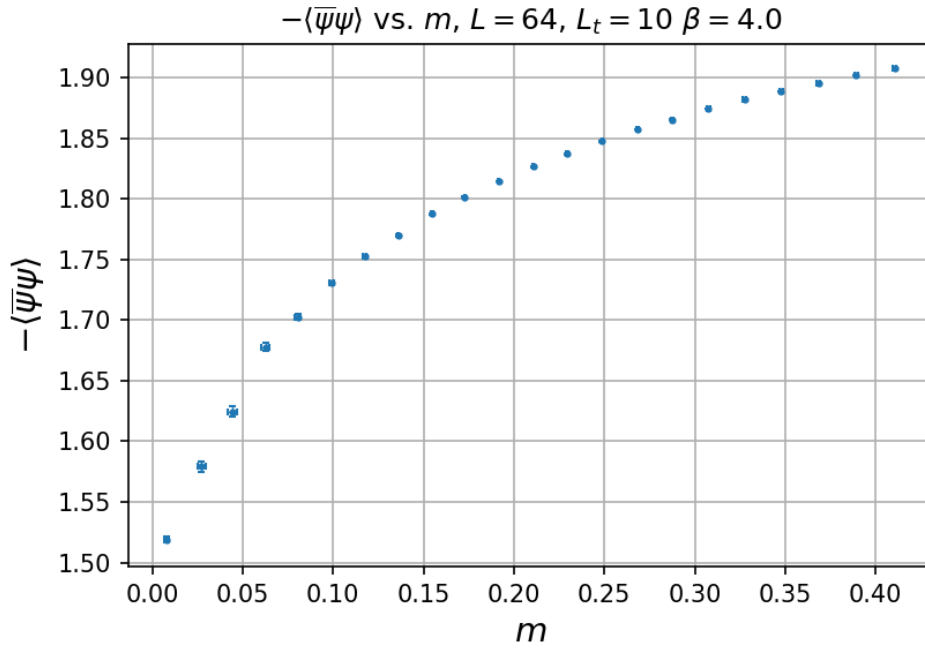
(a) $-\langle \bar{\psi}\psi \rangle$ vs. m obtained with lattice simulations.
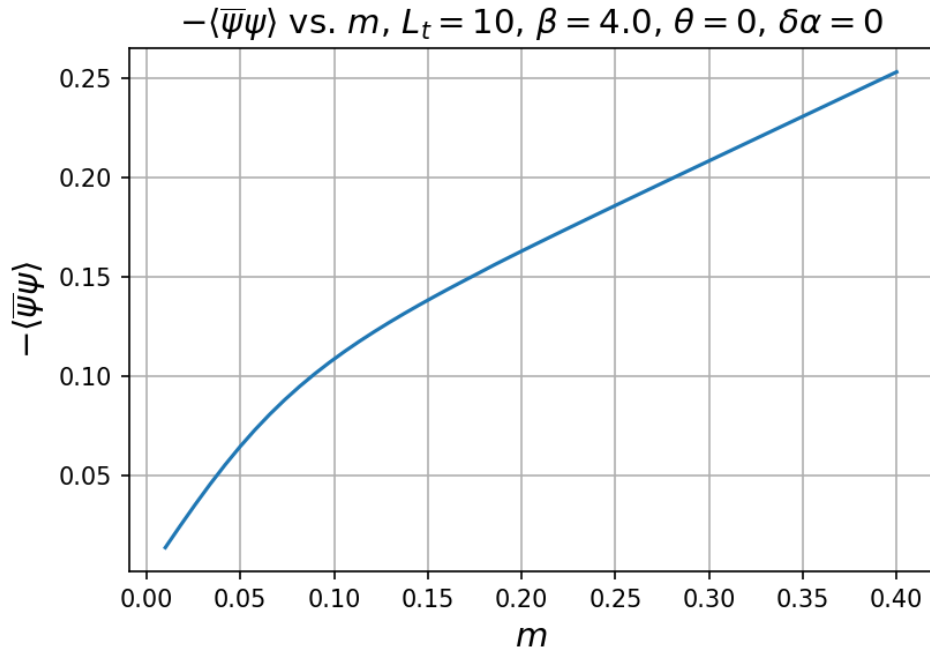
(b) $-\langle \bar{\psi}\psi \rangle$ vs. m obtained with eqs. (3.44) and the last line of eqs. (3.13).

Figure 3.10: In the upper plot, we show the result of $\langle \bar{\psi}\psi \rangle$ obtained with the lattice simulations, while in the lower plot we show the prediction by Hosotani. The former does not vanish in the chiral limit due to the explicit chiral symmetry breaking encoded in the Wilson fermion formulation.

Chapter 4

Chiral Perturbation Theory and the δ-regime

As it was mentioned in Chapter 2, the low energy regime of QCD cannot be treated with perturbation theory, but one can use lattice simulations. A systematic analytical approach to this regime is *Chiral Perturbation Theory*, which is an effective field theory. In virtue of the chiral symmetry breaking of QCD, the Lagrangian of the effective theory is built by introducing a field in the coset space of the symmetry breaking group. This field describes the lightest hadrons, since at low energy they dominate the theory. If the symmetry breaking is spontaneous, the particles that appear are massless and they are known as Nambu-Goldstone Bosons. On the other hand, if the symmetry breaking is explicit, the particles have a light mass and we refer to them as quasi Nambu-Goldstone Bosons, which correspond to light mesons. In principle, the effective Lagrangian contains all the terms that are consistent with the symmetries of the underlying theory. Since the number of terms is infinite, they are truncated in the sense of a low energy expansion. This leads to a consideration of the chiral symmetry of the QCD Lagrangian.

4.1   QCD chiral symmetry

Since we are interested in low energy, we will work with the flavors whose masses satisfy $m_f \ll \Lambda_{\text{QCD}} \approx 300$ MeV. Therefore we only take into account the u and d quarks, with masses in the following range [33]

$$
\begin{aligned}
m_u &= 1.9 \text{ - } 2.65 \text{ MeV}, \\
m_d &= 4.5 \text{ - } 5.15 \text{ MeV}.
\end{aligned}
\tag{4.1}
$$

Then, in Minkowski space-time, the QCD Lagrangian is given by

$$
\mathcal{L} = \sum_{f=u,d} \left(\bar{q}_f i \gamma^\mu D_\mu q_f - m_f \bar{q}_f q_f \right) - \frac{1}{4} \text{tr} \left[G_{\mu\nu} G^{\mu\nu} \right],
$$

$$
D_\mu = (\partial_\mu + ig A_\mu), \;\; G_{\mu\nu} = \partial_\mu A_\nu - \partial_\nu A_\mu + ig[A_\mu, A_\nu],
\tag{4.2}
$$

where q_f and $\bar{q}_f$ are fermion fields associated with the flavor f with mass m_f. The gauge field is $A_\mu(x) = \sum_{a=1}^{8} A_\mu^a(x) T_a$, where $A_\mu^a(x)$ are field components and T_a are the basis elements of the traceless Hermitian 3×3 matrices (generators of SU(3)). This implies that the gauge field is a matrix as well. The Lagrangian is constructed in the same way as we did in Section 2.3, so it is invariant under SU(3) gauge transformations. We are interested in analyzing the chiral symmetry, therefore we apply the chiral projection operators, which

were already introduced in section 1.3.

$$P_R = \frac{1}{2}(\mathbb{I} + \gamma_5), \;\; P_L = \frac{1}{2}(\mathbb{I} - \gamma_5), \tag{4.3}$$

to the quark fields in order to obtain the right-handed and left-handed fields

$$q_{R_f} = P_R q_f, \;\; q_{L_f} = P_L q_f, \;\; \bar{q}_{R_f} = \bar{q}_f P_L, \;\; \bar{q}_{L_f} = \bar{q}_f P_R. \tag{4.4}$$

By using $\{\gamma_5, \gamma^\mu\} = 0$, $\gamma_5^2 = \mathbb{I}$, $\gamma_5^\dagger = \gamma_5$ and the definition (4.3) of the chiral operators one obtains the following properties

$$P_{L,R} = P_{L,R}^\dagger, \;\; P_{L,R}^2 = P_{L,R}, \;\; P_R P_L = P_L P_R = 0, \;\; P_{R,L}\gamma^\mu = \gamma^\mu P_{L,R}, \tag{4.5}$$

$$q_f = q_{R_f} + q_{L_f}, \quad \bar{q}_f = \bar{q}_{R_f} + \bar{q}_{L_f}. \tag{4.6}$$

With eqs. (4.5) and eqs. (4.6) the QCD Lagrangian takes the form

$$\mathcal{L} = \sum_{f=u,d} \left[\bar{q}_{L_f} i\gamma^\mu D_\mu q_{L_f} + \bar{q}_{R_f} i\gamma^\mu D_\mu q_{R_f} - m_f(\bar{q}_{R_f} q_{L_f} + \bar{q}_{L_f} q_{R_f}) \right] - \frac{1}{4}\text{tr}\,[G_{\mu\nu}G^{\mu\nu}]. \tag{4.7}$$

Now, we use global chiral transformations defined by

$$q_{R,L_f} \to q'_{R,L_f} = e^{i\alpha\gamma_5} q_{R,L_f}, \;\; \bar{q}_{R,L_f} \to \bar{q}'_{R,L_f} = \bar{q}_{R,L_f} e^{i\alpha\gamma_5}, \;\; \alpha \in \mathbb{R}. \tag{4.8}$$

By using $\gamma^\mu e^{i\alpha\gamma_5} = e^{-i\alpha\gamma_5}\gamma^\mu$, the quark part of the Lagrangian transforms as

$$\sum_{f=u,d} \left[\left(\bar{q}'_{L_f} i\gamma^\mu D_\mu q'_{L_f} + \bar{q}'_{R_f} i\gamma^\mu D_\mu q'_{R_f} \right) - m_f(\bar{q}'_{R_f} q'_{L_f} + \bar{q}'_{L_f} q'_{R_f}) \right]$$

$$= \sum_{f=u,d} \left[\left(\bar{q}_{L_f} i\gamma^\mu D_\mu q_{L_f} + \bar{q}_{R_f} i\gamma^\mu D_\mu q_{R_f} \right) - m_f(\bar{q}_{R_f} e^{i2\alpha\gamma_5} q_{L_f} + \bar{q}_{L_f} e^{i2\alpha\gamma_5} q_{R_f}) \right]. \tag{4.9}$$

Hence, $\mathcal{L}$ is invariant under the transformations of eq. (4.8) only when $m_f = 0$, for that reason this is called the chiral limit. Let us work in the chiral limit for the moment.

If we express the quark fields as doublets

$$q_R = \begin{pmatrix} q_{R_u} \\ q_{R_d} \end{pmatrix}, \;\; \bar{q}_R = \left(\bar{q}_{R_u}, \bar{q}_{R_d} \right), \;\; q_L = \begin{pmatrix} q_{L_u} \\ q_{L_d} \end{pmatrix}, \;\; \bar{q}_L = \left(\bar{q}_{L_u}, \bar{q}_{L_d} \right), \tag{4.10}$$

we can rewrite the massless Lagrangian as

$$\mathcal{L} = \bar{q}_L i\gamma^\mu D_\mu q_L + \bar{q}_R i\gamma^\mu D_\mu q_R - \frac{1}{4}\text{tr}\,[G_{\mu\nu}G^{\mu\nu}] \tag{4.11}$$

and apply separate global U(2) transformations

$$q_R \to q'_R = R\, q_R, \quad \bar{q}_R \to \bar{q}'_R = \bar{q}_R R^\dagger, \quad R \in \text{U}(2)_R,$$
$$q_L \to q'_L = L\, q_L, \quad \bar{q}_L \to \bar{q}'_L = \bar{q}_L L^\dagger, \quad L \in \text{U}(2)_L. \tag{4.12}$$

Under these transformations, $\mathcal{L}$ is once again invariant. The corresponding symmetry group is $\text{U}(2)_L \otimes \text{U}(2)_R$. An element of U(2) can be decomposed into an element of SU(2) multiplied by a phase factor, thus

$$\text{U}(2)_L \otimes \text{U}(2)_R = \text{SU}(2)_L \otimes \text{SU}(2)_R \otimes \text{U}(1)_B \otimes \text{U}(1)_A, \tag{4.13}$$

where $U(1)_A$ is the axial symmetry, which is broken explicitly under quantization (axial anomaly). $U(1)_B$ is associated with the baryon number conservation, while $SU(2)_L \otimes SU(2)_R$ is the chiral flavor symmetry group. At low energy, the latter breaks spontaneously to $SU(2)$. We analyze this through the chiral condensate

$$\langle 0| \bar{q}q |0\rangle = \langle 0| (\bar{q}_R q_L + \bar{q}_L q_R) |0\rangle . \tag{4.14}$$

Under the transformations in eq. (4.12) the chiral condensate transforms as

$$\langle 0| \bar{q}'q' |0\rangle = \langle 0| (\bar{q}_R R^\dagger L q_L + \bar{q}_L L^\dagger R q_R) |0\rangle , \tag{4.15}$$

where we see that $\langle 0| \bar{q}q |0\rangle$ remains invariant only if $R = L$. Hence, we have the following spontaneous breaking pattern

$$SU(2)_L \otimes SU(2)_R \rightarrow SU(2)_{L=R}. \tag{4.16}$$

The order parameter of this symmetry is $\langle 0| \bar{q}q |0\rangle$, so when it is different from zero the chiral symmetry is indeed spontaneously broken. Because of the Goldstone theorem, this broken symmetry corresponds to

$$\dim(SU(2)_L \otimes SU(2)_R) - \dim(SU(2)) = 3 + 3 - 3 = 3 \tag{4.17}$$

massless Nambu-Goldstone Bosons (NGB). If now we take into account the masses m_u and m_d, the symmetry is explicitly broken and the NGBs turn into light massive quasi NGBs, which can be identified with the pion triplet π^+, π^-, π^0. See refs. [34–36] for extensive reviews.

4.2   Effective Lagrangian

In order to build the effective Lagrangian $\mathcal{L}_{\text{eff}}$, one introduces a field $U(x)$ in the coset space of the symmetry breaking group, *i.e.*

$$U(x) \in (SU(2)_L \otimes SU(2)_R)/SU(2)_{L=R} = SU(2), \tag{4.18}$$

which transforms under global transformations of $SU(2)_L \otimes SU(2)_R$ as

$$U(x) \rightarrow U'(x) = RU(x)L^\dagger, \;\; R \in SU(2)_R, \;\; L \in SU(2)_L. \tag{4.19}$$

For two quark flavors, the field $U(x)$ can be expressed in terms of pseudoscalar pion fields: $\vec{\pi} = \{\pi_1(x), \pi_2(x), \pi_3(x)\}$. Thus, $U(x)$ is written as

$$U(x) = \exp\left(i\frac{\vec{\pi} \cdot \vec{\tau}}{F_\pi}\right), \;\; \vec{\tau} = (\sigma_1, \sigma_2, \sigma_3), \tag{4.20}$$

where F_π is known as the pion decay constant and makes the argument of the exponential dimensionless (the pion fields have dimension of mass in units of $c = \hbar = 1$ in $d = 4$) and where σ_i are the Pauli matrices, which are the generators of $SU(2)$. Hence

$$U(x) = \exp\left(i\frac{\phi(x)}{F_\pi}\right), \;\; \phi(x) = \begin{pmatrix} \pi^0 & \sqrt{2}\pi^+ \\ \sqrt{2}\pi^- & -\pi^0 \end{pmatrix},$$
$$\pi^0 = \pi_3, \;\; \pi^\pm = \frac{\pi_1 \mp i\pi_2}{\sqrt{2}}. \tag{4.21}$$

$\mathcal{L}_{\text{eff}}$ is constructed by using $U(x)$. It must have all the terms that present the symmetries of QCD, in particular Lorentz invariance and chiral symmetry. Each term is accompanied

by a coefficient denominated Low Energy Constant (LEC), which is a free parameter of the effective theory and has to be determined from the underlying theory. However, there are actually an infinite number of terms consistent with the symmetries. They can be organized in increasing powers of momentum, which is the same as increasing number of derivatives, so one can truncate them for low energy. In the massless case, the effective Lagrangian with the least number of derivatives reads

$$\mathcal{L}_{\text{eff}} = \frac{F_\pi^2}{4} \text{tr} \left(\partial_\mu U \partial^\mu U^\dagger \right). \tag{4.22}$$

The factor $F_\pi^2/4$ is required because if one expands in powers of ϕ up to second order, the kinetic term $\frac{1}{2}\text{tr}(\partial_\mu \phi \partial^\mu \phi^\dagger)$ is obtained. Under the transformation of eq. (4.19) the Lagrangian is invariant

$$\mathcal{L}_{\text{eff}} = \frac{F_\pi^2}{4} \text{tr} \left(\Omega_R \partial_\mu U \Omega_L^{-1} \Omega_L \partial^\mu U^\dagger \Omega_R^{-1} \right) = \frac{F_\pi^2}{4} \text{tr} \left(\Omega_R^{-1} \Omega_R \partial_\mu U \partial^\mu U^\dagger \right) = \frac{F_\pi^2}{4} \text{tr} \left(\partial_\mu U \partial^\mu U^\dagger \right), \tag{4.23}$$

where we have used the cyclic property of the trace.

If one introduces the masses m_u and m_d to the theory, a term that explicitly breaks the chiral symmetry is added

$$\mathcal{L}_{\text{s.b.}} = \frac{F_0^2 B_0}{2} \text{tr} \left(M U^\dagger + U M \right), \quad M = \begin{pmatrix} m_u & 0 \\ 0 & m_d \end{pmatrix}, \tag{4.24}$$

where s.b. stands for "symmetry breaking" and F_0 and B_0 are two LECs. To leading order the massive effective Lagrangian reads

$$\mathcal{L}_{\text{eff}} = \frac{F_\pi^2}{4} \text{tr} \left(\partial_\mu U \partial^\mu U^\dagger \right) + \frac{F_0^2 B_0}{2} \text{tr} \left(M U^\dagger + U M \right). \tag{4.25}$$

For degenerate quark masses, $m_u = m_d \equiv m$, the LECs satisfy the following relations [37]

$$F_\pi = F_0 \left[1 + O \left(\frac{m}{\Lambda_{\text{QCD}}} \right) \right],$$

$$\langle 0 | \bar{q} q | 0 \rangle = -2 F_0^2 B_0 \left[1 + O \left(\frac{m}{\Lambda_{\text{QCD}}} \right) \right],$$

$$m_\pi = \sqrt{2 B_0 m} \left[1 + O \left(\frac{m}{\Lambda_{\text{QCD}}} \right) \right]. \tag{4.26}$$

In the chiral limit we obtain $F_\pi = F_0$. For $m \ll \Lambda_{\text{QCD}}$ eqs. (4.26) allow us to write $\mathcal{L}_{\text{eff}}$ in a more convenient way

$$\mathcal{L}_{\text{eff}} = \frac{F_\pi^2}{4} \text{tr} \left(\partial_\mu U \partial^\mu U^\dagger \right) + \frac{\Sigma}{4} \text{tr} \left(M U^\dagger + U M \right), \quad \Sigma \equiv - \langle 0 | \bar{q} q | 0 \rangle. \tag{4.27}$$

The effective Lagrangian can be formulated in terms of a normalized field $\vec{S}(x) \in \text{O}(4)$, $|\vec{S}(x)| = 1$ as well, since there is a local isomorphism between O(4) and $\text{SU}(2)_L \otimes \text{SU}(2)_R$. This is known as the non-linear σ model [38]. The symmetry breaking pattern takes the form

$$\text{O}(4) \to \text{O}(3) \quad \longleftrightarrow \quad \text{SU}(2)_L \otimes \text{SU}(2)_R \to \text{SU}(2). \tag{4.28}$$

In terms of the field $\vec{S}(x)$, the non-trivial $\mathcal{L}_{\text{eff}}$ term with the least number of derivatives reads

$$\mathcal{L}_{\text{eff}} = \frac{F_\pi^2}{2} \partial^\mu \vec{S} \cdot \partial_\mu \vec{S}. \tag{4.29}$$

Now, we introduce an external field $\vec{H}$ that explicitly breaks the symmetry by adding the term

$$\mathcal{L}_{\text{s.b.}} = -\Sigma \vec{H} \cdot \vec{S}, \tag{4.30}$$

where $\vec{H}$ plays the same role as a degenerate quark mass.

4.3 Regimes of Chiral Perturbation Theory

From eq. (4.27) we see that the leading order LECs are F_π, Σ. These constants can be determined through lattice QCD simulations. Still, one cannot simulate an infinite volume, so three regimes with finite volume in Euclidean space, $V = L^3 \times L_t$, have been established. For each one of them, the relation between the LECs can be different from the one that is shown in eqs. (4.26). Nevertheless, the values of these LECs are the same in all the regimes. Let us briefly review them:

- The *p-regime* consists of a large volume compared to the correlation length: $L, L_t \gg \xi = m_\pi^{-1}$. In this regime the finite volume corrections are suppressed by a factor proportional to $\exp(-m_\pi L)$, so eqs. (4.26) are valid [37].

- If $L, L_t \lesssim \xi$ we refer to the *ε-regime* [39]. Here the finite volume corrections cannot be neglected. In the ε-regime the chiral condensate has the following dependence on the LECs, m and the volume when $B_0 m L^2 \ll 1$ (see e.g. ref. [40])

$$\langle 0| \bar{q}q |0\rangle = -2F_0^2 B_0 \left(\frac{I_1'(F_0^2 B_0 mV)}{I_1(F_0^2 B_0 mV)} - \frac{1}{F_0^2 B_0 mV} \right), \tag{4.31}$$

where I_1 is the modified Bessel function of first kind of order one. Let us revise the infinite volume limit of this expression. For that purpose, we denote $x = F_0^2 B_0 mV$ and we use the asymptotic large x form of the modified Bessel functions (see e.g. ref. [28])

$$I_\nu(x) \sim \frac{e^x}{\sqrt{2\pi x}} \left(1 - \frac{4\nu^2 - 1}{8x} \right), \tag{4.32}$$

and therefore

$$\frac{I_1'(x)}{I_1(x)} - \frac{1}{x} \sim -\frac{15 - 30x + 16x^2}{6x - 16x^2}. \tag{4.33}$$

When $x \to \infty$ this expression converges to 1. Thus, the infinite volume limit of eq. (4.31) recovers $\langle 0| \bar{q}q |0\rangle = -2F_0^2 B_0$. On the other hand, we obtain the limit of $\langle 0| \bar{q}q |0\rangle$ when $m \to 0$ in a finite volume. To do so we use the following expressions for the modified Bessel functions and their derivatives

$$I_\nu(x) = \sum_{k=0}^{\infty} \frac{(x/2)^{\nu+2k}}{k!\Gamma(\nu+k+1)}, \quad I_\nu'(x) = I_{\nu-1}(x) - \frac{\nu}{x} I_\nu(x). \tag{4.34}$$

Then we have

$$\frac{I_1'}{I_1} - \frac{1}{x} = \frac{I_0(x) - \frac{1}{x}I_1(x)}{I_1(x)} - \frac{1}{x} = \frac{\sum_{k=0}^{\infty} \frac{(x/2)^{2k}}{k!\Gamma(k+1)}}{\sum_{l=0}^{\infty} \frac{(x/2)^{1+2l}}{l!\Gamma(l+2)}} - \frac{2}{x}$$

$$\underset{x\to 0}{\approx} \frac{\frac{1}{\Gamma(1)}}{\frac{(x/2)}{\Gamma(2)}} - \frac{2}{x} = 0. \tag{4.35}$$

Hence, we see that in the chiral limit $\langle 0| \bar{q}q |0\rangle$ vanishes. This is consistent with the fact that in finite volume there is no spontaneous symmetry breaking.

- Finally, the δ-*regime* is determined by a volume of size $V = L^3 \times L_t$, where the spatial volume is small, but the Euclidean time extent is large, that is $L \lesssim \xi \ll L_t$ [7].

The pion decay constant has been calculated in the p-regime and the ϵ-regime with three flavors several times, giving a result of $F_\pi = 92.1(9)$ MeV [2, 41–43]. On the other hand, the δ-regime is less explored; there F_π has been measured with two flavors obtaining $F_\pi = 78^{+14}_{-10}$ MeV [44].

The ϵ and δ-regime are useful from a technical point of view, because the small volume reduces the computing time of the simulations. In particular, in the δ-regime the fact that $L \lesssim \xi \ll L_t$ has several effects. First, in the chiral limit the pion does not become massless and instead there is a *residual mass* $m_\pi^R \neq 0$ (this is also true for the ϵ-regime). Another consequence is that there is approximately only one dimension, that enables us to treat the system as a quasi one dimensional field theory, *i.e.* quantum mechanics [7]. Then, since O(4) is locally isomorphic to SU(2)$\otimes$SU(2), if we consider again $\vec{S}(x) \in$ O(4), the system describes a particle moving in a unit 3-sphere $\mathbb{S}^3$ [38]. One can express m_π^R as the energy gap of a quantum rotor, which is given by

$$E_j = \frac{j(j + N - 2)}{2\Theta}, \tag{4.36}$$

where Θ is the moment of inertia and N refers to the group O(N). The value of Θ was computed in ref. [8] up to next-to-leading order, for a general dimension $d > 2$ and $N \geq 2$

$$\Theta = F_\pi^2 L^{d-1} \left[1 + \frac{N-2}{4\pi F_\pi^2 L^{d-2}} \left(2\frac{d-1}{d-2} + \cdots \right) \right], \tag{4.37}$$

The leading term had been calculated in ref. [7] for four dimensions already.

The residual pion mass is obtained by substituting $j = 1$ and $N = 4$ in eq. (4.36)

$$m_\pi^R = \frac{3}{2\Theta}. \tag{4.38}$$

In four dimensions we have

$$m_\pi^R = \frac{3}{2F_\pi^2 L^3 (1 + \Delta)}, \quad \Delta = \frac{0.477 \cdots}{(F_\pi L)^2} + \ldots, \quad d = 4. \tag{4.39}$$

Calculations of Δ up to $1/(F_\pi L)^4$ have been done in refs. [45, 46]. In two dimensions there is a divergence of the next-to-leading term, so instead we just consider the leading term, yielding

$$m_\pi^R \simeq \frac{3}{2F_\pi^2 L}, \quad d = 2. \tag{4.40}$$

This dimension has not been considered in this context, because there are no NGBs [47–49]. Still, at finite fermion mass the lightest particles are similar to quasi NGBs and we will refer to them as pions [50]. Note that when $d = 2$, F_π is dimensionless, since the mass has units of inverse of length.

We performed simulations of the two flavor Schwinger model in the δ-regime with the HMC algorithm. This allowed us to obtain m_π^R as a function of L, in order to verify the relation $m_\pi^R \propto 1/L$ and extract the value of F_π from eq. (4.40).

4.4 δ-regime simulation results

As in Chapter 3, we will denote $\beta = 1/g^2$. All the plots shown are in lattice units, *i.e.* the lattice constant a is set to 1. To make the lattice finer, we increment the value of β. Results

for $\beta = 2, 3$ and 4 were obtained through 10^3 measurements, separated by 10 sweeps. 500 sweeps were performed to thermalize the field configurations. It is important to mention that under gauge interaction the mass of the Wilson fermion undergoes renormalization, so it is necessary to measure a renormalized mass m, instead of using the input mass of the simulations. This can be achieved with the *Partial Conservation of Axial Current* (PCAC) relation (see e.g. Section 9.1.4 of [20])

$$\langle \partial_\mu A_\mu^a(x) P^a(0) \rangle = 2m \langle P^a(x) P^a(0) \rangle, \tag{4.41}$$

where A_μ^a is the *isovector axial current*, P^a is the *pseudoscalar density* and m the renormalized fermion mass

$$A_\mu^a(x) = \frac{1}{2} \overline{q}(x) \gamma_\mu \gamma_5 \sigma^a q(x),$$

$$P^a(x) = \frac{1}{2} \overline{q}(x) \gamma_5 \sigma^a q(x), \tag{4.42}$$

where σ^a denotes the Pauli matrices. Equation (4.41) partially restores the broken axial symmetry when $m = 0$. With the PCAC relation, we were able to measure the renormalized fermion mass m for different lattice sizes, and thus to express m_π as a function of m.

In figure 4.1 (a), m_π is shown as a function of the degenerate quark mass m for $L = 6$, $L_t = 64$ and $\beta = 4$. We see that close to the chiral limit, the value of m_π becomes very unstable, so one cannot simply measure m_π at $m = 0$. Instead one extrapolates the value to $m = 0$. However, that is easier to do with figure 4.1 (b), where m_π is plotted against $(m^2 g)^{1/3}$. A function of the form $y = \sqrt{a + b\,x^3}$, where $x = (m^2 g)^{1/3}$ and a and b are fit parameters, was fitted to extrapolate to m_π^R. Many attempts with functions of the form $y = \sqrt{a + b\,x^c}$ and $y = a + bx^c$ were performed. The best results were obtained by taking $c = 3$ in the former expression. We do not have an explanation for this behavior, but it works best to infer m_π^R. We observe that in figure 4.1 (a) there are results for negative fermion mass. In the simulation both signs of the mass are measured, but the negative values do not have physical meaning and they were ignored in the extrapolations.

This same procedure was performed for different L between 5 and 12 and $L_t = 64$. In figure 4.2 we show plots of m_π vs. $(m^2 g)^{1/3}$ for $\beta = 2$, in figure 4.3 for $\beta = 3$ and in figure 4.4 for $\beta = 4$.

Finally, we plot m_π^R as a function of L and fit a function of the form $3/(2LF_\pi^2)$, see figures 4.5, 4.6 and 4.7.
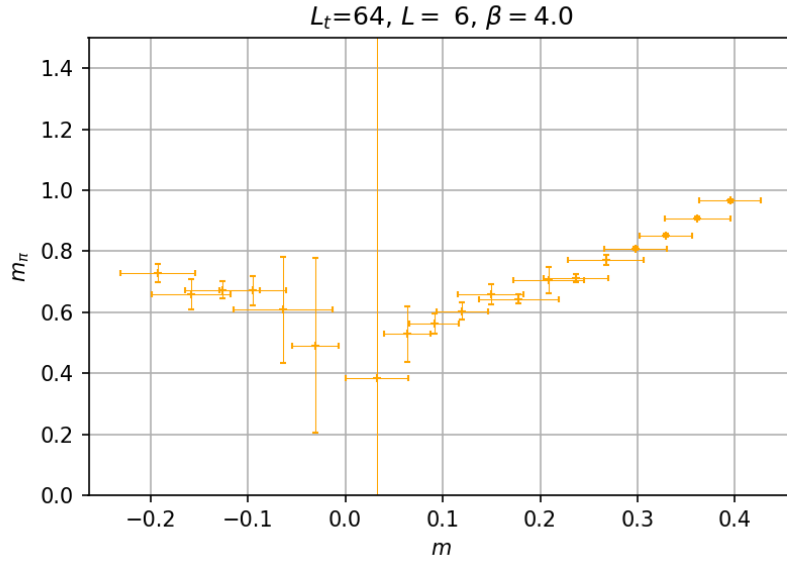
(a) m_π vs. m. We see that near $m = 0$ the pion mass result is plagued by large errors.
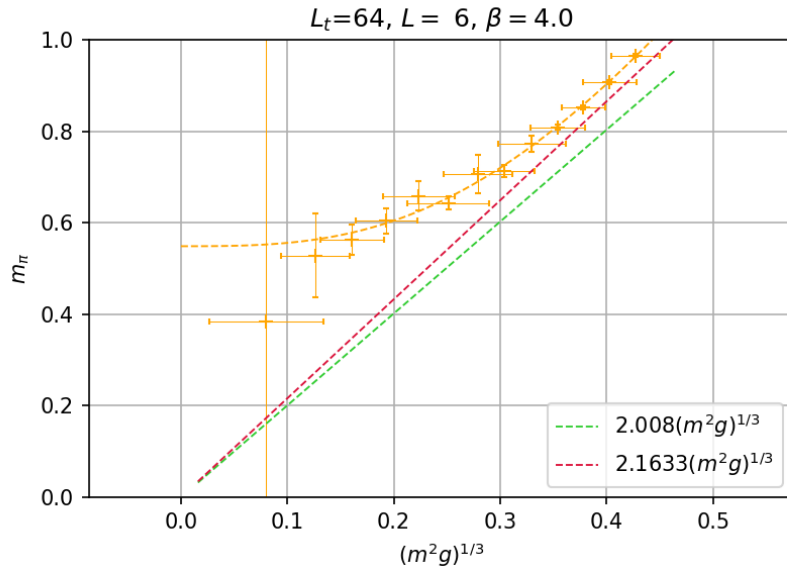
(b) m_π vs. $(m^2 g)^{1/3}$. We fit a function of the form $m_\pi^R = \sqrt{a + b\, m^2 g}$ to obtain the value of the residual pion mass: $m_\pi^R = 0.549(12)$. The predictions for m_π in infinite volume, mentioned in Chapter 3, are shown for comparison.

Figure 4.1: Results of m_π and m. Note that there are also values for $m < 0$, but they are unphysical. However, in the simulation both signs of the mass are measured. In the lower plot only $m > 0$ was considered. The errors were computed by using the *jackknife method*, see Appendix C.
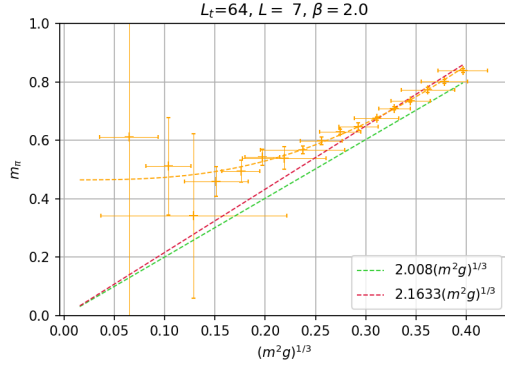
(a) m_π vs. $(m^2 g)^{1/3}$ for $L = 7$. $m_\pi^R =0.4645(72)$
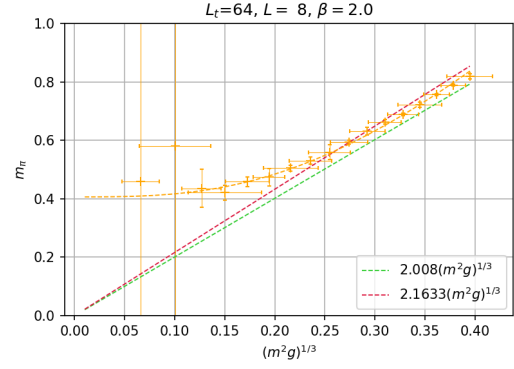
(b) m_π vs. $(m^2 g)^{1/3}$ for $L = 8$. $m_\pi^R =0.4063(45)$
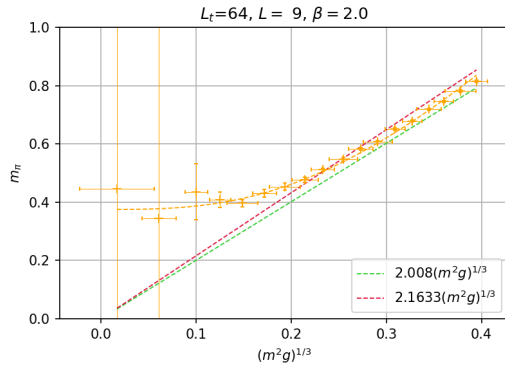
(c) m_π vs. $(m^2 g)^{1/3}$ for $L = 9$. $m_\pi^R =0.3749(47)$
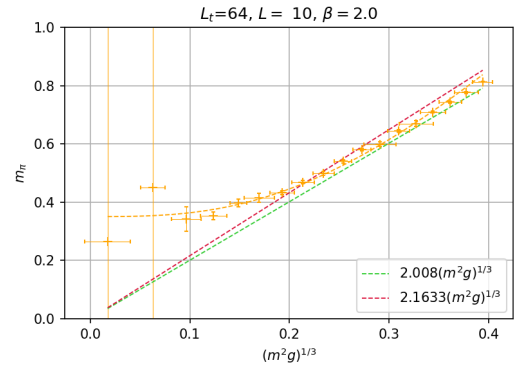
(d) m_π vs. $(m^2 g)^{1/3}$ for $L = 10$. $m_\pi^R =0.3505(58)$
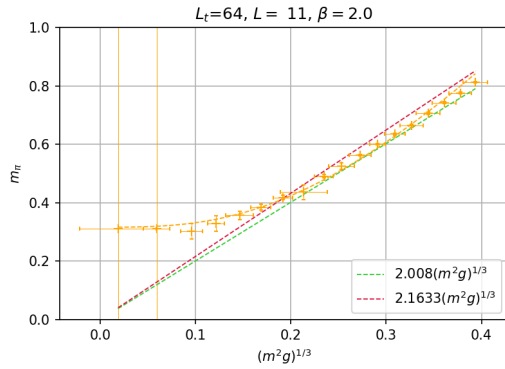
(e) m_π vs. $(m^2 g)^{1/3}$ for $L = 11$. $m_\pi^R =0.3163(59)$
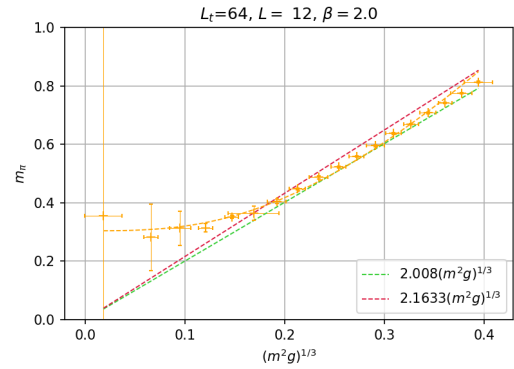
(f) m_π vs. $(m^2 g)^{1/3}$ for $L = 12$. $m_\pi^R =0.3040(51)$

Figure 4.2: Results for $\beta = 2$. Each value of m_π and m was obtained by averaging 10^3 measurements of different configurations. Between each configuration used, 10 sweeps were performed. All the fits were made with gnuplot.
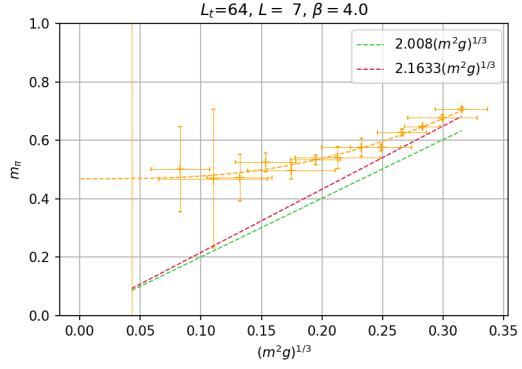
(a) m_π vs. $(m^2 g)^{1/3}$ for $L = 7$. $m_\pi^R = 0.4639(103)$

(b) m_π vs. $(m^2 g)^{1/3}$ for $L = 8$. $m_\pi^R = 0.4057(58)$

(c) m_π vs. $(m^2 g)^{1/3}$ for $L = 9$. $m_\pi^R = 0.3722(29)$

(d) m_π vs. $(m^2 g)^{1/3}$ for $L = 10$. $m_\pi^R = 0.3437(42)$

(e) m_π vs. $(m^2 g)^{1/3}$ for $L = 11$. $m_\pi^R = 0.3104(30)$

(f) m_π vs. $(m^2 g)^{1/3}$ for $L = 12$. $m_\pi^R = 0.2832(51)$
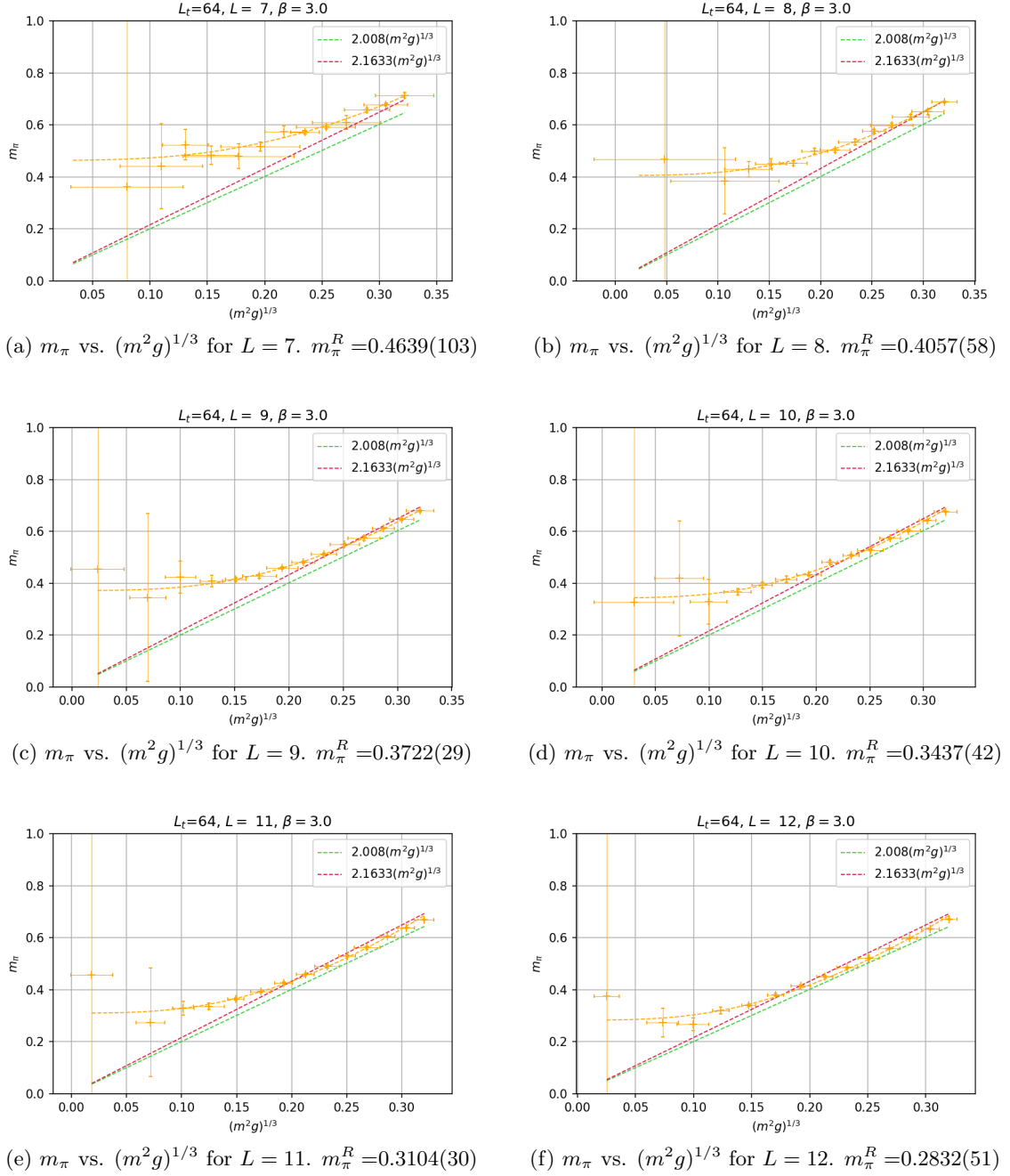
Figure 4.3: Results for $\beta = 3$. Each value of m_π and m was obtained by averaging 10^3 measurements of different configurations. Between each configuration used, 10 sweeps were performed.
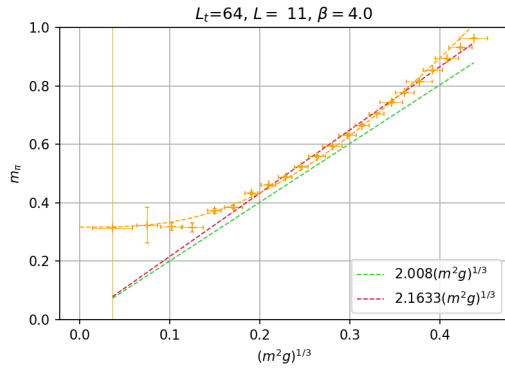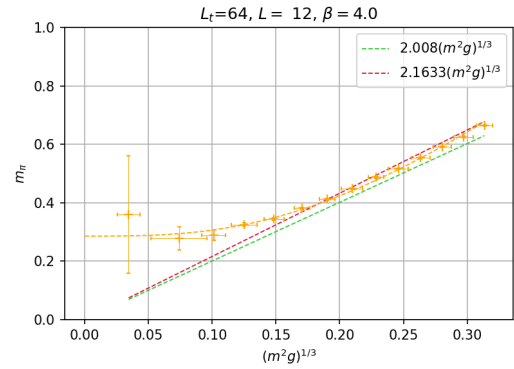
(a) m_π vs. $(m^2 g)^{1/3}$ for $L = 7$. $m_\pi^R = 0.4684(75)$
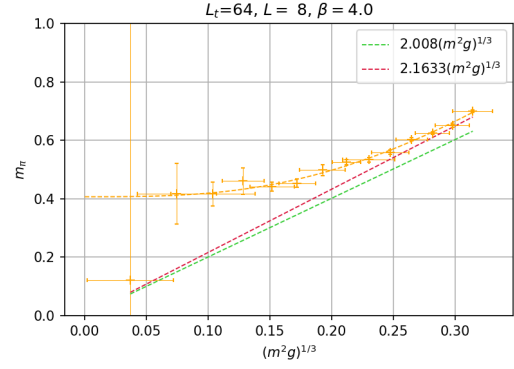
(b) m_π vs. $(m^2 g)^{1/3}$ for $L = 8$. $m_\pi^R = 0.4068(63)$
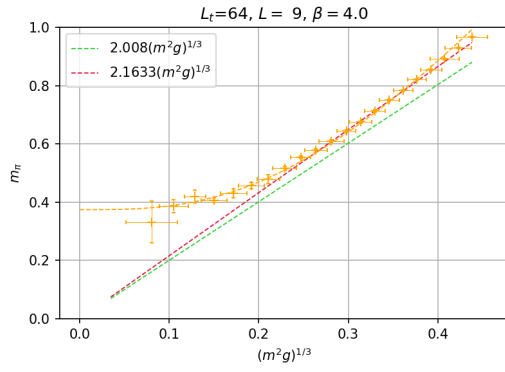
(c) m_π vs. $(m^2 g)^{1/3}$ for $L = 9$. $m_\pi^R = 0.3741(40)$
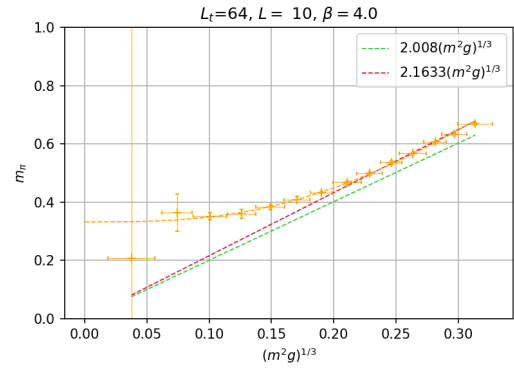
(d) m_π vs. $(m^2 g)^{1/3}$ for $L = 10$. $m_\pi^R = 0.3323(22)$

(e) m_π vs. $(m^2 g)^{1/3}$ for $L = 11$. $m_\pi^R = 0.3167(54)$

(f) m_π vs. $(m^2 g)^{1/3}$ for $L = 12$. $m_\pi^R = 0.2857(41)$

Figure 4.4: Results for $\beta = 4$. Each value of m_π and m was obtained by averaging 10^3 measurements of different configurations. Between each configuration used, 10 sweeps were performed.
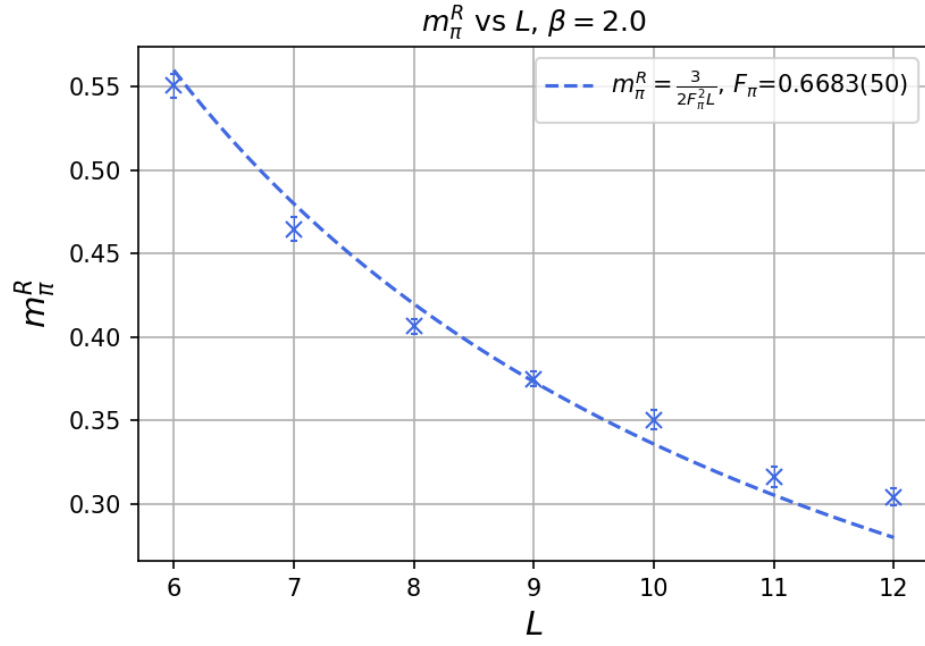
Figure 4.5: Behavior of m_π^R vs. L for $\beta = 2$. The dashed line is a fit of a function of the form $m_\pi^R = a/L$. The chi-square per degree of freedom is $\chi_\nu^2 = 7.932$.
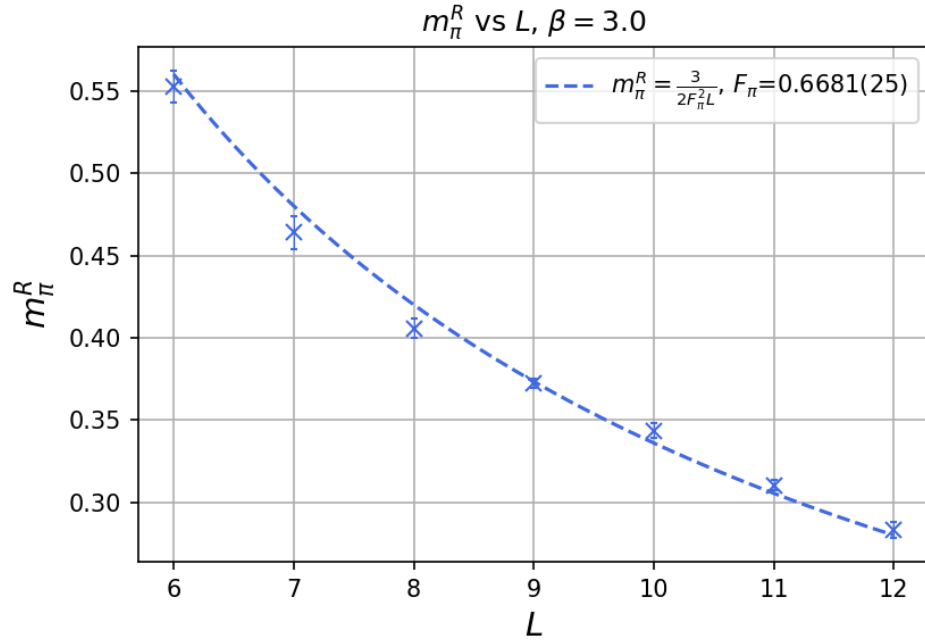

Figure 4.6: Behavior of m_π^R vs. L for $\beta = 3$. The chi-square per degree of freedom is $\chi_\nu^2 = 2.581$.
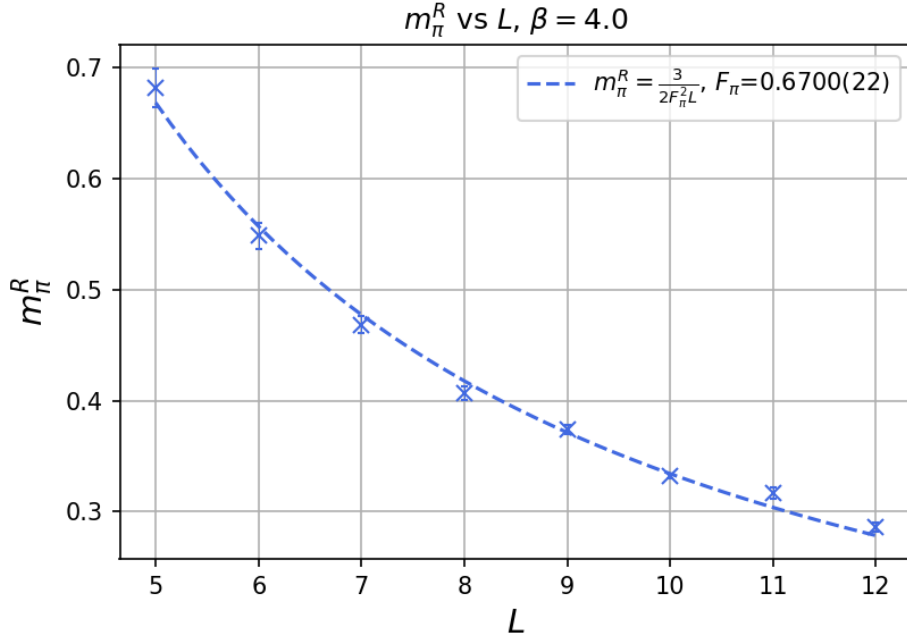
Figure 4.7: Behavior of m_π^R vs. L for $\beta = 4$. $\chi_\nu^2 = 2.213$. We can see that the data matches well the relation of $1/L$ described in eq. (4.40).

From figures 4.5, 4.6 and 4.7 we see that indeed $m_\pi^R \propto 1/L$, as we conjectured for the δ-regime. This can be best seen for $\beta = 4$, because the lattice is finer than for $\beta = 2, 3$ and as a consequence there are less lattice artifacts. Still, for $\beta = 2, 3$ the $1/L$ relation is noticeable. For all the β values that we used, we see that when L becomes large, m_π^R vanishes, as it should do for an infinite volume. From the fits we were able to extract F_π (see table 4.1).

β	2	3	4
F_π	0.6683(50)	0.6681(25)	0.6700(22)

Table 4.1: Pion decay constant for different values of β.

For $\beta = 4$ the error and χ_ν^2 are the smallest. Again, this is due to the fact that there are less lattice artifacts. In order to determine F_π in the continuum, one has to extrapolate to $\beta \to \infty$. However, in this case we observe that for the β values that we used, the results are the same within errors. Then, in principle we could use F_π for $\beta = 4$ as our final result. Still, the measurements could be not so well decorrelated and we have to analyze their autocorrelation time (see Appendix D for the definition) first.

We measured the autocorrelation time of the topological charge Q (see Chapter 5 for a definition of the topological charge), because this quantity tends to be the one with the highest autocorrelation. In figures 4.8, 4.9 and 4.10 we show the number of Monte Carlo configurations sorted according to each topological sector, for simulations with different masses. We see that the distribution of Q obeys approximately a Gaussian relation and, in most cases, it is compatible with $\langle Q \rangle = 0$. The exponential autocorrelation time $\tau_{\exp}$ and the integrated autocorrelation time τ_{int} with respect to Q are shown in figures 4.11, 4.12 and 4.13. In some plots (e.g. figures 4.12 (b), (c), (e), (f) and 4.13 (d), (f)) we see that close to $m = 0$, the autocorrelation time has a peak. In some other plots, $\tau_{\exp}$ and τ_{int} are scattered. We also observe that in general τ_{int} is more stable than $\tau_{\exp}$, since the procedure to measure it is more systematic and does not rely on a fit.

For $\beta = 2$, the autocorrelation time does not have a peak and in most cases it is below 2.5, which is a good sign of decorrelation. In a few cases, the exponential autocorrelation time reaches values larger than 2.5, for instance in figure 4.11 (a) and (b). In those situations, it is very likely that $\tau_{\exp}$ was not properly determined by fitting eq. (D.2). For $\beta = 3$, $\tau_{\exp}$ and τ_{int} increase close to $m = 0$, but their maximum values remain below 4.

For $\beta = 4$, $\tau_{\exp}$ and τ_{int} reach maximum values beyond 14, which implies that for this fine lattice the number of sweeps between each measurement should be increased in order to suppress correlations, although that also increases significantly the computing time of the simulations. Given the autocorrelation times obtained with $\beta = 4$, we do not take the value of F_π corresponding to this β and instead we take an average of the values obtained for F_π
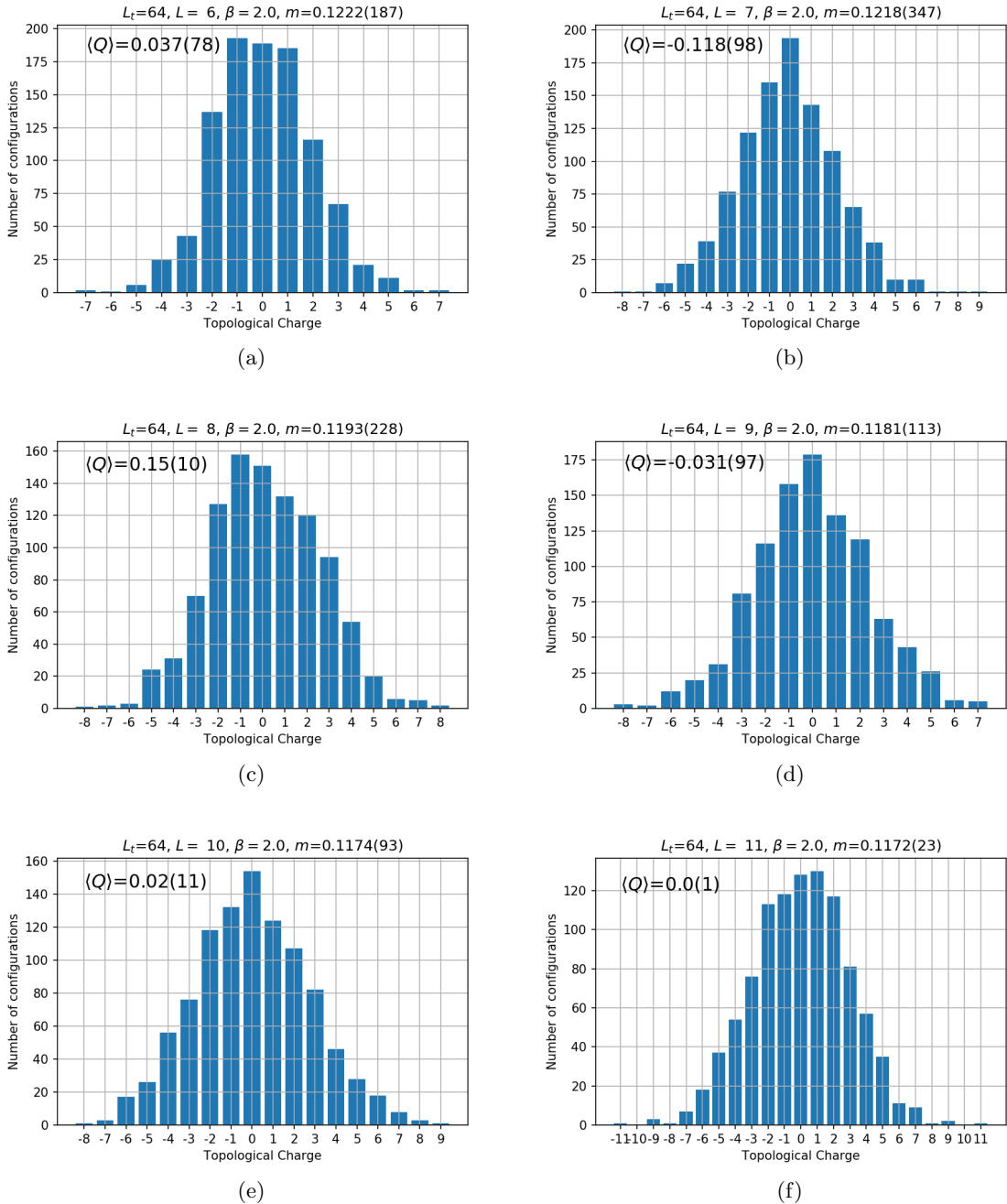
$$F_\pi = 0.6688(5). \tag{4.43}$$

Figure 4.8: Topological charge distribution for different lattices and fermion mass, $\beta = 2$.

Figure 4.9: Topological charge distribution for different lattices and fermion mass, $\beta = 3$. In figure (e) the value of $\langle Q \rangle$ is four sigmas deviated from 0, so it is not compatible with zero.
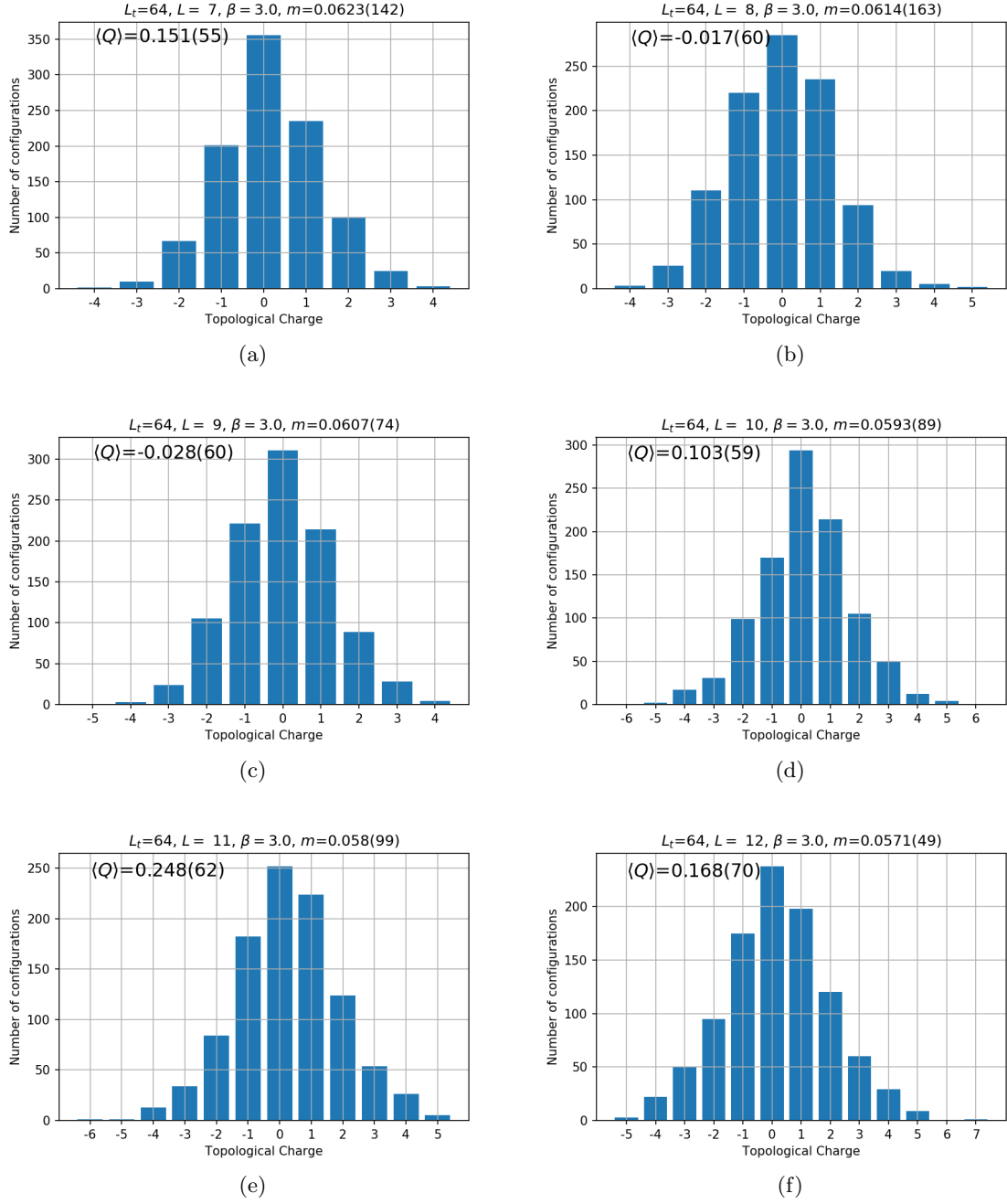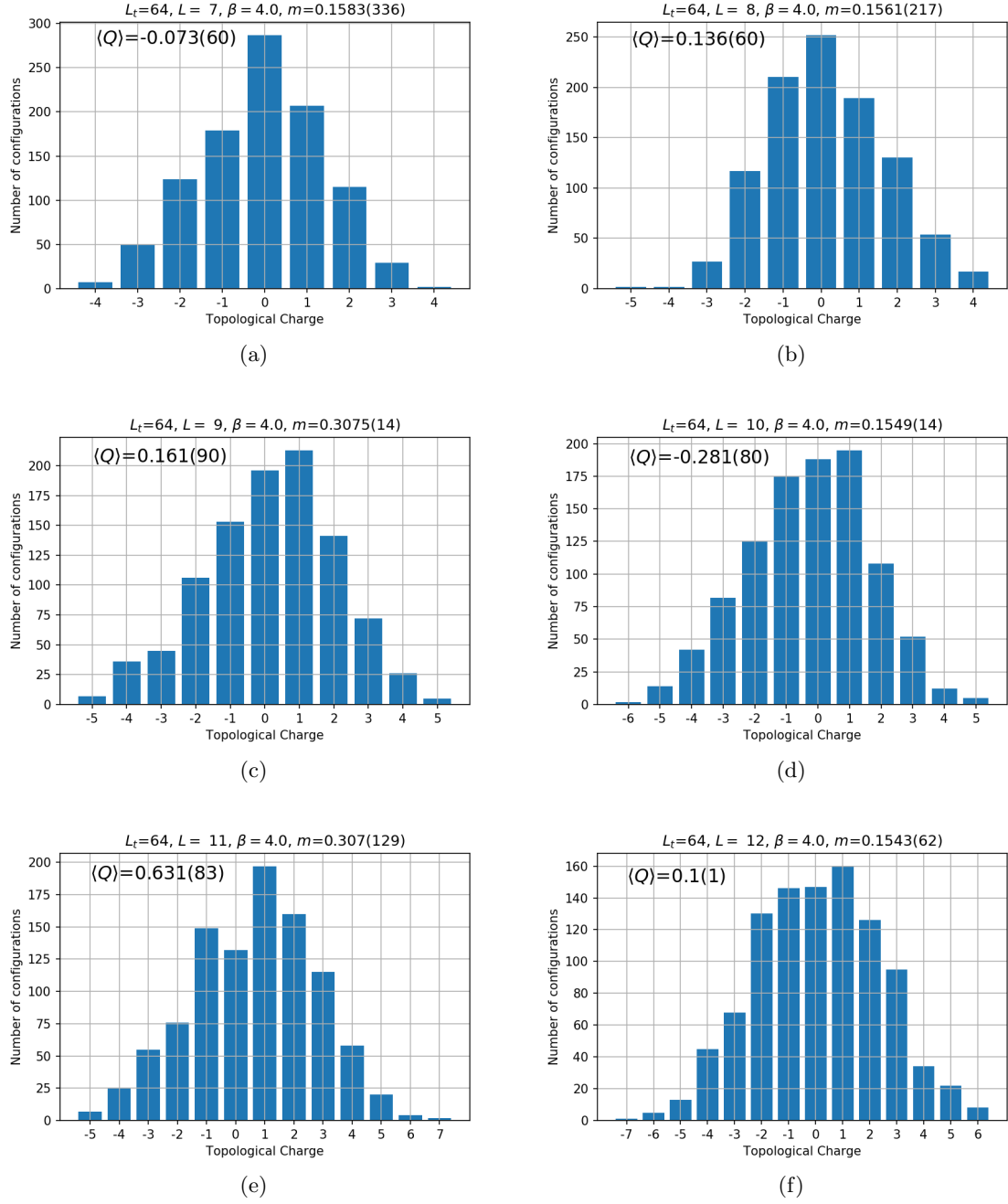
Figure 4.10: Topological charge distribution for different lattices and fermion mass, $\beta = 4$. In figure (e) the value of $\langle Q \rangle$ is 7.6 sigmas deviated from 0, so it is not compatible with zero. This is an effect of the autocorrelation of the measurements.
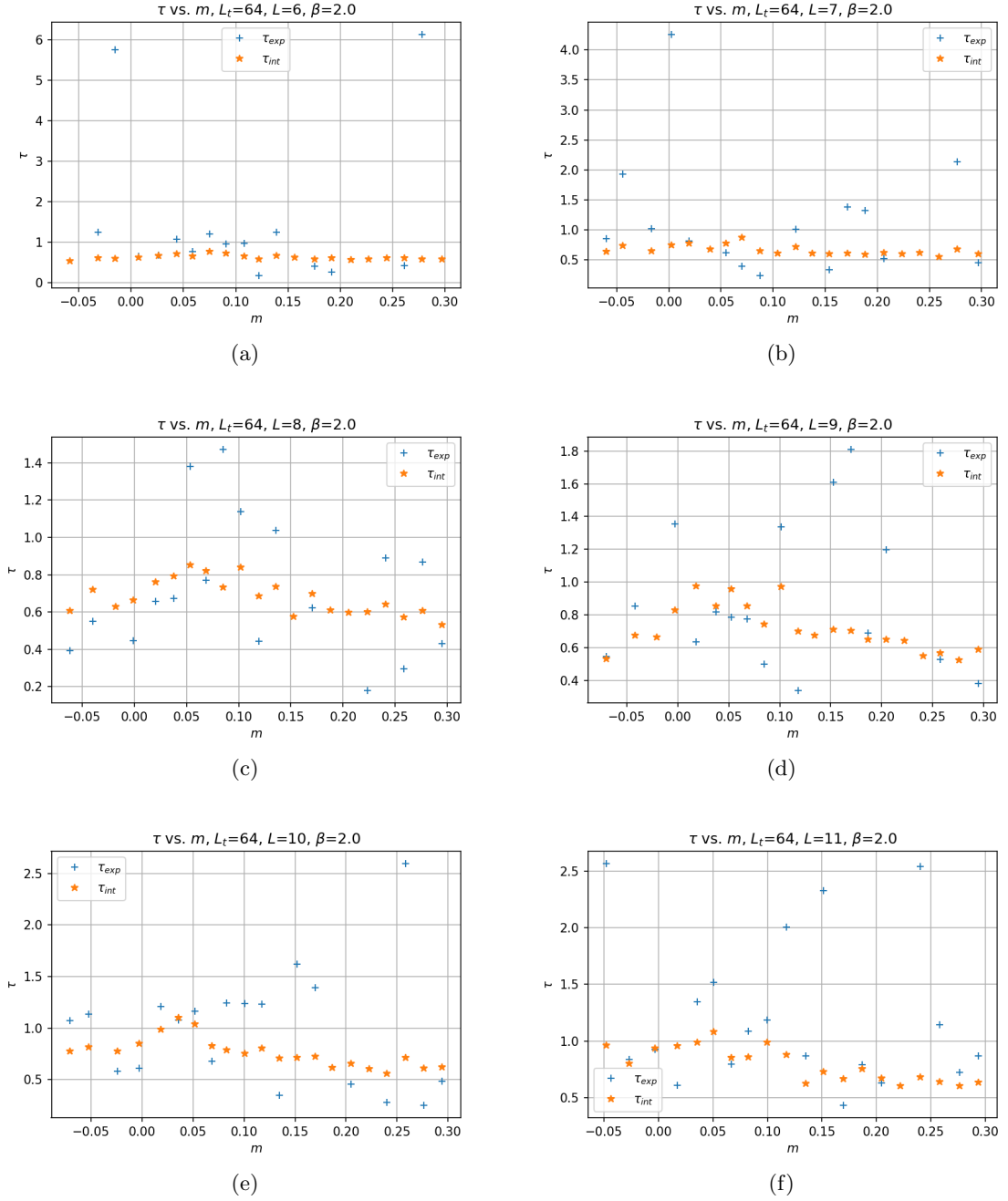
Figure 4.11: Exponential and integrated autocorrelation time of the topological charge for different lattices, $\beta = 2$.
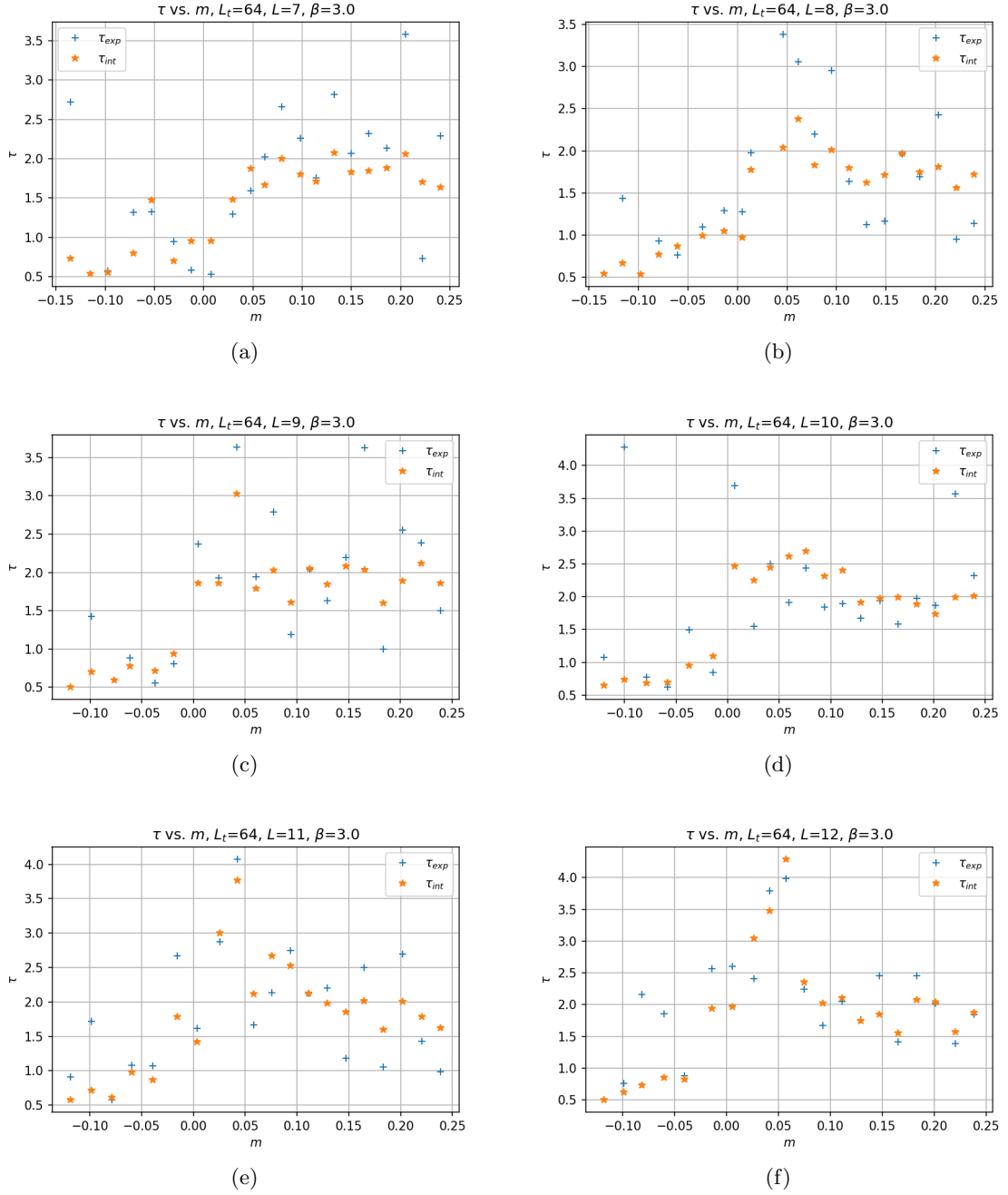
Figure 4.12: Exponential and integrated autocorrelation time of the topological charge for different lattices, $\beta = 3$.
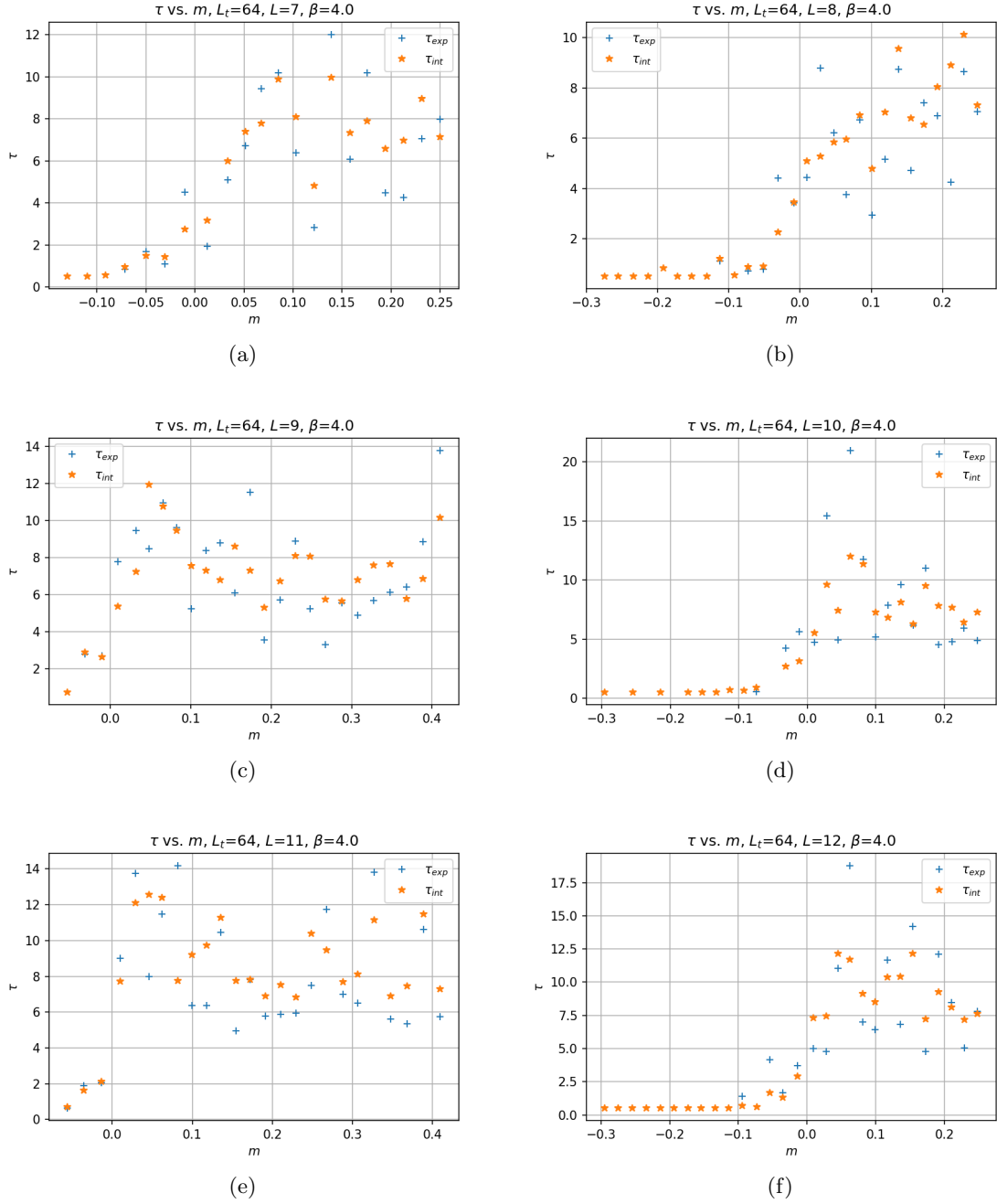
Figure 4.13: Exponential and integrated autocorrelation time of the topological charge for different lattices, $\beta = 4$.

Chapter 5

The Witten-Veneziano formula

In this chapter we compute the decay constant of the η meson, F_η, in two dimensions and attempt to make a connection to the value of F_π that we measured in the previous chapter. To do so we rely on the Witten-Veneziano formula [9, 10], which in 3-flavor QCD relates the mass of the η' meson with m_η, m_K, F_π and the quenched *topological susceptibility* χ_T^{que}, defined below. This formula is obtained by taking the *'t Hooft limit* of a $1/N_c$ expansion, where N_c is the number of colors. In this limit one considers $N_c \to \infty$ and $g_s \to 0$, while leaving the product $g^2 = g_s^2 N_c$ finite (g_s is the strong coupling constant).

In theory one introduces two η mesons, with the valence quark composition

$$\eta_1 = \frac{1}{\sqrt{3}} \left(\overline{u}u + \overline{d}d + \overline{s}s \right), \quad \eta_8 = \frac{1}{\sqrt{6}} \left(\overline{u}u + \overline{d}d - 2\overline{s}s \right). \tag{5.1}$$

η_1 is a flavor singlet and η_8 belongs to an octet of states. In nature one observes the particles η and η', which are mixed by an angle θ_P

$$\begin{pmatrix} \eta \\ \eta' \end{pmatrix} = \begin{pmatrix} \cos\theta_P & -\sin\theta_P \\ \sin\theta_P & \cos\theta_P \end{pmatrix} \begin{pmatrix} \eta_8 \\ \eta_1 \end{pmatrix}. \tag{5.2}$$

Since the measured value of θ_P is small, $\theta_P = -11.3°$ [33], we have

$$\eta \approx \frac{1}{\sqrt{6}} \left(\overline{u}u + \overline{d}d - 2\overline{s}s \right), \quad \eta' \approx \frac{1}{\sqrt{3}} \left(\overline{u}u + \overline{d}d + \overline{s}s \right). \tag{5.3}$$

Veneziano [10] obtained the following formula by taking into account the three lightest quark flavors and assuming $m_u = m_d = 0$ and $m_s > 0$ to order $1/N_c$

$$m_{\eta'}^2 + m_\eta^2 - 2m_K^2 = \frac{6}{F_{\eta'}^2} \chi_T^{\text{que}}. \tag{5.4}$$

where $F_{\eta'}$ is the decay constant of the meson η' and "que" stands for quenched, *i.e.* its value when the degenerate fermion mass $m \to \infty$. In the chiral limit we obtain the formula deduced by Witten

$$m_{\eta'}^2 = \frac{6}{F_{\eta'}^2} \chi_T^{\text{que}}. \tag{5.5}$$

To lowest order in a $1/N_c$ expansion, we have $F_{\eta'} = F_\pi$ [9]. This leads to the question if this relation between the decay constants holds in the Schwinger model. In general, the literature refers to eq. (5.4) or (5.5), as the Witten-Veneziano formula.

In the two-flavor Schwinger model, in the limit of massless fermions, eq. (5.4) is simplified to[1] [51, 52]

$$m_\eta^2 = \frac{2N}{F_\eta^2} \chi_T^{\text{que}}, \tag{5.6}$$

where N is the number of flavors. We compute F_η in the Schwinger model with eq. (5.6) and based on the result we verify whether the relation $F_\eta \simeq F_\pi$ holds. This would also enable us to determine F_π by an independent method that does not involve the δ-regime.

The topological susceptibility χ_T is defined for the Euclidean Schwinger model in the continuum as

$$\chi_T = \int d^2x \left(\langle q(x)q(0) \rangle - \langle q(x) \rangle \langle q(0) \rangle \right), \tag{5.7}$$

where

$$q(x) = \frac{g}{4\pi} \epsilon_{\mu\nu} F_{\mu\nu}(x) = \frac{g}{2\pi} F_{12}(x) \tag{5.8}$$

is the *topological charge density*. With $q(x)$ we define the *topological charge* as

$$Q = \int d^2x \, q(x) \in \mathbb{Z}. \tag{5.9}$$

We can formulate χ_T in terms of Q as well

$$\chi_T = \frac{\langle Q^2 \rangle - \langle Q \rangle^2}{V}, \tag{5.10}$$

where V is the space-time volume. An important property of the topological charge is that it is an integer number. We can see that fact if we rewrite $q(x)$ as a total divergence

$$q(x) = \partial_\mu \Omega_\mu(x), \quad \Omega_\mu(x) = \frac{g}{2\pi} \epsilon_{\mu\nu} A_\nu(x). \tag{5.11}$$

If we consider field configurations of finite action, $F_{\mu\nu}(x)$ has to vanish at infinity, so the gauge field must be gauge equivalent to 0 when $|x| \to \infty$

$$0 = A'_\mu(x) = A_\mu(x) - \frac{1}{g} \partial_\mu \varphi(x). \tag{5.12}$$

Then

$$Q = \int d^2x \, \partial_\mu \left(\frac{g}{2\pi} \epsilon_{\mu\nu} \frac{1}{g} \partial_\nu \varphi(x) \right) = \frac{1}{2\pi} \int_{\partial V} d\sigma_\mu \, \epsilon_{\mu\nu} \partial_\nu \varphi(x), \tag{5.13}$$

where we have used the Gauss theorem and where we assume ∂V to be the boundary of a large volume in $\mathbb{R}^2$. Now, if we consider a circumference of length L, we identify Q with the following integral

$$\lim_{L \to \infty} \frac{1}{2\pi i} \int_0^L dx \, U^*(x) \partial_x U(x), \quad \text{where} \quad U(x) = e^{i\varphi(x)}, \quad U(L) = U(0). \tag{5.14}$$

This expression is equal to

$$\frac{1}{2\pi} \left[\varphi(L) - \varphi(0) \right] = n \in \mathbb{Z}, \tag{5.15}$$

hence Q is an integer.

---

[1]One can make an analogy of the flavor singlet of the two-flavor Schwinger model, $(\overline{u}u + \overline{d}d)/\sqrt{2}$, with the singlet η_1 of QCD. Since η_1 is close to η', in the literature they often refer to the flavor singlet of the two-flavor Schwinger model as η' [51, 52]. However, it is not the actual η' particle from QCD and for simplicity we will denote it as η.

As we mentioned in Chapter 3, we can relate m_η with the gauge coupling as follows

$$m_\eta^2 = N \frac{g^2}{\pi}. \tag{5.16}$$

Thus, by determining χ_T^{que} we obtain a value for F_η. According to refs. [51, 52], the theoretical expression for χ_T^{que} in infinite volume and in the continuum is

$$\chi_T^{\text{que}} = \frac{g^2}{4\pi^2} \simeq 0.0253\, g^2. \tag{5.17}$$

This implies that theoretically $F_\eta = 0.3989$. This result was also deduced in ref. [53].

To numerically measure the topological susceptibility by using lattice simulations we have to discretize the topological charge density. This can be done most easily through the plaquette variables defined in Chapter 2. From eq. (2.94), we know that for a small lattice spacing a, the plaquette variables have the following expression

$$U_{\mu\nu}(\vec{n}) = e^{iga^2 F_{\mu\nu}(\vec{n})}, \quad F_{\mu\nu}(\vec{n}) = -\frac{i}{ga^2} \ln U_{\mu\nu}(\vec{n}). \tag{5.18}$$

That way, we have

$$q(\vec{n}) = -\frac{i}{2\pi a^2} \ln U_{12}(\vec{n}) \tag{5.19}$$

and

$$Q = \sum_{\vec{n}} a^2 q(\vec{n}), \tag{5.20}$$

where the sum runs over all lattice sites $\{\vec{n} = (n_1, n_2) \mid n_\mu = 0, 1, \ldots, N_\mu - 1; \mu = 1, 2\}$.

The lattice configurations generated through Monte Carlo algorithms are sorted in different sectors, where each one is characterized by a topological charge. Furthermore, there is evidence (see e.g. refs. [54, 55]) that the distribution of these configurations corresponds approximately to a Gaussian function. Due to parity symmetry, we also have

$$\langle Q \rangle = 0. \tag{5.21}$$

Then, one can calculate χ_T on the lattice using the following weighted average

$$\chi_T = \frac{\sum_Q Q^2 N_Q}{V \sum_Q N_Q}, \tag{5.22}$$

where N_Q are the number of configurations in the topological sector labeled by Q.

In Chapter 5 we have shown the histograms for Q obtained with simulations for several lattice sizes, using low statistics (10^3 measurements separated by 10 sweeps). We attempted to compute the topological susceptibility using those results. Unfortunately, even though the topological charge is compatible with $\langle Q \rangle = 0$, χ_T as a function of the fermion mass m does not have a clear behavior, see for instance figure 5.1. This does not allow us to perform a fit and to extrapolate to the quenched value of χ_T. Usually the autocorrelation time for Q is larger than with other observables. Separating the measurements by 10 sweeps could be enough to decorrelate other observables, but here we see that it affects the result of χ_T. For that reason, we incremented the number of measurements to 10^4, separated by 100 sweeps, and simulated a 10×64 lattice for $\beta = 4$. This improved the results. In figure 5.2 we show the distribution of the configurations and in figure 5.3 we show the topological susceptibility as a function of the degenerate fermion mass. We used two functions to extrapolate χ_T, from their average we obtain

$$\chi_T^{\text{que}} \beta = 0.029(1). \tag{5.23}$$

This result is in agreement with ref. [56], which reported $\chi_T^{\text{que}}\beta = 0.0300(8)$ at $\beta = 4$, and with our quenched simulations $\chi_T^{\text{que}}\beta = 0.0304(2)$ (see below).

Now, we substitute eq. (5.16) in eq. (5.6) and solve for F_η

$$F_\eta^2 = \chi_T^{\text{que}} \frac{2\pi}{g^2}. \tag{5.24}$$

Using the result in eq. (5.23) yields

$$F_\eta = 0.4243(76). \tag{5.25}$$

To check the lattice artifacts of this quantity, we compute F_η for more values of β.
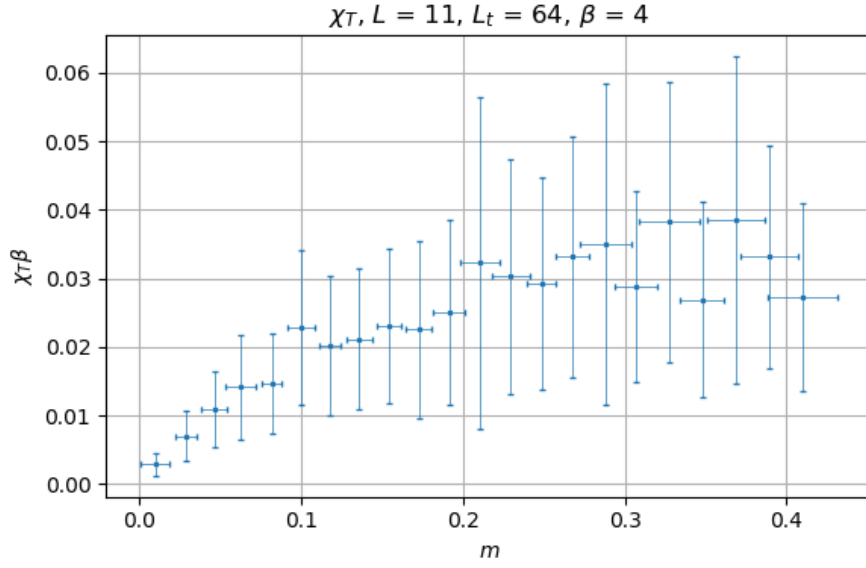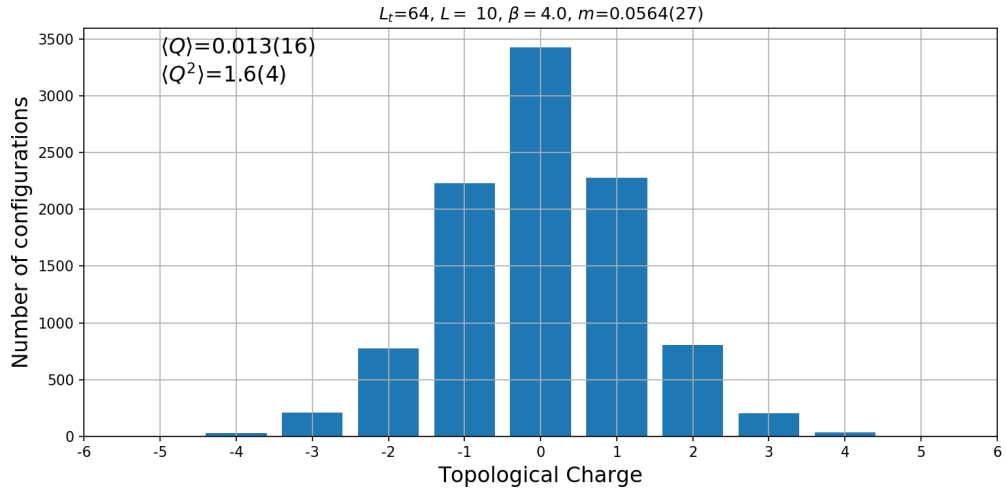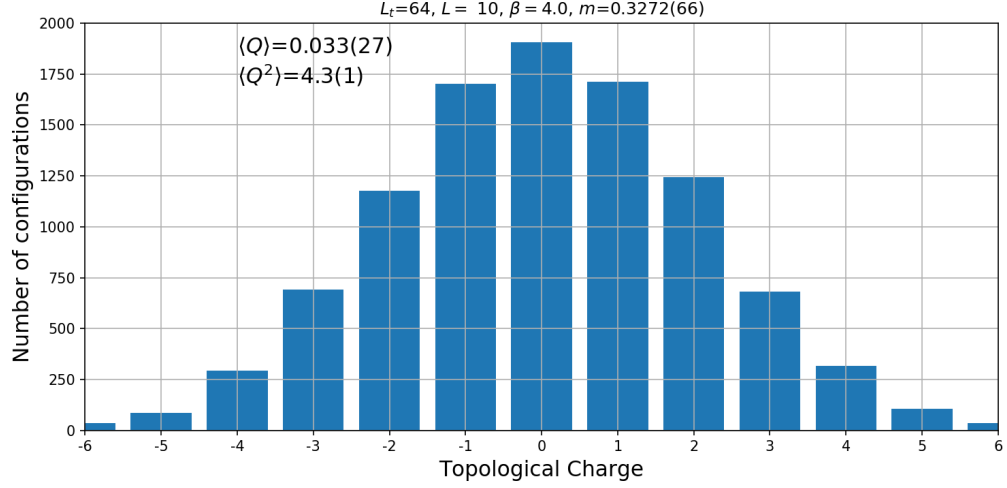

Figure 5.1: Topological susceptibility as a function of the fermion mass m, computed for 10^3 measurements with 10 sweeps between each of them on a 11×64 lattice. χ_T does not have a clear behavior for this number of measurements.

(a) Configurations sorted by their topological charge for $m = 0.0564(27)$.

(b) Configurations sorted by their topological charge for $m = 0.3272(66)$.

Figure 5.2: Distribution of the Monte Carlo configurations in different topological sectors for $\beta = 4$. We see approximately a Gaussian distribution. m denotes the degenerate PCAC fermion mass. When the mass is smaller, the configurations occupy less topological sectors.
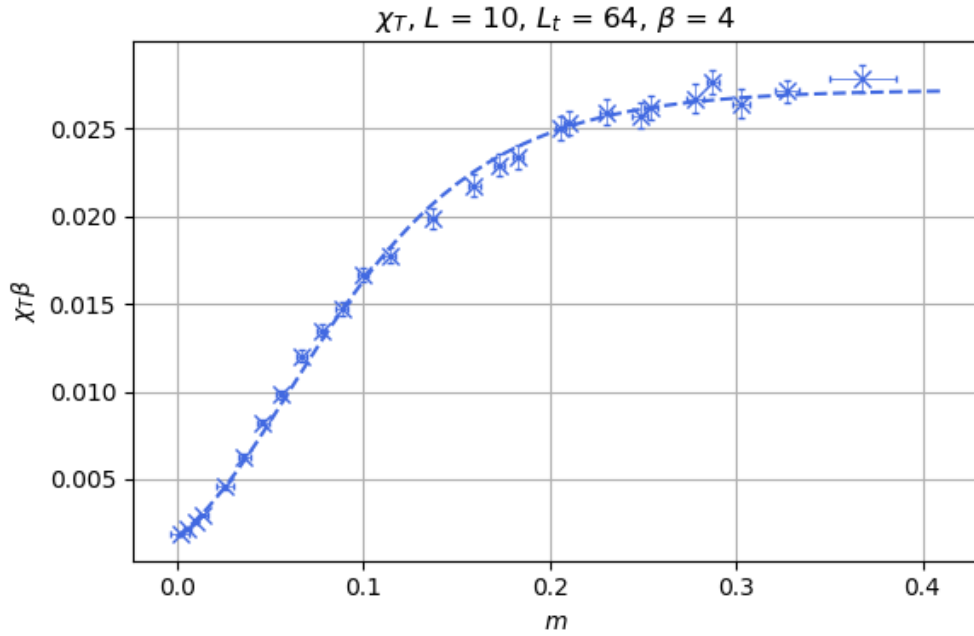
(a) A function of the form $y = ae^{-be^{-cx}}$ was fitted to the data.

(b) We also fitted a function of the form $y = \frac{a+bx+cx^2}{d+fx+gx^2}$.

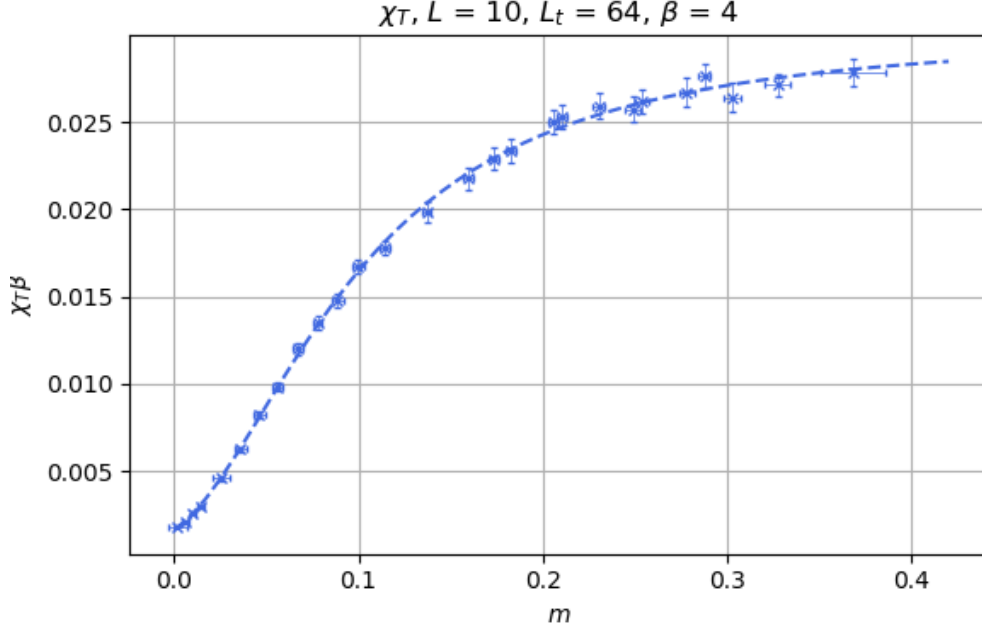Figure 5.3: Topological susceptibility as a function of the degenerate fermion mass obtained with 10^4 measurements. The plots are in lattice unites. We performed two fits in order to extract the value of χ_T when $m \to \infty$. The results yield $\chi_T^{\text{que}}/g^2 = \chi_T^{\text{que}}\beta = 0.029(1)$.

To do so, we performed more simulations to determine χ_T in the quenched approximation by working with pure gauge theory, *i.e.* by generating Monte Carlo configurations using only the gauge action

$$S_G = \frac{1}{4} \int d^4x \, F_{\mu\nu}F_{\mu\nu}. \tag{5.26}$$

This is more convenient than extrapolating χ_T to infinite m, because the simulations are faster and they yield results for $m \to \infty$. Still, the extrapolation of χ_T to infinite m works as a cross-check with the results of $\beta = 4$ that we obtain with the quenched simulations.

In figure 5.4, we show $\chi_T^{\text{que}}\beta$ for different lattices of dimension $L \times L$ and $\beta = 2, 3, 4, 5, 6, 7$ and 8. We took 10^4 measurements separated by 10 sweeps for $\beta = 2$ and 3; 10^4 measurements separated by 100 sweeps for $\beta = 4$ and 5 and 10^4 measurements separated by 10^3 sweeps for $\beta = 6, 7$ and 8. In table 5.1 we show $\chi_T^{\text{que}}\beta$ for the different β values that we simulated, together with F_η computed with the Witten-Veneziano formula.

| β	$\chi_T^{\text{que}}\beta$	F_η
2	0.0389(2)	0.495(1)
3	0.0335(3)	0.459(2)
4	0.0304(2)	0.437(1)
5	0.0285(4)	0.423(3)
6	0.0283(4)	0.422(2)
7	0.0261(11)	0.404(9)
8	0.0256(19)	0.399(15)

Table 5.1: Results of $\chi_T^{\text{que}}\beta$ and F_η for different β values obtained with pure gauge theory simulations.

We observe that $\chi_T^{\mathrm{que}}\beta$ still depends on β. As β increases, $\chi_T^{\mathrm{que}}\beta$ decreases monotonically. For $\beta = 4$ the number that we obtain by means of the quenched simulations is compatible, within errors, with the large m extrapolation that we performed before. In figure 5.5, we show a comparison of our results for $\chi_T^{\mathrm{que}}\beta$ with the values of refs. [52, 56]. Since $\chi_T^{\mathrm{que}}\beta$ is not independent of β, F_η also has lattice artifacts. We can perform an extrapolation to the continuum limit by fitting the ansatz $\chi_T^{\mathrm{que}}\beta = a + b/\beta$, where a and b are fit parameters, in order to determine F_η. The extrapolation yields

$$\chi_T^{\mathrm{que}}\beta = 0.0223(3), \quad F_\eta = 0.374(3). \tag{5.27}$$

The result of eq. (5.27) is slightly below the theoretical prediction for infinite volume and in the continuum, given by eq. (5.17). We also compare our result of $\chi_T^{\mathrm{que}}\beta$ for large β with the value that was obtained in ref. [57]: $\chi_T^{\mathrm{que}}\beta \simeq 0.023$. Our result is in agreement with this value.

When we compare F_η with the value that we obtained in the δ-regime: $F_\pi = 0.6688(5)$, we observe that they do not agree. Furthermore, in the δ-regime the result is essentially independent of β, so the lattice artifacts are mild, in contrast to the outcome of F_η. This confirms that the hypothesis that F_η could be equal to F_π in the Schwinger model is not correct, although they are of the same order of magnitude.
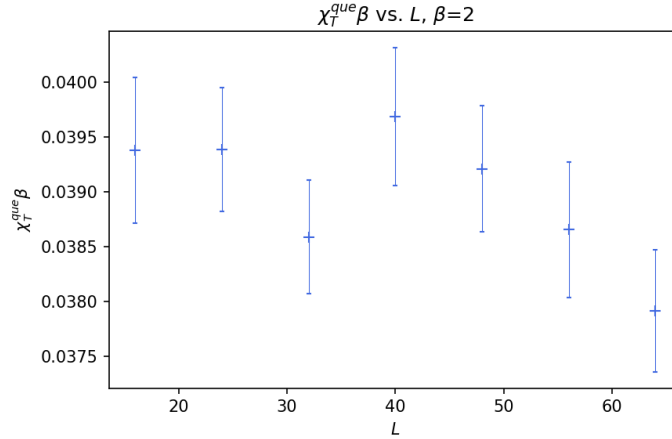
(a) $\chi_T^{\mathrm{que}}\beta$ vs. L for $\beta = 2$. An average yields $\chi_T^{\mathrm{que}} = 0.0389(2)$.
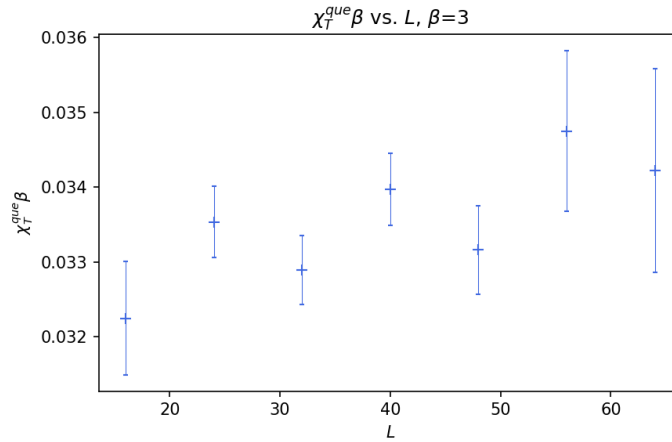
(b) $\chi_T^{\mathrm{que}}\beta$ vs. L for $\beta = 3$. An average yields $\chi_T^{\mathrm{que}} = 0.0335(3)$.
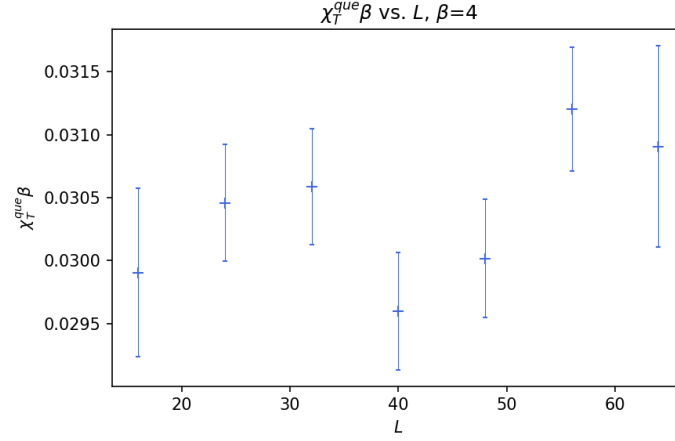
(c) $\chi_T^{\mathrm{que}}\beta$ vs. L for $\beta = 4$. An average yields $\chi_T^{\mathrm{que}} = 0.0304(2)$.
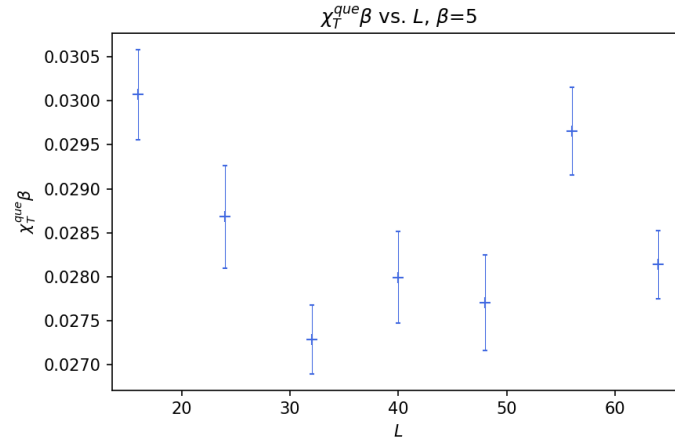
(d) $\chi_T^{\mathrm{que}}\beta$ vs. L for $\beta = 5$. An average yields $\chi_T^{\mathrm{que}} = 0.0285(4)$.

Figure 5.4: $\chi_T\beta$ measured for different β and lattices of dimensions $L \times L$.

Figure 5.5: $\chi_T^{\mathrm{que}}\beta$ vs. $1/\beta$. Bautista *et al.* refers to ref. [56] and Dürr, Hoelbling to ref. [57]. HMC algorithm denotes the results that we computed with pure gauge theory simulations. In order to determine $\chi_T^{\mathrm{que}}\beta$ in the continuum we fitted a function of the form $\chi_T^{\mathrm{que}}\beta = a + b/\beta$, which yielded $\chi_T^{\mathrm{que}}\beta = 0.0223(3)$.

Chapter 6

Conclusions

In this work we computed the masses of the bosons that appear in the two-flavor Schwinger model at finite temperature by 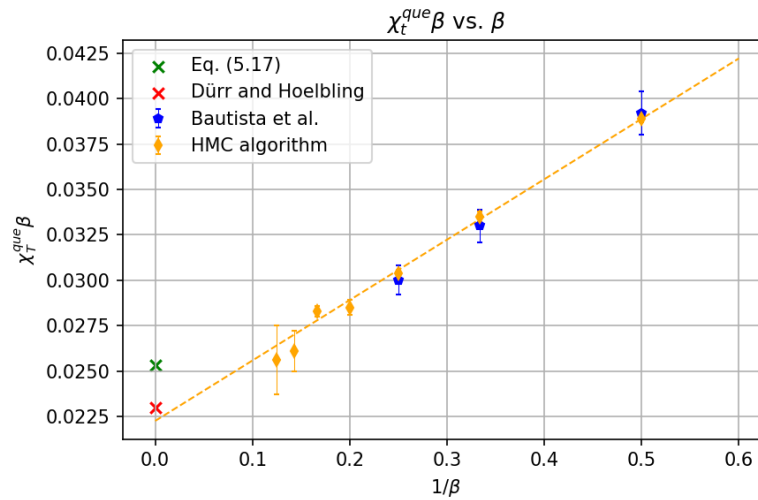using lattice simulations. We compared the results with the analytic approach by Hosotani *et al.*, which is only valid for $m \ll \mu = \sqrt{2g^2/\pi}$, so we did not expect a perfect agreement with lattice simulations. Still, we confirm the validity of Hosotani's equations in the low mass regime. We saw that they are not very useful to obtain predictions for m_π and m_η for arbitrary fermion masses. However, they would be applicable to compute m_π and m_η for arbitrary values of the vacuum angle θ, when the degenerate fermion mass is much smaller than μ. This cannot be easily done by lattice simulations, because the Euclidean action becomes complex and $\exp(-S[x])$ does not represent a probability measure for $\theta \neq 0$.

In the δ-regime, we observed that the residual pion mass m_π^R is proportional to $1/L$ for $d = 2$, as we conjectured based on the higher dimensional results previously shown by Leutwyler, Hasenfratz and Niedermayer. Thus, we were able to compute the pion decay constant in two dimensions. Our final result is

$$F_\pi = 0.6688(5).$$
(6.1)

It also turned out that this quantity does not depend on the parameter β and shows mild lattice artifacts.

We determined the η decay constant, F_η, in two dimensions by computing the quenched topological susceptibility and applying the Witten-Veneziano formula to the Schwinger model. We verified that our results for χ_T^{que} are compatible with the literature. From an extrapolation to the continuum limit we obtained

$$\chi_T^{\text{que}}\beta = 0.0223(3).$$
(6.2)

This value is below of the theoretical prediction by Seiler, which states that $\chi_T^{\text{que}}\beta \simeq 0.0253$, but is in agreement with the value determined by Dürr and Hoelbling: $\chi_T^{\text{que}}\beta \simeq 0.023$. With our result of $\chi_T^{\text{que}}\beta$ we obtained

$$F_\eta = 0.374(3).$$
(6.3)

As we mentioned in Chapter 5, in large N_c QCD, to the order $1/N_c$ we can relate $F_{\eta'} = F_\pi$. On the other hand, in the Schwinger model nothing assures that this relation holds. Our results obtained with the Witten-Veneziano formula and in the δ-regime suggest that in Schwinger model the relation $F_\eta = F_\pi$ is not valid. Still, both decay constants are of the same order of magnitude in two dimensions.

Appendix

A Hybrid Monte Carlo algorithm

In Chapter 2 we described how to implement the Metropolis algorithm to update a scalar field configuration $[\Phi]$ in order to achieve configurations distributed according to $p \propto \exp(-S[\Phi])$, where $S[\Phi]$ is the discretized Euclidean action. To update the configuration from $[\Phi]$ to $[\Phi']$ with this algorithm, one performs local updates $\Phi_x \to \Phi'_x$ which are accepted based on the ratio

$$\frac{p[\Phi']}{p[\Phi]} = e^{-\Delta S[\Phi, \Phi']}, \tag{A.1}$$

where

$$\Delta S = S[\Phi'] - S[\Phi]. \tag{A.2}$$

Now, when we consider gauge fields interacting with fermions, the partition function is given by

$$Z = \int \mathcal{D}[U]\, \mathcal{D}[\overline{\psi}, \psi]\, e^{-S[\psi, \overline{\psi}, U]} = \int \mathcal{D}[U]\, \mathcal{D}[\overline{\psi}, \psi]\, e^{-S_F[\psi, \overline{\psi}, U]} e^{-S_G[U]}, \tag{A.3}$$

where ψ and $\overline{\psi}$ are Grassmann fields and where U denotes the link variables. If we use eq. (2.50) and the first line of eqs. (2.98), we can rewrite the partition function as

$$Z = \int \mathcal{D}[U]\, e^{-S_G[U]} \det D[U], \tag{A.4}$$

where $D[U]$ is a discretization of the Dirac operator. Thus, the probability of a configuration $[U]$ is

$$p[U] = \frac{1}{Z} e^{-S_G[U]} \det D[U]. \tag{A.5}$$

We observe that in order to update the link variables, we will have to compute the ratio $\det D[U']/\det D[U]$, which is computationally expensive . Therefore, algorithms that perform local updates are not very efficient when one deals with fermions and gauge fields, since one has to consider complete configurations to calculate determinants.

Several algorithms that update entire configurations in one step have been introduced. For fermions interacting with gauge fields, the most efficient is the Hybrid Monte Carlo (HMC) algorithm [58], which introduces auxiliary momenta π, distributed according to $p[\pi] \propto \exp(-\pi^2/2)$, conjugated to the link variables U. By solving the Hamilton equations we can evolve (π, U) to (π', U') for N steps along a trajectory in the phase space. This is known as molecular dynamics evolution. After these N steps, one performs a *Langevin*

$step^1$, that is, the momenta are generated again and the molecular dynamics evolution is repeated. We describe the HMC procedure for a scalar field. The steps are the same for the implementation in QED; however, it involves a more subtle treatment of the fermion fields and the link variables, which is reviewed in refs. [20, 59, 60].

Let us suppose a scalar field configuration $[\Phi]$ with Euclidean action $S[\Phi]$. By introducing the conjugate momenta

$$\pi_x = \frac{\partial \mathcal{L}}{\partial \dot{\Phi}_x}, \tag{A.6}$$

the Hamiltonian is given by

$$H[\Phi, \pi] = \frac{1}{2}\pi^2 + S[\Phi], \tag{A.7}$$

where $\pi^2 = \sum_x \pi_x^2$ and where x runs over all the lattice sites. The momentum configuration is generated with a Gaussian distribution

$$p[\pi] \propto e^{-\frac{1}{2}\pi^2} \tag{A.8}$$

and $[\Phi]$ with a cold or hot start. From eq. (2.42), we know that the expectation value of an observable A is given by

$$\langle A \rangle = \frac{\int \mathcal{D}[\Phi] e^{-S[\Phi]} A[\Phi]}{\int \mathcal{D}[\Phi] e^{-S[\Phi]}}, \quad \mathcal{D}[\Phi] = \prod_x \Phi_x. \tag{A.9}$$

We can insert the momentum to this expression without modifying its outcome

$$\langle A \rangle = \frac{\int \mathcal{D}[\Phi]\mathcal{D}[\pi] e^{-\frac{1}{2}\pi^2} e^{-S[\Phi]} A[\Phi]}{\int \mathcal{D}[\Phi]\mathcal{D}[\pi] e^{-\frac{1}{2}\pi^2} e^{-S[\Phi]}}, \quad \mathcal{D}[\pi] = \prod_x \pi_x. \tag{A.10}$$

Now, we evolve Φ_x and π_x along a trajectory, parametrized by τ, with the Hamilton equations

$$\frac{d\Phi_x}{d\tau} = \frac{\partial H}{\partial \pi_x} = \pi_x, \quad \frac{d\pi_x}{d\tau} = -\frac{\partial H}{\partial \Phi_x} = -\frac{\partial S}{\partial \Phi_x}. \tag{A.11}$$

After $N\Delta\tau$ steps, the system arrives at a new configuration (π', ϕ'). As we mentioned in Chapter 2, the detailed balance condition

$$\frac{W([\Phi] \to [\Phi'])}{W([\Phi'] \to [\Phi])} = \frac{p[\Phi']}{p[\Phi]} = \frac{e^{-S[\Phi']}}{e^{-S[\Phi]}}, \quad p[\Phi] \propto e^{-S[\Phi]} \tag{A.12}$$

has to be fulfilled. We will show that the condition is satisfied when the transitions are reversible, *i.e.* if we can go from (π, Φ) to (π', Φ') with the same probability as from $(-\pi', \Phi')$ to $(-\pi, \Phi)$, and when the measure does not change, $\mathcal{D}[\Phi]\mathcal{D}[\pi] = \mathcal{D}[\Phi']\mathcal{D}[\pi']$. Since eqs. (A.11) are deterministic, there is a transformation rule

$$f(\pi, \Phi) = (\pi', \Phi') \tag{A.13}$$

that maps $(\pi, \Phi) \to (\pi', \Phi')$ and reversibility means that

$$f(\pi, \Phi) = (\pi', \Phi') \Leftrightarrow f(-\pi', \phi') = (-\pi, \phi). \tag{A.14}$$

Both conditions can be achieved numerically by solving eqs. (A.11), for instance with the so-called *leapfrog integrator*, which we describe below.

---

[1]This comes from another algorithm, known as Langevin algorithm (see for instance ref. [21]). Mixing this step with molecular dynamics is the reason of the "hybrid" name.

The Hamiltonian is a constant of motion and the configurations are constrained to $H = H[\Phi, \pi]$; so, in principle, (π', Φ') could be used as the new configuration of the Markov chain. However, eqs. (A.11) cannot be solved exactly, thus $H[\Phi, \pi] \neq H[\Phi', \pi']$. A way to correct this defect is to apply a Metropolis step, *i.e.* to calculate $\Delta H = H[\Phi', \pi'] - H[\Phi, \pi]$ and only accept the change $(\pi, \Phi) \rightarrow (\pi', \Phi')$ when $\Delta H \leq 0$, or if $\Delta H > 0$, accept it with probability $\exp(-\Delta H)$.

The leapfrog integrator updates the values of Φ_x and π_x in a trajectory of length $N\Delta\tau$, $N \in \mathbb{N}$, by evolving the value of Φ_x in N steps of size $\Delta\tau$ and evolving π_x in N steps consisting of two intermediate steps of length $\Delta\tau/2$

$$
\begin{aligned}
\Phi_x\left[(i-1)\Delta\tau\right] &\longrightarrow & \Phi_x(i\Delta\tau), \\
\pi_x\left[(i-1)\Delta\tau\right] &\rightarrow \pi_x\left[(i-\tfrac{1}{2})\Delta\tau\right] \rightarrow & \pi_x(i\Delta\tau), \quad i = 1, \dots N.
\end{aligned}
\tag{A.15}
$$

The equations for updating the values are

$$
\begin{aligned}
\Phi_x(i\Delta\tau) &= \Phi_x\left[(i-1)\Delta\tau\right] + \Delta\tau \left.\frac{d\Phi_x}{d\tau}\right|_{\tau=(i-1/2)\Delta\tau}, \\
\pi_x\left[\left(i-\frac{1}{2}\right)\Delta\tau\right] &= \pi_x\left[(i-1)\Delta\tau\right] + \frac{\Delta\tau}{2}\left.\frac{d\pi_x}{d\tau}\right|_{\tau=(i-1)\Delta\tau}, \\
\pi_x(i\Delta\tau) &= \pi_x\left[\left(i-\frac{1}{2}\right)\Delta\tau\right] + \frac{\Delta\tau}{2}\left.\frac{d\pi_x}{d\tau}\right|_{\tau=i\Delta\tau}.
\end{aligned}
\tag{A.16}
$$

We can substitute the derivatives by using eqs. (A.11) and combine eqs. (A.16) to obtain

$$
\begin{aligned}
\Phi_x(i\Delta\tau) &= \Phi_x\left[(i-1)\Delta\tau\right] + \Delta\tau\,\pi_x\left[(i-1)\Delta\tau\right] - \frac{\Delta\tau^2}{2}\left.\frac{\partial S}{\partial\Phi_x}\right|_{\Phi_x[(i-1)\Delta\tau]}, \\
\pi_x(i\Delta\tau) &= \pi_x\left[(i-1)\Delta\tau\right] - \frac{\Delta\tau}{2}\left[\left.\frac{\partial S}{\partial\Phi_x}\right|_{\Phi_x[(i-1)\Delta\tau]} + \left.\frac{\partial S}{\partial\Phi_x}\right|_{\Phi_x(i\Delta\tau)}\right].
\end{aligned}
\tag{A.17}
$$

Let us verify that the Jacobian of the transformation $(\Phi_x[(i-1)\Delta\tau], \pi_x[(i-1)\Delta\tau]) \rightarrow (\Phi_x(i\Delta\tau), \pi_x(i\Delta\tau))$ is equal to one. A computation of the matrix of derivatives of eqs. (A.17) yields

$$
J = \det \begin{pmatrix} 1 - \frac{\Delta\tau^2}{2}\frac{\partial}{\partial\Phi_x[(i-1)\Delta\tau]}\left.\frac{\partial S}{\partial\Phi_x}\right|_{\Phi_x[(i-1)\Delta\tau]} & \Delta\tau \\ -\frac{\Delta\tau}{2}\frac{\partial}{\partial\Phi_x[(i-1)\Delta\tau]}\left.\frac{\partial S}{\partial\Phi_x}\right|_{\Phi_x[(i-1)\Delta\tau]} & 1 \end{pmatrix} = 1.
\tag{A.18}
$$

Thus, the measure does not change in any integration step $i - 1 \rightarrow i$. Since the Jacobian of the transformation from $\tau = 0$ to $\tau = N\Delta\tau$ is the multiplication of all the Jacobians of eqs. (A.17) for $i = 1, \dots, N$, we conclude that the measure does not change after N steps, *i.e.* $\mathcal{D}[\Phi]\mathcal{D}[\pi] = \mathcal{D}[\Phi']\mathcal{D}[\pi']$.

To show the reversibility we identify eqs. (A.17) as the transformation rule f that we mentioned in eq. (A.13). To check eq. (A.14) we interchange

$$
\Phi_x\left[(i-1)\Delta\tau\right] \leftrightarrow \Phi_x(i\Delta\tau), \quad \pi_x\left[(i-1)\Delta\tau\right] \leftrightarrow -\pi_x(i\Delta\tau)
\tag{A.19}
$$

on the right-hand side of eqs. (A.17)

$$\Phi_x(i\Delta\tau) - \Delta\tau\,\pi_x(i\Delta\tau) - \frac{\Delta\tau^2}{2}\frac{\partial S}{\partial\Phi_x}\bigg|_{\Phi_x(i\Delta\tau)}$$

$$= \Phi_x(i\Delta\tau) - \Delta\tau\,\pi_x[(i-1)\Delta\tau] + \frac{\Delta\tau^2}{2}\left[\frac{\partial S}{\partial\Phi_x}\bigg|_{\Phi_x[(i-1)\Delta\tau]} + \frac{\partial S}{\partial\Phi_x}\bigg|_{\Phi_x(i\Delta\tau)}\right] - \frac{\Delta\tau^2}{2}\frac{\partial S}{\partial\Phi_x}\bigg|_{\Phi_x(i\Delta\tau)}$$

$$= \Phi_x[(i-1)\Delta\tau] - \pi_x(i\Delta\tau) - \frac{\Delta\tau}{2}\left[\frac{\partial S}{\partial\Phi_x}\bigg|_{\Phi_x[(i-1)\Delta\tau]} + \frac{\partial S}{\partial\Phi_x}\bigg|_{\Phi_x(i\Delta\tau)}\right]$$

$$= -\pi_x[(i-1)\Delta\tau]. \tag{A.20}$$

Therefore eq. (A.14) is established.

Now, we still have to show that the HMC algorithm obeys detailed balance. But first, let us summarize the algorithm steps as a recipe:

1. We generate an auxiliary momentum configuration $[\pi]$ distributed according to $p[\pi] \propto \exp(-\sum_x \pi_x^2/2)$.

2. Then, we solve the Hamilton equations (A.11) by using the leapfrog integrator in order to evolve the system from $(\pi, \phi) \to (\pi', \phi')$.

3. If $\Delta H = H[\pi', \phi'] - H[\pi, \phi] \leq 0$ the configuration is updated, otherwise the update $(\pi, \phi) \to (\pi', \phi')$ is accepted only with probability $\exp(-\Delta H)$. This is equivalent to accepting the change with probability $W_M = \min(1, \exp(-\Delta H))$.

These three steps are repeated the required number of times and together they conform a sweep. It is important to mention that for each new sweep, the momentum configuration has to be generated again.

To demonstrate detailed balance, we begin with the transition probability to move from $[\Phi]$ to $[\Phi']$

$$W(\Phi'|\Phi) = \int \mathcal{D}[\pi]\mathcal{D}[\pi']\, W_M(\pi', \Phi'|\pi, \Phi) W_R(\pi', \Phi'|\pi, \Phi) e^{-\pi^2/2}, \tag{A.21}$$

where we introduced the simplified notation $W(A|B)$, which means "the probability to move from B to A" (here we deviate from the notation in eq. (A.12)). W_R stands for the probability to evolve the system from (π', Φ') to (π, Φ), which satisfies reversibility $W_R(\pi', \Phi'|\pi, \Phi) = W_R(-\pi, \Phi| - \pi', \Phi')$. W_M is the probability to accept the update (step 3 of the recipe). We can rewrite $W_M(\pi', \Phi'|\pi, \Phi)$ as follows

$$W_M(\pi', \Phi'|\pi, \Phi) = \min(1, \exp(-\Delta H)) = \exp(-\Delta H)\min(\exp(\Delta H), 1)$$

$$= \exp(-\Delta H)W_M(\pi, \Phi|\pi', \Phi'). \tag{A.22}$$

Since H does not depend on the sign of π, we obtain the relation

$$W_M(\pi', \Phi'|\pi, \Phi) = \exp(-\Delta H)W_M(-\pi, \Phi| - \pi', \Phi'), \tag{A.23}$$

and therefore

$$W(\Phi'|\Phi) = \int \mathcal{D}[\pi]\mathcal{D}[\pi']\, W_M(\pi', \Phi'|\pi, \Phi) W_R(\pi', \Phi'|\pi, \Phi) e^{-\pi^2/2}$$

$$= \int \mathcal{D}[\pi]\mathcal{D}[\pi']\, e^{-\Delta H} W_M(-\pi, \Phi| - \pi', \Phi') W_R(-\pi, \Phi| - \pi', \Phi') e^{-\pi^2/2}$$

$$= \int \mathcal{D}[\pi]\mathcal{D}[\pi']\, W_M(-\pi, \Phi| - \pi', \Phi') W_R(-\pi, \Phi| - \pi', \Phi') e^{-S[\Phi']+S[\Phi]-\pi'^2/2}. \tag{A.24}$$

Under sign flip $\pi \to -\pi$, $\pi' \to -\pi'$ the measure does not change, thus

$$
\begin{aligned}
W(\Phi'|\Phi) &= \int \mathcal{D}[\pi]\mathcal{D}[\pi'] \, W_M(\pi, \Phi|\pi', \Phi')W_R(\pi, \Phi|\pi', \Phi')e^{-S[\Phi']+S[\Phi]-\pi'^2/2} \\
&= W(\Phi|\Phi')e^{-S[\Phi']+S[\Phi]}.
\end{aligned}
$$

Hence

$$
\frac{W(\Phi'|\Phi)}{W(\Phi|\Phi')} = \frac{e^{-S[\Phi']}}{e^{-S[\Phi]}} = \frac{p[\Phi']}{p[\Phi]}, \tag{A.25}
$$

i.e. detailed balance is satisfied.

B   Second order numerical integral

In Chapter 3 we have to evaluate several integrals of the form

$$
I = \int_a^b f(x)\,dx \tag{B.1}
$$

to solve the equations obtained by Hosotani. In order to do so, we construct a numerical integral up to second order. Let us consider a lattice of N points separated by a length Δx, with the condition $f(x_1) = f(a)$, $f(x_N) = f(b)$. For the interior points of the lattice, we can approximate the second derivative as

$$
f_i'' \approx \frac{f_{i+1} - 2f_i + f_{i-1}}{\Delta x^2}, \tag{B.2}
$$

where we denote $f_i \equiv f(x_i)$. If N is an odd number, then eq. (B.1) can be written, up to second order, by using a Taylor series, as

$$
I \approx \sum_{i=1}^{\frac{N-1}{2}} \int_{x_{2i}-\Delta x}^{x_{2i}+\Delta x} \left[f_{2i} + f_{2i}'(x - x_{2i}) + f_{2i}''\frac{(x - x_{2i})^2}{2} \right] dx, \tag{B.3}
$$

where we are only integrating on the even sites. Simplifying eq. (B.3) yields

$$
I \approx \sum_{i=1}^{\frac{N-1}{2}} 2\Delta x f_{2i} + \frac{\Delta x^3}{3}f_{2i}''. \tag{B.4}
$$

If we substitute eq. (B.2) we obtain an expression that allows us to evaluate eq. (B.1) when N is odd

$$
I \approx \sum_{i=1}^{\frac{N-1}{2}} \frac{\Delta x}{3}\left(f_{2i+1} + 4f_{2i} + f_{2i-1}\right). \tag{B.5}
$$

On the other hand, if N is an even number, we can use the following variant of eq. (B.5)

$$
I \approx \sum_{i=1}^{\frac{N}{2}-1} \frac{\Delta x}{3}\left(f_{2i+2} + 4f_{2i+1} + f_{2i}\right). \tag{B.6}
$$

However, we still need to integrate from the site x_1 to x_2 (see figure 1 for a graphical depiction). In this case, eq. (B.2) is not valid for the derivatives, because we do not have any more points to the left of the grid. Thus, we use the following discretization for the derivatives (see e.g. ref. [61]), which only relies on forward steps

$$
f_1' \approx \frac{-3f_1 + 4f_2 - f_3}{2\Delta x}, \quad f_1'' \approx \frac{2f_1 - 5f_2 + 4f_3 - f_4}{\Delta x^2}. \tag{B.7}
$$

Then, the contribution of the interval $[x_1, x_1 + \Delta x]$ to the integral is

$$\int_{x_1}^{x_1+\Delta x} \left[f_1 + f_1'(x - x_1) + f_1'' \frac{(x - x_1)^2}{2} \right] dx = f_1 \Delta x + \frac{f_1'}{2} \Delta x^2 + \frac{f_1''}{6} \Delta x^3$$

$$= \Delta x \left(\frac{7}{12} f_1 + \frac{1}{6} f_2 + \frac{5}{12} f_3 - \frac{1}{6} f_4 \right). \quad \text{(B.8)}$$

Therefore, the general result for the second order numerical integral reads

$$I \approx \begin{cases} \sum_{i=1}^{\frac{N-1}{2}} \frac{\Delta x}{3} \left(f_{2i+1} + 4 f_{2i} + f_{2i-1} \right) & \text{for odd } N, \\ \sum_{i=1}^{\frac{N}{2}-1} \frac{\Delta x}{3} \left(f_{2i+2} + 4 f_{2i+1} + f_{2i} \right) + \Delta x \left(\frac{7}{12} f_1 + \frac{1}{6} f_2 + \frac{5}{12} f_3 - \frac{1}{6} f_4 \right) & \text{for even } N. \end{cases} \quad \text{(B.9)}$$

We test the result with the following definite integrals

$$\int_{-1/\sqrt{2}}^{1/\sqrt{2}} x e^{-x^2} \, dx = 0, \quad \int_0^\pi e^x \cos(x) \, dx = -\frac{1}{2}(1 + e^\pi). \quad \text{(B.10)}$$

In figure 2 we show the numerical value of these integrals as a function of the number of points, N, on the lattice. We also compare the result of eq. (B.9) with a calculation of the integrals by using midpoint Riemann sums. In figure 2 (a) we observe that the Riemann sum converges faster and that the numerical integral computed with eq. (B.9) oscillates around the right value for small N. In figure 2 (b), eq. (B.9) converges faster.

$$\sum_{i=1}^{\frac{5-1}{2}} \frac{\Delta x}{3} \left(f_{2i+2} + 4 f_{2i+1} + f_{2i} \right)$$

$$x_1 \quad x_2 \quad x_3 \quad x_4 \quad x_5$$

$$\sum_{i=1}^{\frac{6}{2}-1} \frac{\Delta x}{3} \left(f_{2i+2} + 4 f_{2i+1} + f_{2i} \right)$$

$$\Delta x \left(\frac{7}{12} f_1 + \frac{1}{6} f_2 + \frac{5}{12} f_3 - \frac{1}{6} f_4 \right)$$

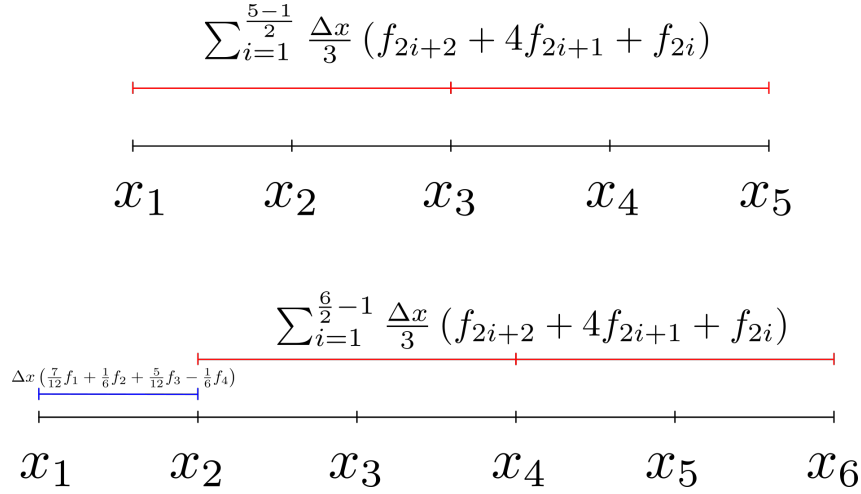$$x_1 \quad x_2 \quad x_3 \quad x_4 \quad x_5 \quad x_6$$

Figure 1: In the upper image we show a lattice with an odd number of points, where we see that by integrating only in the even sites from $x_{2i} - \Delta x$ to $x_{2i} + \Delta x$, we can compute the numerical integral. In the lower image we show the case of a lattice with even N. There, we can compute the integral from x_2 up to the last site (x_6 in the figure); however, the contribution from x_1 to x_2 would be missing if we only use eq. (B.6). For that reason, we have to use eqs. (B.7) to calculate the contribution from the blue region, which is given by eq. (B.8).
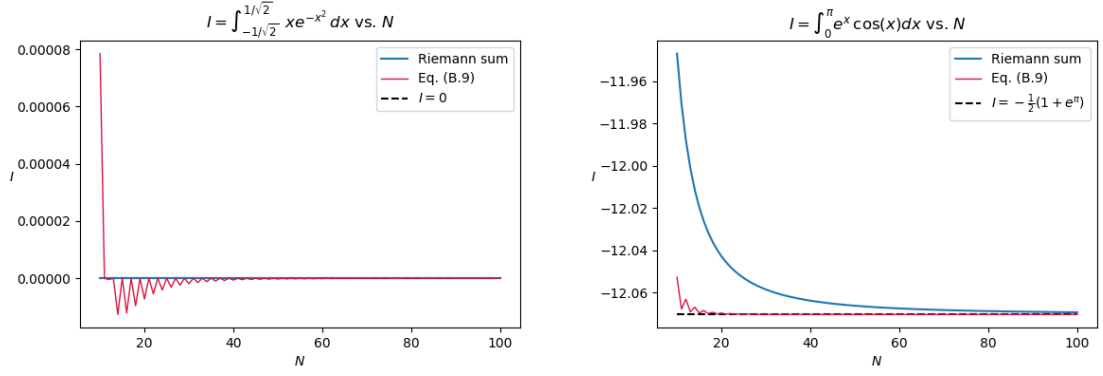
(a) $\int_{-1/\sqrt{2}}^{1/\sqrt{2}} xe^{-x^2}\, dx$ as a function of the number of points used to evaluate the integral.

(b) $\int_0^\pi e^x \cos(x)\, dx$ as a function of the number of points used to evaluate the integral.

Figure 2: Test of the convergence of the numerical integral with the examples of eq. (B.10). We compare the results of the numerical integral presented in this section with the results obtained with Riemann sums.

C   Jackknife error

The jackknife error, σ_J, is a special kind of error that allows us to compute the uncertainty of a set of measurements by taking into account possible autocorrelations. It is also useful to determine the error of a fit parameter. For instance, an error to the energy gap given by the correlation function (eq. (2.44)) can be obtained by fitting a cosh function to several data subsets and by estimating σ_J, using the resultant parameter of each fit as a measurement.

Let us suppose that we have N measurements of a variable x. We describe the calculation of σ_J as a recipe:

- We calculate the average $\langle x \rangle$ of the N measurements.

- We divide the N measurements in M blocks. M should preferably be a number that satisfies $N/M \in \mathbb{N}$.

- For each block $m = 1 \dots M$, we consider the set of the N measurements without the block m and calculate its average $\langle x \rangle_m$.

- The jackknife error is defined as follows

$$\sigma_J = \sqrt{\frac{M-1}{M} \sum_{m=1}^{M} \left(\langle x \rangle_m - \langle x \rangle \right)^2}. \tag{C.1}$$

An important remark is that when $M = N$, σ_J coincides with the standard error, since for that case we have

$$\langle x \rangle_m = \frac{1}{N-1} \sum_{m' \neq m}^{N} x_{m'} \implies \langle x \rangle_m - \langle x \rangle = \frac{1}{N-1} \left(\langle x \rangle - x_m \right). \tag{C.2}$$

Then

$$\sigma_J = \sqrt{\frac{N-1}{N(N-1)^2} \sum_{m=1}^{N} \left(x_m - \langle x \rangle \right)^2} = \sqrt{\frac{1}{N(N-1)} \sum_{m=1}^{N} \left(x_m - \langle x \rangle \right)^2}. \tag{C.3}$$

However, it is not the idea to take $M = N$, but to work with $M \ll N$. In general, σ_J changes for a different number of blocks M and it tends to be larger than the standard error. Therefore, normally one calculates the right-hand side of eq. (C.1) for several M and chooses the error as the largest value of the σ_J that were computed.

D Autocorrelation time

The autocorrelation time is a quantitative measure of the autocorrelation between the Markov chain configurations. It depends on a specific observable X. To define it, we make use of the correlation function

$$C_X(t) = \langle X_i X_{i+t} \rangle - \langle X_i \rangle \langle X_{i+t} \rangle, \tag{D.1}$$

where $t = |i - j|$, $i, j = 1, \ldots, N$, with N the number of measurements of X. For large t, the following behavior is known

$$C_X(t) \propto e^{-t/\tau_{\exp}}, \tag{D.2}$$

where we refer to $\tau_{\exp}$ as the *exponential autocorrelation time*. $\tau_{\exp}$ can be obtained by measuring $C_X(t)$ for large t and fitting eq. (D.2). A small $\tau_{\exp}$ means that the configurations are well decorrelated. When that is not the case, it is recommendable to increment the number of sweeps between each configuration that is used to take measurements.

There is another autocorrelation time that can be defined, known as the *integrated autocorrelation time*

$$\tau_{\text{int}} = \frac{1}{2} + \sum_{t=1}^{N} \frac{C_X(t)}{C_X(0)}. \tag{D.3}$$

It can be proved that for large N (see e.g. ref. [62]), the statistical error σ_X is related to the variance

$$\text{Var} = \langle (X - \langle X \rangle)^2 \rangle \tag{D.4}$$

by

$$\sigma_X^2 = 2\tau_{\text{int}} \frac{\text{Var}}{N}. \tag{D.5}$$

Thus, τ_{int} provides a way of finding an error that takes into account correlations between measurements, different from the jackknife error. Another interpretation of eq. (D.5) is that it tells us that we are using an effective sample of $N/(2\tau_{\text{int}})$ measurements. If $\tau_{\text{int}} = 1/2$, the effective sample is N, which indicates a perfect decorrelation. This is motivated by the fact that with decorrelated data the uncertainty is simply the standard error $\sqrt{\text{Var}/N}$. Deeper discussions of the autocorrelation time can be found in refs. [62–64].

Bibliography

[1] K. G. Wilson. Confinement of quarks. *Phys. Rev. D*, 10:2445–2459, 1974.

[2] S. Aoki et al. Review of lattice results concerning low-energy particle physics. *Eur. Phys. J. C*, 77:112, 2017.

[3] J. Schwinger. Gauge Invariance and Mass. *Phys. Rev.*, 125:397–398, 1962.

[4] J. Schwinger. Gauge Invariance and Mass. II. *Phys. Rev.*, 128:2425–2429, 1962.

[5] S. R. Coleman, R. Jackiw, and L. Susskind. Charge Shielding and Quark Confinement in the Massive Schwinger Model. *Ann. Phys.*, 93:267, 1975.

[6] S. R. Coleman. More About the Massive Schwinger Model. *Ann. Phys.*, 101:239, 1976.

[7] H. Leutwyler. Energy Levels of Light Quarks Confined to a Box. *Phys. Lett. B*, 189:197–202, 1987.

[8] P. Hasenfratz and F. Niedermayer. Finite size and temperature effects in the AF Heisenberg model. *Z. Phys. B*, 92:91, 1993.

[9] E. Witten. Current Algebra Theorems for the U(1) Goldstone Boson. *Nucl. Phys. B*, 156:269–283, 1979.

[10] G. Veneziano. U(1) Without Instantons. *Nucl. Phys. B*, 159:213–224, 1979.

[11] S. L. Adler. Axial vector vertex in spinor electrodynamics. *Phys. Rev.*, 177:2426–2438, 1969.

[12] J. S. Bell and R. Jackiw. A PCAC puzzle: $\pi^0 \to \gamma\gamma$ in the σ model. *Nuovo Cim. A*, 60:47–61, 1969.

[13] L. V. Belvedere, K. D. Rothe, B. Schroer, and J. A. Swieca. Generalized Two-dimensional Abelian Gauge Theories and Confinement. *Nucl. Phys. B*, 153:112–140, 1979.

[14] W. Dittrich and M. Reuter. *Selected Topics in Gauge Theories*. Springer, 1986.

[15] D. Tong. Lectures on Gauge Theory. Cambridge. `http://www.damtp.cam.ac.uk/user/tong/gaugetheory/gt.pdf`, 2018. Accessed: 2021-03.

[16] J. E. Hetrick, Y. Hosotani, and S. Iso. Interplay between mass, volume, vacuum angle and chiral condensate in N flavor QED in two-dimensions. *Phys. Rev. D*, 53:7255–7259, 1996.

[17] G. Roepstorff. *Path Integral Approach to Quantum Physics*. Springer, 1994.

[18] L. S. Schulman. *Techniques and Applications of Path Integration*. Dover Publications,

1981.

[19] W. Bietenholz and U. W. Wiese. *Quantum Field Theory and the Standard Model of Particle Physics: From Fundamental Concepts to Dynamical Mechanisms.* To appear in Cambridge University Press.

[20] C. Gattringer and C. B. Lang. *Quantum Chromodynamics on the Lattice.* Springer, 2010.

[21] H. J. Rothe. *Lattice gauge theories: An Introduction,* volume 43. World Scientific, 1992.

[22] M. Creutz and B. Freedman. A statistical approach to quantum mechanics. *Ann. Phys.*, 132:427–462, 1981.

[23] W. Bietenholz. Optimised Dirac Operators on the Lattice: Construction, Properties and Applications. *Fortsch. Phys.*, 56:107–180, 2008.

[24] I. Montvay and G. Münster. *Quantum Fields on a Lattice.* Cambridge Monographs on Mathematical Physics. Cambridge University Press, 1994.

[25] J.E. Hetrick, Y. Hosotani, and S. Iso. The massive multi-flavor Schwinger model. *Phys. Lett. B*, 350:92–102, 1995.

[26] Y. Hosotani. More about the massive multiflavor Schwinger model. In *Nihon University Workshop on Fundamental Problems in Particle Physics*, pages 64–69, 1995.

[27] Y. Hosotani and R. Rodriguez. Bosonized massive N-flavour Schwinger model. *J. Phys. A: Math. Gen*, 31:9925–9955, 1998.

[28] M. Abramowitz and I. A. Stegun. *Handbook of Mathematical Functions with Formulas, Graphs, and Mathematical Tables.* Dover, 1964.

[29] C. Gattringer, I. Hip, and C.B. Lang. The chiral limit of the two-flavor lattice Schwinger model with Wilson fermions. *Phys. Lett. B*, 466:287–292, 1999.

[30] A. V. Smilga. Critical amplitudes in two-dimensional theories. *Phys. Rev. D*, 55:R443–R447, 1997.

[31] D. Y. Hsieh. On Mathieu equation with damping. *J. Math. Phys.*, 21:722–725, 1980.

[32] N. W. McLachlan. *Theory and application of Mathieu functions.* Clarendon Press, Oxford, 1951.

[33] P.A. Zyla et al. Review of Particle Physics. *Prog. Theor. Exp. Phys.*, 2020:083C01, 2020.

[34] A. Pich. Chiral perturbation theory. *Rept. Prog. Phys.*, 58:563–610, 1995.

[35] S. Scherer and M. R. Schindler. *A Primer for Chiral Perturbation Theory.* Springer, 2012.

[36] H. Leutwyler. Chiral perturbation theory. *Scholarpedia*, 7:8708, 2012.

[37] J. Gasser and H. Leutwyler. Light Quarks at Low Temperatures. *Phys. Lett. B*, 184:83–88, 1987.

[38] P. Hasenfratz and H. Leutwyler. Goldstone Boson Related Finite Size Effects in Field Theory and Critical Phenomena With O(N) Symmetry. *Nucl. Phys. B*, 343:241–284, 1990.

[39] J. Gasser and H. Leutwyler. Thermodynamics of chiral symmetry. *Phy. Lett. B*, 188:477–481, 1987.

[40] M. Golterman. Applications of chiral perturbation theory to lattice QCD. In *Les Houches Summer School: Session 93: Modern perspectives in lattice QCD: Quantum field theory and high performance computing*, pages 423–515, 2009.

[41] A. Bazavov et al. Results for light pseudoscalar mesons. *PoS*, LATTICE2010:074, 2010.

[42] R. Arthur et al. Domain wall QCD with near-physical pions. *Phys. Rev. D*, 87:094514, 2013.

[43] E. Follana, C. T. H. Davies, G. P. Lepage, and J. Shigemitsu. High-Precision Determination of the π, K, D, and D_s Decay Constants from Lattice QCD. *Phys. Rev. Lett.*, 100:062002, 2008.

[44] W. Bietenholz, M. Göckeler, R. Horsley, Y. Nakamura, D. Pleiter, P.E.L. Rakow, G. Schierholz, and J.M. Zanotti. Pion in a box. *Phys. Lett. B*, 687:410–414, 2010.

[45] P. Hasenfratz. The QCD rotator in the chiral limit. *Nucl. Phys. B*, 828:201–214, 2010.

[46] F. Niedermayer and P. Weisz. Matching effective chiral Lagrangians with dimensional and lattice regularizations. *JHEP*, 04:110, 2016.

[47] N. D. Mermin and H. Wagner. Absence of Ferromagnetism or Antiferromagnetism in One- or Two-Dimensional Isotropic Heisenberg Models. *Phys. Rev. Lett.*, 17:1133–1136, 1966.

[48] P. C. Hohenberg. Existence of Long-Range Order in One and Two Dimensions. *Phys. Rev.*, 158:383–386, 1967.

[49] S. R. Coleman. There are no Goldstone bosons in two-dimensions. *Commun. Math. Phys.*, 31:259–264, 1973.

[50] A. V. Smilga and J. J. M. Verbaarschot. Scalar susceptibility in QCD and the multiflavor Schwinger model. *Phys. Rev. D*, 54:1087–1093, 1996.

[51] E. Seiler and I. O. Stamatescu. Some remarks on the Witten-Veneziano formula for the η' mass. *MPI-PAE-PTh-10-87*.

[52] E. Seiler. Some more remarks on the Witten-Veneziano formula for the eta-prime mass. *Phys. Lett. B*, 525:355–359, 2002.

[53] P. H. Damgaard, H. B. Nielsen, and R. Sollacher. Gauge symmetric approach to effective Lagrangians: The eta-prime meson from QCD. *Nucl. Phys. B*, 414:541–578, 1994.

[54] C. R. Gattringer, I. Hip, and C. B. Lang. Quantum fluctuations versus topology: A Study in $U(1)_2$ lattice gauge theory. *Phys. Lett. B*, 409:371–376, 1997.

[55] S. Dürr, Z. Fodor, C. Hoelbling, and T. Kurth. Precision study of the SU(3) topological susceptibility in the continuum. *JHEP*, 04:055, 2007.

[56] I. Bautista, W. Bietenholz, A. Dromard, U. Gerber, L. Gonglach, C. P. Hofmann, H. Mejía, and M. Wagner. Measuring the Topological Susceptibility in a Fixed Sector. *Phys. Rev. D*, 92:114510, 2015.

[57] S. Dürr and C. Hoelbling. Scaling tests with dynamical overlap and rooted staggered fermions. *Phys. Rev. D*, 71:054501, 2005.

[58] S. Duane, A. D. Kennedy, B. J. Pendleton, and D. Roweth. Hybrid Monte Carlo. *Phys. Lett. B*, 195:216–222, 1987.

[59] T. R. Haar. *Optimisations to Hybrid Monte Carlo for Lattice QCD*. PhD thesis, Adelaide U., 2019.

[60] A. Sternbeck. Simulations with (hybrid) Monte Carlo Algorithms. *Helmholtz International Summer School, JINR Dubna*, 2014.

[61] B. Fornberg. Generation of finite difference formulas on arbitrarily spaced grids. *Math. Comp.*, 51:699–699, 1988.

[62] A. Sokal. *Monte Carlo Methods in Statistical Mechanics: Foundations and New Algorithms*, pages 131–192. Springer, 1997.

[63] F. Niedermayer. Cluster algorithms. *Lect. Notes Phys.*, 501:36, 1998.

[64] B. A. Berg. *Markov Chain Monte Carlo Simulations and Their Statistical Analysis*. World Scientific, 2004.